# PHYSICAL AND NUMERICAL INVESTIGATION OF FLIP ANCHORS

**A Thesis Submitted to**
**the Graduate School of**
**İzmir Institute of Technology**
**in Partial Fulfillment of the Requirements for Degree of**

**MASTER OF SCIENCE**

**in Civil Engineering**

**by**
**Yıllar Meral KAYALI YÜK**

**June 2024**
**İZMİR**

We approve the thesis of **Yıllar Meral KAYALI YÜK**

**Examining Committee Members:**

**Prof. Dr. Nurhan ECEMİŞ**
Department of Civil Engineering, İzmir Institute of Technology

**Asst. Prof. Dr. Selçuk SAATCI**
Department of Civil Engineering, İzmir Institute of Technology

**Asst. Prof. Hasan Emre DEMİRCİ**
Department of Civil Engineering, İzmir Katip Çelebi University

**27 June 2024**

**Prof. Dr. Nurhan ECEMİŞ**
Supervisor, Department of Civil Engineering, İzmir Institute of Technology

**Prof. Dr. Cemalettin DÖNMEZ**
Head of the Department of Civil Engineering

**Prof. Dr. Mehtap EANES**
Dean of the Graduate School

# ACKNOWLEDGMENTS

I would like to thank my advisor, Prof. Dr. Nurhan Ecemiş, for his assistance in this scientific study, guiding me in the planning, research, and execution of my thesis, and instilling scientific confidence in me with his knowledge and experience. She was always patient with me and showed a high degree of understanding.

Also, I would like to thank the jury members Selçuk Saatcı and Hasan Emre Demirci for their participation in my thesis defense seminar and their valuable comments on this study.

Finally, I am grateful to my family for their support throughout my education, especially my mother and friends, who always believed in me and encouraged me to continue my graduate education.

# ABSTRACT

PHYSICAL AND NUMERICAL INVESTIGATION OF FLIP ANCHORS

The tensile capacity of driven earth anchors is important in maintaining slope stability. This study aims to summarize the results of field pull-out experiments conducted on two types of driven earth anchors that were installed in three different soil layers. The galvanized cast steel material was used in the construction of driven earth anchors. The large driven earth anchor (FPA-I) weighed 10 kg, while the small driven earth anchor (FPA-II) weighed approximately 5 kg. The FPA-I anchor was initially driven vertically into the clayey sand layer at a depth of 1.5 m, followed by the silty sand layer at a depth of 2.5 m, and ultimately the low-plastic clay layer at a depth of 3.25 m. FPA-II anchor was then driven vertically to a depth of 1.5 m and 2.5 m. The flip anchor heads were then rotated to allow sufficient earth pressure to act on them. Pull-out tests determined the maximum tensile resistance of two differently designed flip anchors at different depths. The flip anchors were then modeled using a commercially available finite element program (PLAXIS-2D) based on the data obtained from the field pull-out tests, and the ultimate tensile resistances obtained from the field were used as the applied tensile load values for the numerical analysis. As a result of the numerical analysis, both displacements and total principal stresses were obtained at the top and bottom of the soil surrounding the flip anchors. The main findings from the field tests and numerical analysis results are that the behavior of the flip anchors exhibits different behavior in each soil profile and is affected by the principal stress and displacement in the soil profile near the surface.

# ÖZET

## DÖNEL ANKRAJLARIN FİZİKSEL VE SAYISAL OLARAK ARAŞTIRILMASI

Darbeli zemin ankrajlarının çekme kapasitesinin anlaşılması, şev stabilitesinin korunması açısından çok önemlidir. Bu çalışma, üç farklı zemin tabakasına sürülen iki farklı darbeli zemin ankrajının sahada yapılan çekme testlerinden elde edilen bulguları sunmayı amaçlamaktadır. Her iki ankrajın yapımında da galvanizli çelik döküm malzeme kullanılmıştır. Büyük darbeli zemin ankrajı (FPA-I) ağırlığı 10 kg, küçük darbeli zemin ankrajı (FPA-II) ağırlığı ise yaklaşık 5 kg'dır. FPA-I, önce 1.5 metre derinlikteki killi kum kum tabakasına, ardından 2.5 metre derinlikteki siltli kum tabakasına ve son olarak 3,25 metre derinlikteki düşük plastisiteli kil tabakasına dikey olarak sürüldü. Daha sonra, FPA-II ankrajı dikey olarak 1.5 metre ve 2.5 metre derinliğine kadar sürüldü. Darbeli zemin ankrajı yeterli toprak basıncının üzerlerine etki etmesine izin verecek şekilde döndürüldü. Çekme testleri ile farklı derinliklerdeki iki farklı tasarıma sahip darbeli zemin ankrajının maksimum çekme direnci belirlendi. Darbeli zemin ankrajları daha sonra saha testlerinden elde edilen verilere dayalı olarak piyasada bulunan bir sonlu elemanlar programı (PLAXIS-2D) kullanılarak modellenmiş ve sahadan elde edilen nihai çekme dayanımları sayısal analiz için uygulanan çekme yükü değerleri olarak kullanılmıştır. Sayısal analiz sonucunda, darbeli zemin ankrajlarını çevreleyen zeminin üst ve alt kısımlarında hem yer değiştirmeler hem de toplam asal gerilmeler elde edilmiştir. Saha deneylerinden ve sayısal analiz sonuçlarından elde edilen ana bulgular, darbeli zemin ankrajlarının çekme davranışının her zemin profilinde farklı davranış sergilediği ve yüzeye yakın zemin profilindeki asal gerilme ve yer değiştirmeden etkilendiği sonucuna varılmıştır.

# TABLE OF CONTENTS

# LIST OF FIGURES

**Figure** **Page**

**Figure** **Page**

**Figure** **Page**

**Figure** **Page**

**Figure** **Page**

**Figure** **Page**

# LIST OF TABLES

**Table** **Page**

# CHAPTER 1

# INTRODUCTION

## 1.1. Research Background and Problem Statement

Today, globally, there is a significant increase in the construction of urban infrastructure (Abdi & Arjomand, 2011). However, due to the lack of available urban spaces, new developments such as buildings, bridges, tunnels, highways, and railways are increasingly being constructed near existing structures (Chan & Lam,2002). Construction can become highly problematic since these structures are sensitive to nearby soil movements (Gue & Tan, 1998). The new geotechnical engineering developments have been used to analyze and minimize the consequences of surrounding soil movement.

There are several types of soil anchors to minimize soil movements and provide stability. They are divided into active and passive earth anchors under two main headings. These are further divided based on their specific characteristics. Passive earth anchors utilize existing soil structures for stabilization without applying external forces. These systems typically employ grout or soil nails to reinforce the soil matrix, enhancing its load-bearing capacity and stability. Passive anchors find application in scenarios where minimal disturbance to the surrounding environment is desired, such as urban redevelopment projects or environmentally sensitive areas. Active earth anchors rely on external forces to stabilize soil structures, unlike passive earth anchors. This category includes mechanical anchors, ground screws, and tension soil anchors. Active anchorage mechanisms are used when robust stabilization measures are required due to significant loads or dynamic forces. Active earth anchors are widespread, with applications in various sectors. These include civil engineering projects such as retaining walls, slope stabilization, and offshore installations requiring secure foundation systems.

Flip anchors are one of the economical and safe mechanical type passive earth anchors. Flip anchors have several advantages over traditional anchors, making them suitable for various construction applications. These anchors are affordable and simple to set up, making them especially appealing for projects with financial or time limitations. In addition, flip anchors can be installed directly into the ground without jet grout during

construction. It also stabilizes embankments requiring repair and facilitates slope stabilization by fixing geogrids, geotextiles and fiber mats. This section will include a detailed description of the problem's current status and the study's aims and objectives.

The problem statement of this thesis is on the tensile resistance capacity of driven earth anchors and specifically focuses on the tensile resistance capacity of flip anchors in different soil properties. Due to their low cost and ease of installation, flip anchors are becoming a common product in construction for stabilizing slopes and supporting retaining walls and foundations. While past research has delved into the pull-out(tensile) capacity of various embedded plate anchors, the pull-out resistance mechanism of flip anchors has not been thoroughly investigated (Das, 1990; Niroumand & Kassim, 2016). There is a lack of knowledge regarding their performance under different soil layers and the factors that affect their pull-out resistance. The lack of understanding regarding the tensile behavior of flip anchors in various soil layers and the impact of overload pressure near the surface on this behavior is a significant gap in current knowledge. Consequently, field tests are required for a comprehensive understanding of the tensile resistance capacity limitations of flip anchors.

Although numerical models such as PLAXIS-2D have been used to analyze anchor performance (Abdi & Arjomand, 2011), few comprehensive field studies validate these models, especially applying flip anchors at various soil profiles. A thorough investigation into the field pull-out test of flip anchors in various soil layers is required. This will enable comparison with numerical models, enhance prediction accuracy, and streamline the design and deployment of flip anchors. Therefore, conducting further research to fully understand flip anchors' capabilities and limitations in these applications is important.

## 1.2. Aim and Scope of Thesis

This aim of this research is to contribute to the existing literature by explaining the tensile strength mechanism of flip anchors through a field study and to investigate the possible future use of flip-type anchors in construction projects. Considering previous studies in the literature, field testing of flip anchors is limited. In contrast, this study includes field pull-out testing of the new concept of flip anchors. In field tests, the tensile resistance forces obtained from different soil profiles and depths were compared with the

tensile resistance force of similar flip anchors, and an equation based on ultimate tensile resistance ($P_{ult}$) was obtained. The ultimate tensile resistance values obtained from this equation were integrated into the commercially available PLAXIS-2D program and numerical analyses were performed. In these analyses, displacements and soil principal stress changes in the soil surrounding the flip anchor about the ultimate tensile resistance of flip anchors across different soil profiles and embedment depths were examined.

## 1.3. Outline of Thesis

This thesis consists of five chapters. **The first chapter** introduces the research, including a brief description of the problem, the aims and scope of the study, and an outline of the thesis. The second chapter provides an overview of literature research on earth anchors that function based on similar principles. It also provides a comprehensive summary of the major focus of this study, which is the type of driven earth anchor known as the flip anchor. Additionally, case studies of flip anchors used in real applications are included. **The third chapter first** presents the results of field soil investigation tests. Then, the maximum tensile resistances of the flip anchor samples in different soil layers and depths were determined by the pull-out tests. Finally, the tensile resistances of FPA-I and FPA-II anchor were compared with similar flip anchors on the market. **In the fourth chapter,** the PLAXIS-2D numerical modeling was presented. The field test soil parameters were introduced to the model. Finally, the analysis results, displacements, and principal stresses in the soil resulting from applying maximum tensile forces during the loading phase were presented. **The fifth chapter** includes the conclusions and recommendations for future studies.

# CHAPTER 2

# LITERATURE SURVEY OF FLIP ANCHOR

## 2.1. Introduction

In this section, various earth anchors (grouted anchors, plate anchors, drag anchors, anchor piles and suction caissons) are explained based on literature studies. Then, the flip anchor (type of driven earth anchor) was introduced, which was designed to respond to tensile loads along the axis of the anchor rod and thus could be easily driven into the soil. Finally, the previous laboratory, numerical and field studies on these anchors are presented.

## 2.2. Earth Anchors

Earth anchors in both soil and rock have been used for centuries. These anchors are essential components of construction that provide stability to various structures such as foundations, retaining walls, and slopes by transferring external forces to deeper soil and rock layers (Yu et al., 2011). Earth anchors used in soil and rock are important for providing stability in structures such as foundations, retaining walls, and slopes. These anchors effectively distribute the load and increase structural integrity by transferring it to deeper layers of soil and rock to withstand external stresses applied to these structures. Earth anchors serve as essential components in the construction and strengthening of structures and contribute to their durability and longevity.

Buried anchors have been successful in stabilizing structures for thousands of years. The earliest uses of this technology were the stabilization of tents using piles or anchors. Until the 19th century, earth anchors were used in structures with shallow foundations. Then, the advance of extensive suspension bridge construction created the need for durable anchor systems capable of supporting significant stresses on bridge foundations, particularly in mountainous terrain. Due to these developments, specialized tensile anchor systems were introduced to resist wind loads, which often exceeded the weight of the structures themselves.

Today, earth anchors are widely used to increase tensile resistance in a variety of applications, including transmission towers, power poles and submerged pipelines. Earth anchors are generally divided into many types according to their design and usage. The types of anchors used on land are plate anchors, helical anchors, and grouted anchors. Also, anchor piles and drilled shafts are used as deep foundation options specifically designed for marine environments, such as suction caissons and tensile anchors. This classification indicates the variety of anchor techniques that have been created to meet the specific requirements of various structures and soil types. In this section, the anchors described above were described in overview form.

### 2.2.1. Grouted Earth Anchors

The fundamental principle of earth anchor technology is that steel pieces buried in the ground are then exposed to tensile forces to stabilize the slope or structure (Barley & Mothersille 2007). This phenomenon is commonly referred to as an anchor in the field of geotechnical engineering. Elton and Whitbeck (1997) define anchor operations as the process of creating a hole in rock or soil and then introducing a steel member (such as a rod or rope) together with the grouting mix. The United States Federal Highway Transportation Administration released a publication called "Ground Anchors and Anchored Systems" which served as the authoritative definition of anchors (FHWA, 1999). Strom & Ebelling (2001) offer an extra description in a technical paper produced for activities carried out by the US Army Corps of Engineers Research and Development Center. As defined in the technical paper, prestressed or injected anchors are utilized to transmit tensile stresses to the surrounding environment via structural elements embedded in rock or soil. This definition defines anchors as systems of prestressed steel elements mixed with cement to restrict and control potential deformations in structural elements like walls and slabs utilized in soil or rock.

Grouted anchors transfer compressive forces from the soil to the structural system. The anchors are inserted in drilled boreholes (Fang H.Y. 1991). Steel tendons used as the foundation material for anchors, are described by Petros P. Xanthakos (1991) as load-bearing elements that can be positioned in practically any direction under improper soil conditions. The anchor's load-carrying capability is determined by the combination of the mobilization of resistance forces in the soil and the tension in the anchor zone (Xanthakos, 1991). Various sources provide definitions of anchors, which are commonly utilized in

civil and geotechnical engineering projects as a form of ground technology. When the anchor structure is examined, it is determined that the anchor consists of 3 main parts:

- Anchor (anchor head)
- Free Length
- Root Length

The classification of anchors based on their operational principle divides them into two main types. These are active and passive anchor systems.

Active anchors function by preloading to impart forces into a structure, with the timing of this preloading tailored to the project's specific requirements. This tension process aims to achieve a predetermined load capacity that the active anchors will support throughout the service life of the structure or system they are reinforcing. These anchors primarily facilitate the transfer of tensile loads into the surrounding soil or rock. According to Cestelli-Gudi (1974) and further on by Xanthakos (1991), active anchors are installed with a predetermined tension load that remains unaffected by the following interaction between the structure and the natural soil conditions. Using an active anchor is especially beneficial for reducing and managing deformations a structure may experience when exposed to different loads. Their applications encompass several projects, such as providing support during excavation, stabilizing slopes, and mitigating the uplift forces exerted by water on structures. Active anchors are used in deep excavations to reduce any motions that may occur during the excavation operation and the installation of the anchors.

In passive anchors, which are obtained by using steel and cement-water mixture placed in the soil, prestressing is not applied. Ground nail and rock bolt applications, categorized as passive anchors, reinforce unstable slopes, carry out relatively shallow excavations compared to systems with active anchors, and prevent regional collapses in underground tunnels or subway excavations. The load-carrying capacity of passive anchors can be achieved when the earth or the structure it supports begins to move (Xanthakos 1991). The steel members forming the passive anchorage carry the tensile loads mobilized by movements in the rock mass or soil and transfer them to the system. In passive anchors, where there is no distinction between free length and root length, the steel member and the surrounding grout interact throughout the drilling process to transfer the load to the soil or rock environment.

The primary distinction between active and passive anchors is that the former are preloaded to prevent the structure from deforming excessively due to pressures arising

from excavation or other factors. Conversely, soil/anchor interaction occurs when passive anchors are loaded by the movement of the system or structure they support. Petros P. Xanthakos (1991) provided a summary of the procedures, tools, and stages of production for each of the three types of anchors, which are separated based on how they function, as Table 2.1 illustrates. This table includes the general framework lines and varies depending on the injection techniques utilized, particularly in the fabrication of anchors.

Table 2.1 Classification of anchors according to degree of tension and function (Source:Xanthakos,1991)

| Anchor type | Anchor steel type | Anchor head type | Ground Root Zone (Anchorage Zone) | Stages of Injection |
|---|---|---|---|---|
| Active | Prestressed | Prestressed steel device, apparatus | With the end zone limited | 1) Injection of the end zone (root zone)<br>2)Grouting for connection of pipes to the ground<br>3) Injection of pipes |
| Passive | Non-prestressed | Apparatus and equipment used for connection and docking | Through anchor in progress | 1) Pipes to the floor to connect injection<br>2) Pipes Injection |
| Interme diary | Semi-prestressed | Prestressed steel device, apparatus | With the end zone limited | 1) Injection of the end zone (root zone)<br>2)Grouting for connection of pipes to the grout<br>3) Protection of Steel Element (without grouting) |

The following is a summary of the advantages of retaining walls using anchor systems or retaining structures like piles, sheet piles, diaphragm walls, etc., overweight type or externally supported (steel pipes or reinforced concrete beams) excavation systems.

- Lowering the amount of material needed for excavation and doing away with the need for backfilling,

- Reducing the quantity of reinforcement and concrete utilized in the construction of the reinforced concrete components that make up the retaining wall's body
- The suitability of various soil profiles and conditions, as well as the affordability of rehabilitating or repairing an existing structure

The following is a summary of the benefits of passive anchors over active anchors (Fang H.-Y. (1991):

- Lightweight and cost-effective solution production in comparison to prestressed anchors and systems (diaphragm wall, bored pile, sheet pile, etc.)
- Quick and flexible in comparison to systems where prestressed (active) anchors are applied using shotcrete and unstressed nails
- The adaptability of tools, processes, etc. utilized in the manufacturing of shotcrete and other coating technologies, as well as passive anchor (ground nail, non-tensioned anchor),
- The benefit of the low weight and small size of the nail manufacturing machinery and equipment, particularly in locations with constrained access in the city center or narrow building sites
- Compared to prestressed (active) anchors, the number of pieces per $m^2$ is very high, and thus, the whole system is not affected after damage to the ground nails, and effective and fast measures can be taken,
- The advantages of soil-nailed systems compared to reinforced concrete retaining structures (bore piles, diaphragm walls, etc.) are that they are flexible, withstand large movements and different displacements, and have a damping structure suitable for earthquake zones.

### 2.2.2. Drag Anchors and Suction Caisson

Mooring systems can employ several types of anchors, including suction anchors, pile anchors, screw-in anchors, plate anchors, deadweight anchors, and drag embedment anchors. Drag anchors are widely utilized in marine and offshore engineering to secure floating constructions and have an essential function. The mooring mechanism enhances the ability to withstand the force created when the specifically engineered anchor is pulled

over the ocean floor (Richardson, 2008). The advantage of this technology is the utilization of natural seabed features to generate adequate holding force. This force is combined with sea currents, winds, and waves to provide stability against environmental forces such as seafloor material and the design of the anchor to optimize penetration and resistance, affecting the effectiveness of drag anchors (Richardson, 2008). Drag anchors are used primarily for the temporary mooring of ships and as part of the mooring systems of offshore platforms. They provide a reliable and reversible means of securing marine assets (Richardson,2008). Floating platforms typically utilize mooring systems comprised of steel wire chains, synthetic ropes, and steel tendons. Typically, these systems are attached to the base using tension anchors and suction caissons, as shown in Figure 2.1. To install drag anchors, position the anchor in a designated position on the seabed, and force must be applied to the chain to achieve the intended load. The tensile anchor's resistance is generated from the friction between the shank and the bearing resistance of the caterpillars.

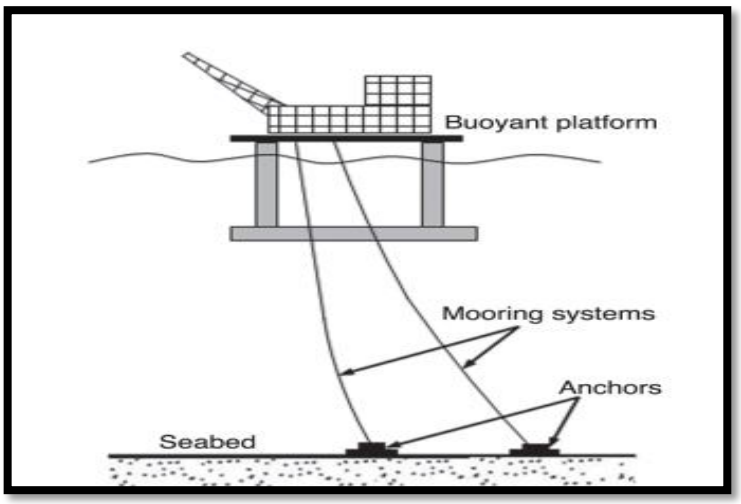


Figure 2.1 Floating platform moored to the seabed (Source: Richardson, 2008)

Drag anchors are efficient in withstanding horizontal forces but are ineffective in withstanding vertical forces and 8 m in diameter, featuring an open lower section and a sealed upper section. The length-to-diameter ratio typically ranges from 3 to 6 meters (Randolph & Gourvenec, 2011). The typical drag anchor, referred to as a fixed fluke plate anchor, consists of a substantial fluke securely affixed to a shaft. The angle formed between the shaft and the fluke of the anchor is pre-established.

The suction caisson, an essential element in marine engineering, experiences self-weight penetration during its initial installation. Then, water is extracted inside the caisson, creating a negative pressure or suction force. The pressure difference causes a downward pull, making it easier for the suction caisson to be embedded into the bottom. However, the considerable distances that anchors need to be pulled lead to higher costs for doing field surveys (Richardson, 2008). Moreover, Liu et al. (2021) proposed a unified model to analyze the comprehensive behavior of deep-water anchors and demonstrated applications in drag anchors in various soil conditions (Liu et al., 2021; Gui et al., 2021), investigating the uplift resistance capacity of the anchor. Installing suction caissons requires many trips or extra vessels due to their large dimensions, even though they may be deployed using cost-effective anchor-handling vessels. This methodical approach ensures the secure anchor of marine structures while also emphasizing the logistical challenges inherent in their installation process.

### 2.2.3. Plate Anchors

Plate anchors are crucial elements in geotechnical engineering as they provide stability and anchor for various structures in different soil conditions. These anchor systems can be manufactured from a variety of materials, each of which contributes to the overall versatility of the application. Such materials include steel sheets, precast concrete sheets, on-site concrete sheets, and wooden sheets. Steel sheets are a durable choice, often used in environments that require high strength and resistance to corrosion. Precast concrete slabs, on the other hand, allow fast installation and consistent quality due to their production under controlled factory conditions. In contrast, poured or on-site concrete slabs provide flexibility in design, as they can be poured into any shape on-site, adapting to unique project requirements. Finally, wooden planks are a renewable, cost-effective option offering unique aesthetic appeal and easy workability. Additionally, the direction of the anchor system to be applied is also important in terms of being able to withstand the required loads.

The orientation of plate anchors can vary depending on the load they must resist. Vertical placement is used to withstand horizontal tensile loads, inclined positioning is used for axial tensile loads, and horizontal orientation is used to counter vertically oriented lifting weights. Multiple studies have forecasted the maximum load-bearing capacity of both horizontal and vertical plate anchors in sandy soil. While there has been

limited research on plate anchors in the sand, especially for deeply buried ones, a wealth of information is available on the behavior of plate anchors placed in clay. The installation entails digging the ground to the necessary depth, filling it, and compressing the soil. Sheet pile walls are commonly built utilizing direct-bearing plate anchors or vertical fill, especially for constructions located along the shore. Figure 2.2 is a diagram of a sheet pile wall with vertical anchors, illustrating its cross-sectional view. The vertical anchors are connected to the sheet pile wall at a specific height (h), width (B), and a center-to-center distance (Das 2013). Horizontal anchor beams are commonly employed for building sheet pile walls with batter piles.

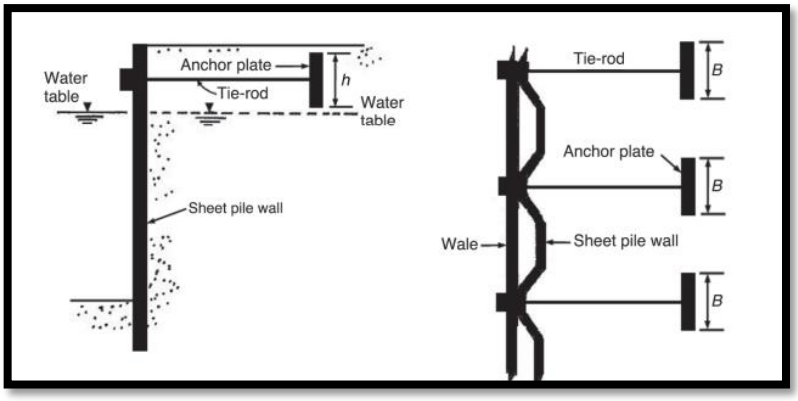


Figure 2.2 Use of vertical plate anchors in section, plan, and sheet pile wall (Source:Das,2013)

Numerous studies have examined the effectiveness of plate anchors in many soil conditions. Rowe and Davis (1982) carried out a significant investigation into the undrained behavior of anchor plates in saturated clay while also examining the positions of these plates in both vertical and horizontal orientations. This study investigated the impact of anchor positioning on performance. The work conducted by Yu et al. (2011) includes a comprehensive quantitative evaluation of the stability of plate anchors in clay soils, approached from a perspective. The research emphasized the importance of taking into account the slope of the anchor, the uneven distribution of clay, and the weight of the anchor when designing anchor systems for maximum efficiency. Bildik et al. (2013) examined the uplift behaviour of anchor plates on slopes. The study aimed to investigate the findings, with a particular emphasis on the importance of understanding the tensile resistance capacity of horizontal anchors on slopes and examining the effect on the performance of anchor plates.

In a recent study, Hu et al. (2022) presented a comprehensive, integrated model to analyze the efficiency of deep-water anchors. Through his research, they have acquired a comprehensive understanding of the factors that need to be considered while developing anchor plates, therefore providing a significant contribution to the existing knowledge in this field. This chapter described the various forms of plate anchors and their principles of working, as well as some theorems for finding the ultimate tensile resistance of the anchor.

### 2.2.3.1. Direct Embedment Anchor

Direct embedment anchors are a type of plate anchor that resembles the direct bearing plate anchors shown in Figure 2.3. They are inserted vertically by driving a rod to the required depth and can be shaped like triangles or any other type of drilling. Once the necessary depth is reached, the anchor is rotated to its final position at a 90° angle by pulling out the rod and tensioning the cable.

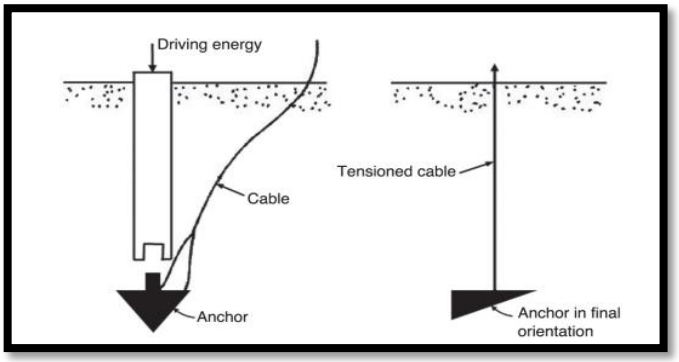


Figure 2.3 Direct embedment anchor and installation process (Source: Kulhawy ,1985, redrawn by Das,2013)

Suction-embedded plate anchors (SEPLAs) are a specific type of embedded plate anchor that offers a handy alternative for precisely positioning plate anchors at desired depths. This technique entails the insertion of a vertical plate into the foundation of a suction caisson. SEPLAs are highly compatible with cohesive clayey soils (Aubeny 2017). Barron's (2014) study emphasized the benefits of this method, including its capacity to offer accurate location and predetermined burial depth, hence mitigating any issues with preexisting seabed infrastructure.

The installation process for SEPLAs consists of several consecutive phases. First, the plate anchor is inserted vertically into the suction caisson and then gently descended till it hits the bottom. The plate anchor is released, and water is then pumped into the caisson, causing it to rise and the plate anchor to be vertically embedded into the seabed. Following the burying stage, tension is applied to the anchor chain, which is tied in the intended direction of the weight. When the chain comes into contact with the soil, the plate anchor turns or 'locks' into the desired position. It is important to note that some embedment loss may occur during this process. Figure 2.4 illustrates the installation stages of a SEPLA (Al Hakeem, 2019).

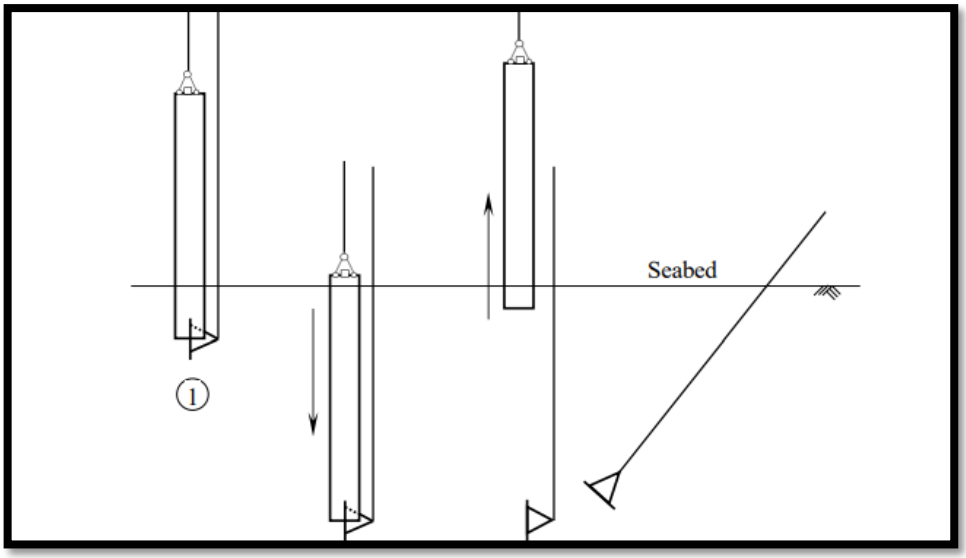


Figure 2.4 Installation procedure of SEPLA (Source: Al Hakeem, 2019)

The Dynamically Embedded Plate Anchor (DEPLA) is a notable hybrid anchor that combines dynamically installed and plate anchors' advantageous features. It is characterized by a tubular cylinder with a conical tip and four symmetric cylindrical fins. DEPLA is engineered to offer robust anchorage solutions in various marine and offshore applications (Lai, 2017). During installation, DEPLA uses a special procedure similar to the SEPLA. While the mooring line is fixed to the top of the follower, the mooring rope is attached to the padding located on the flukes. The installation stage procedures are illustrated in Figure 2.5. The flukes serve as an anchor and are essential for the keying process, which enhances stability and load-bearing capability. DEPLA is a notable breakthrough in anchor technology, providing enhanced performance and adaptability in difficult marine conditions. DEPLA utilizes dynamic installation methods and plate

anchors to effectively meet the intricate anchor needs in maritime engineering projects. This approach guarantees the dependability and longevity of the anchors, even when subjected to dynamic pressures and weather conditions.

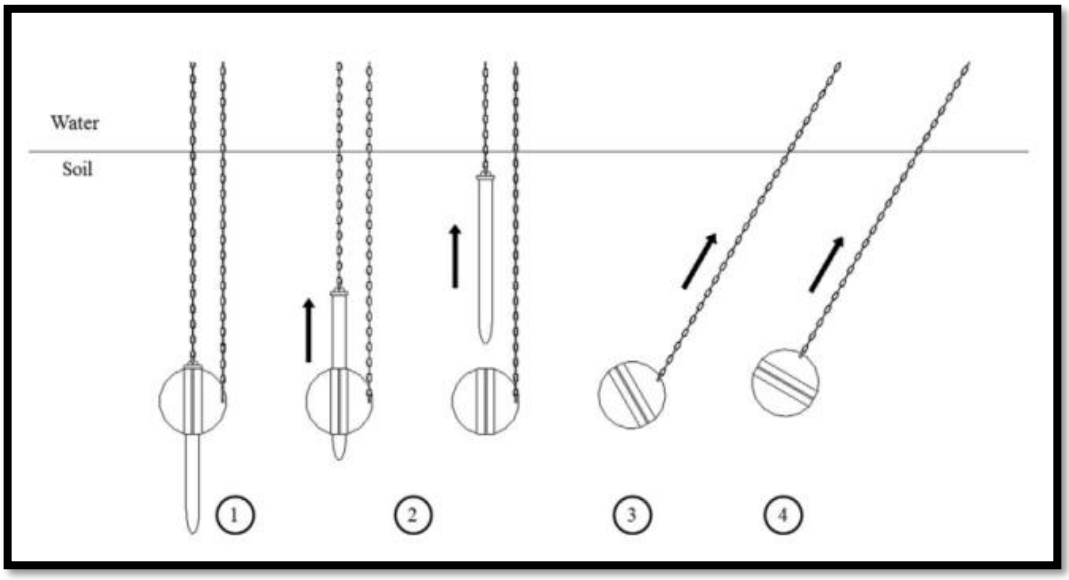


Figure 2.5 Installation procedure of DEPLA (Source: O'Loughlin et al., 2014)

Another type of embedded anchor is a helical anchor. Helical anchors have been relatively neglected despite their long-standing use in the anchor of ships and subsea pipelines. These anchors offer distinct advantages in terms of fast, simple, and cost-effective installation. They consist of one or more helical plates attached to a central shaft, as shown in Figure 2.6 (Das, 2013).

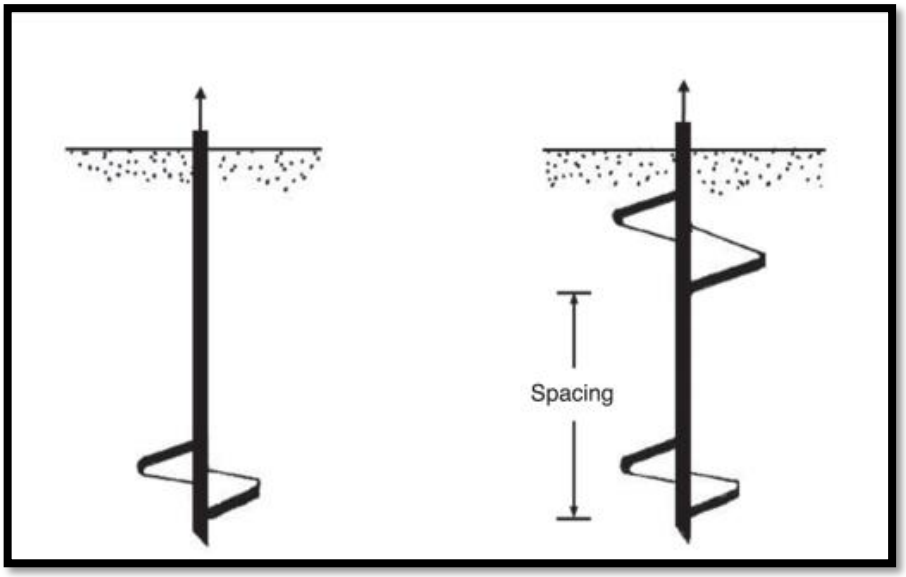


Figure 2.6 Single and multi-helical anchors (Source: Das, 2013)

Helical anchors are becoming more widely used in foundation applications, particularly in constructing electrical transmission tower foundations. Helical anchors are characterized by helical plates that are fixed to a central shaft. These anchors are installed by rotating them into the ground with drilling equipment, taking into account the specific characteristics of the soil. These anchors are designed to resist tensile forces acting on the foundation (Al Hakeem, 2019). The enhanced load-bearing capability is leaned on the interaction between the spiral plates and the earth at their interface. Helical anchors exhibit adaptability by being capable of installation in several orientations, such as vertical and inclined positions, thereby fulfilling diverse technical and design specifications (Randolph & Gourvenec, 2011).

### 2.2.3.2. Horizontal Plate Anchor

A horizontal plate anchor is a type of anchor that resists horizontal tensile loads. It is oriented parallel to the ground surface. Unlike other plate anchors, which can be placed vertically to resist different types of loads, a horizontal plate anchor is specifically designed to withstand forces acting in a horizontal direction. Horizontal plate anchors are utilized in foundation construction to withstand increasing loads. The unique orientation of the horizontal plate anchor enables it to provide adequate stability and anchorage in situations where horizontal forces must be resisted. The studies on horizontal plate anchors have provided valuable insights into their behavior and performance under

various conditions. Kumar and Rahaman (2019) investigated the pulling mechanism of horizontal and inclined plate anchors in cemented clay. Their study examined how varying burial depths and aspect ratios impact the effectiveness of horizontal plate anchors in clay soils. Roy et al. (2022) studied the pullout behavior of inclined shallow plate anchors in sand. They specifically examined how the conditions at the interface between the sand and the anchor affected the performance of horizontal plate anchors. A comprehensive understanding of the interaction between sand and the anchor contact is essential for maximizing the efficiency of horizontal plate anchors in sand conditions.

Several theories have been formulated to forecast the maximum uplift capacity of horizontal plate anchors embedded in various soil types. The pullout capability of horizontal plate anchors is commonly quantified using a break-out factor. The factor in question is influenced by the shape of the anchor, the depth at which it is embedded, the pressure exerted by the overlying soil, and the properties of the soil itself (Niroumand & Kassim, 2016).

### 2.2.3.2.1. Soil Cone and Friction Cylinder Method

The soil cone method was first proposed by Mors in 1959. This method suggests that the surface within the soil that experiences the net tensile resistance capacity ($P_{ult}$) can be approximated as a truncated cone with a distinct apex angle. The soil cone method proposed by Mors represents one of the earliest idealizations associated with the uplift capacity of shallow horizontal plate anchors in cohesionless soil. Figure 2.7 illustrates the failure surface in the soil at the ultimate load as a truncated cone with a peak angle of $\theta = 90° + \phi$ where $\theta$ denotes the apex angle, and $\phi$, the friction angle of the soil (Mors, 1959).

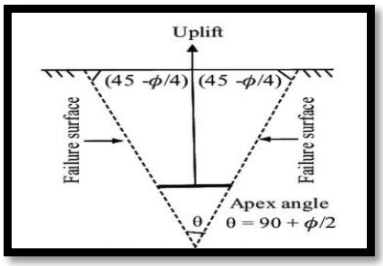


Figure 2.7 Soil Cone Method (Source:Mors,1959 cited in Kalaga,2018)

The net ultimate uplift tensile resistance of shallow circular plate anchors is estimated by assuming it is equivalent to the weight of the soil inside the failure surface (Robertson, 2009). The $P_{ult}$ was calculated as in Equation 2.1(Mors,1959). In this equation, "V" represents the volume of soil in the truncated cone, while "γ" represents the unit weight of soil.

$$Pult = V\,\gamma \tag{2.1}$$

A thorough assessment was carried out to compare the theoretical predictions of the maximum uplift capacity of individual piles, such as the soil cone approach, with empirical data gathered from scale laboratory experiments (Shanker et al., 2006). This study has verified the dependability and accuracy of the soil cone approach in determining uplift capacities.

The friction cylinder method was widely used to calculate the uplift capacity of shallow circular anchor plates. This method, frequently used to calculate the shallow circular anchor plates' uplift capability, assumes that the soil has a cylindrical failure surface. This computation assumed the soil's failure mechanism was cylindrical as illustrated in Figure 2.8.

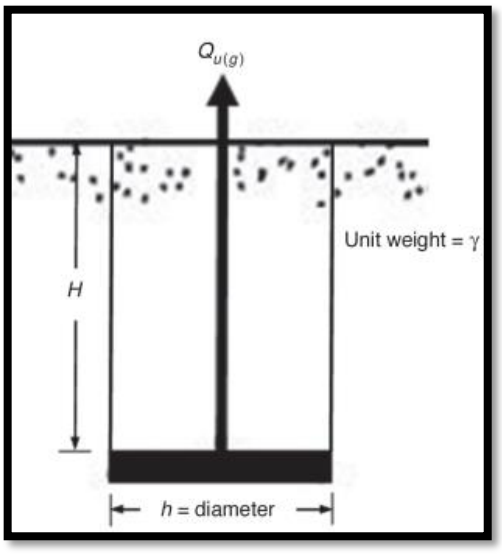


Figure 2.8 Failure mechanism of friction cylinder method (Source: Das, 2013)

The net ultimate load for cohesionless soil is determined by adding the weight of the soil inside the failure cylinder to the frictional resistance mobilized over the failure

surface. In the friction cylinder method, the net ultimate tensile resistance is defined as in Equation 2.2:

$$P_{ult} = \left(\frac{\pi h^2}{4}\right)(\mathrm{H})(\gamma) + \int_0^H (\sigma'_0 \tan\phi)\mathrm{dz} \qquad (2.2)$$

$\sigma'_0$ is effective overburden pressure measured at a specified depth (z) from the ground surface, and $\phi$ is soil friction angle. Friction cylinder method is beneficial for cohesionless soils, where the mobilized frictional resistance along the failure surface and the weight of the soil inside the failure cylinder are added to determine the net ultimate load (Gore et al., 2013). This approach contributes to the knowledge of soil-structure interaction by providing upper-bound estimates for evaluating the uplift capability of plate anchors through the implementation of multiple failure modes (Forcelini, 2023).

## 2.2.3.2.2. Balla's Theory

Balla's theory, derived from field tests conducted in dense soils, focuses on the behavior and capacity of shallow circular anchors (Balla, 1961). This theory states that the failure mechanism extends from around the anchor to the ground surface. As shown in Figure 2.9, the failure surface of this type is the arc of a circle, extends from the edge of the plate, and intersects the free surface at an angle of approximately 45º - $\phi$/2.

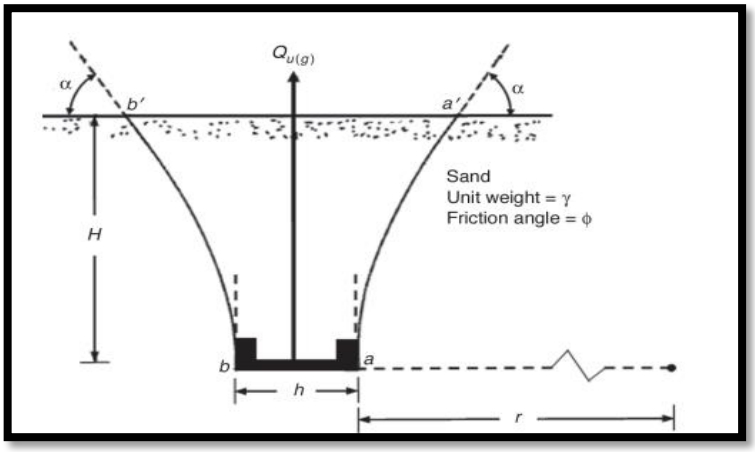


Figure 2.9 Failure mechanism of friction cylinder method (Source: Das, 2013)

The net uplift capacity, the shearing resistance created along the failure surface, and the weight of the mobilized soil within the failure zone add up to the $Q_{u(g)}$ of an anchor embedded at shallow depth, which may be expressed as follows in Equation 2.3:

$$Q_{u(g)} = H^3 \lambda (F_1\left(\phi, \frac{H}{h}\right) + F_3\left(\phi, \frac{H}{h}\right)) \quad (2.3)$$

The sums of the functions $F_1$ (ϕ, H/h) and $F_3$ (ϕ, H/h) stated in Equation 2.1 depend on the values of friction angle (ϕ) and embedment ratio (H/h) as seen in Figure 2.10.

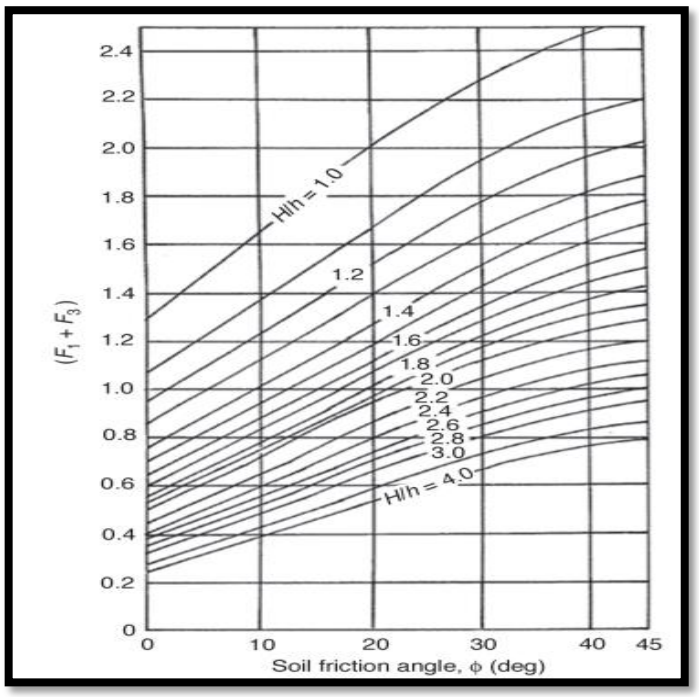


Figure 2.10 Variation of F1+F3 with friction angle according to Balla's theory(1961)

Balla's method represents notable progress in estimating uplift capability for shallow circular anchors in dense sand. Further studies have expanded upon this initial groundwork to investigate diverse parameters that affect anchor behavior and the reasons for failure in different soil types. Wang et al., (2013) aimed to analyze the uplift behavior of helical anchors in clay. The researchers used numerical studies to understand the failure mechanisms of multi-plate anchors and evaluate the suitability of existing semi-theoretical approaches. Their work contributes to the broader understanding of anchor behavior in different soil conditions.

## 2.2.3.2.3. Meyerhof and Adams Theory

In 1968, Meyerhof and Adams proposed an approximation universal theory regarding the soil's resistance to tensile resistance. Their influential study was based on empirical observations and test data from a complete series of model uplift tests conducted under different soil conditions, such as loose and compacted sand and clay. The tests were performed on strip and rectangular anchors (Meyerhof and Adams, 1968). The ultimate tensile resistance ($P_{ult}$) is determined by the combined effect of the landslide resistance activated by a specific failure surface caused by the weight of the soil on the foundation. The configuration and size of the failure surface differ based on the ratio of burial depth to width and the soil's hardness or relative density. The theory was designed for a strip and then modified to accommodate circular and rectangular foundations. It also incorporated considerations for group behaviors (Das, 2013). The general expression incorporates theoretical form factors to accommodate the three-dimensional impact of square or circular foundations. To simplify the theory, analyze the forces exerted on a cylindrical surface above the plate anchor. Furthermore, the intricate nature of these surfaces results in simplified damaged areas. Figure 2.11 illustrates two distinct failure modes, shallow and great depth, determined by the depth at which the object is buried (Al Hakeem, 2019).

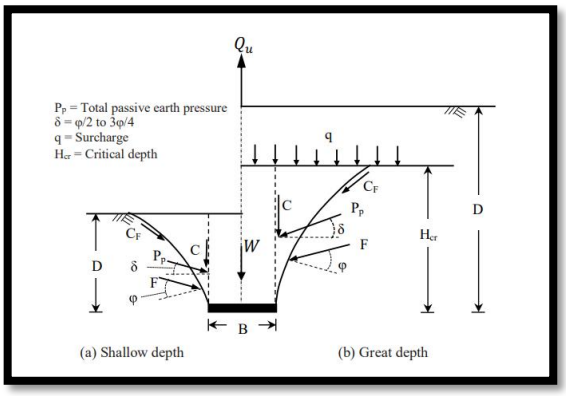


Figure 2.11 According to Meyerhof and Adams, soil failure above a strip plate anchor under ultimate tensile resistance (Source: Al Hakeem, 2019)

According to Meyerhof and Adams (1968), rectangular anchor plates' maximum pullout capacity as Equation 2.4:

$$Pu = W + \gamma H^2(2S_f \text{L} + \text{B-L})K_u.\tan\phi$$
$$S_f = 1 + m\frac{L}{D}$$
$$N_q = 1 + \frac{L}{D}K_u tan\phi \quad (2.4)$$

In Equation 2.4, $K_u$ represents the nominal uplift coefficient according to Figure 2.12. $S_f$ is the shape factor, W is the weight of the anchor plate, m represents the coefficient that is a function of the soil friction angle, and the relationship is shown in the graph in Figure 2.13.

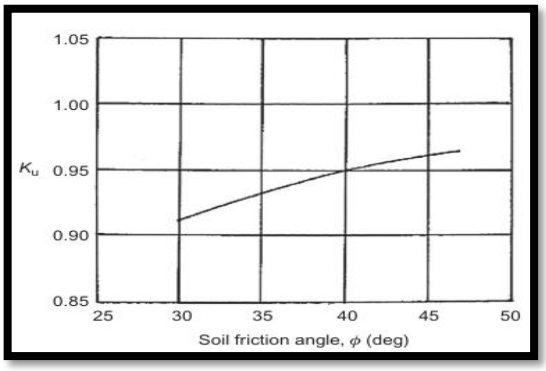


Figure 2.12 Variation of Ku based on soil friction angle(ϕ) (Source: Mayerhofs & Adam,1968)

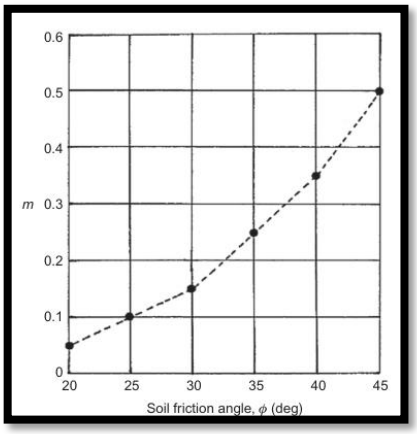


Figure 2.13 Variation of m based on soil friction angle(ϕ) (Source: Mayerhofs & Adams,1968)

The study of tensile resistance capacity ($P_u$) in foundation engineering presents a unique set of challenges, differing significantly from the conventional bearing capacity

theory. This uniqueness stems from the distinct stress distribution pattern above the footing, influenced by the surface boundary (Meyerhof,1973). Numerous studies have contributed to this field. For instance, the work on the stability of plate anchors in undrained clay using numerical techniques has provided vital insights into the factors that impact uplift resistance (Meyerhof, 1973). Research on the uplift behaviour of pipelines in clayey seabed's has enhanced our understanding of uplift capacity mechanisms in spatially varying soils (Radhakrishna & Adams, 1973).

### 2.2.3.2.4. Meyerhof and Adams Theory

In 1971, Vesic developed a mathematical equation to calculate vertical resistance against uplift for strips and circular plate anchors. This was accomplished by considering the expansion of cylindrical and spherical cavities in a semi-infinite, uniform, and isotropic half-space as shown in Figure 2.14. The concept has significantly contributed to understanding shallow circular anchors' uplift potential. Vesic's (1971) research thoroughly examined the ability of horizontal circular plate anchors to resist being pulled out in various types of clay formations.

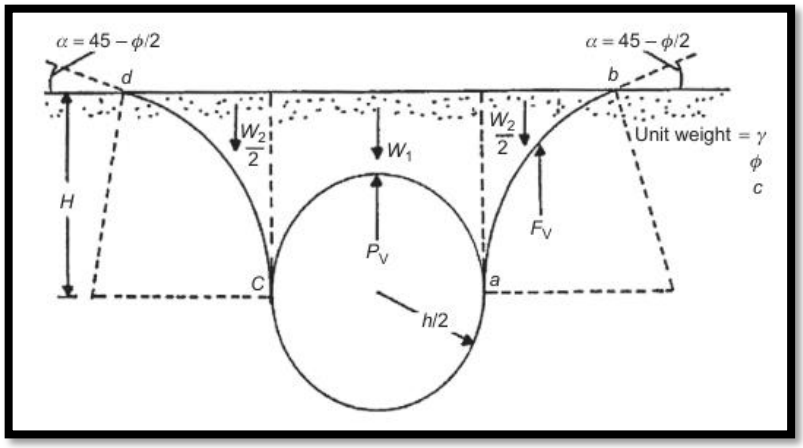


Figure 2.14 Schematic test representation (Source: Vesic,1971)

The vertical component of the force inside the cavity (Pv), the effective self-weight of the soil (W = W1+W2) and the vertical component of the resultant of the internal force (Fv) are assumed. Equation 2.5 shows the pull-out capacity in sand according to the Vesic method.

$$P_u = \gamma \, H \, N_q$$
$$N_q = [1 + A_1(\frac{H}{h1/2}) + A_1(\frac{H}{h1/2})^2 \quad (2.5)$$

In Equation 2.5, the embedment depth H is interpreted as half of the depth of the soil subsidence wedge $h_1/2$, $A_1$ and $A_2$ represent the areas of the soil subsidence wedges. Vesic's (1971) study was built upon prior research performed by Ali (1968) and Bhatnagar (1969), which focused on the analysis of bentonite clay and silty clay, respectively. Vesic's research investigated several key parameters, including soil remoulding, load characteristics, adhesion, suction force, ocean bottom slope, load inclination, and soil fluidity. The characteristics mentioned significantly impact the anchors' pullout resistance, emphasizing the complex relationship between soil and structure in clay environments (Vesic, 1971). However, there was a significant difference between theoretical predictions and actual laboratory results. This showed that further development of theoretical models for anchor capacity prediction is necessary.

## 2.2.3.2.5. Other Methods

The investigation of the ultimate tensile resistance ($P_{ult}$)of horizontal plate anchors in the sand has been a subject of fascination for various researchers, resulting in a multitude of analytical and numerical examinations. Rowe and Davis (1982), Smith (1988, 2012), Merifield and Sloan (2006), Kumar and Kouzer (2008b), and White et al., (2008) have made noteworthy contributions to the literature regarding this topic.

Rowe and Davis (1982) focused their research on the maximum tensile load of horizontal plate anchors and laid the groundwork for future studies. Following this, Tagaya et al. (1983, 1988) and Smith (1988, 2012) have expanded the existing knowledge base by delving more deeply into analytical and numerical predictions of ultimate tensile load in sand. These investigations have enhanced comprehension of the variables that influence the tensile load of horizontal plate anchors. Kumar (2001) examined the theoretical effects of horizontal earthquake acceleration on the vertical uplift capability of shallow strip anchors implanted in cohesionless material. This research employed the upper bound theorem of boundary analysis and assumed planar fracture surfaces. Kumar observed that applying static horizontal seismic stresses led to a steady decrease in the ability of shallow anchors to resist uplift. The decrease was shown to be more pronounced

as the earthquake acceleration coefficient magnitudes increased, the soil friction angle (ϕ) decreased, and the embedment ratio (H/h) increased. For strip anchors, Das and Seeley (1975) formulated the ultimate tensile resistance capacity in Equation 2.6.

$$P_{ult} = F_q \gamma \, AH \tag{2.6}$$

Where,

A = area of the anchor

H= embedment depth of the anchor

$Fq = W + K_u \gamma H^2 \tan\phi$

$K_u$ =nominal tensile coefficient (relevant to soil friction angle)

By substituting the value of W = γBH, Equation 2.6 has been modified to Equation 2.7.

$$P_{ult} = [1 + K_u(\frac{H}{B}) \tan\phi]\gamma \, AH \tag{2.7}$$

As can be seen in Equation 2.7, "H" represents the embedment depth of the anchor, while "B" represents the width of the strip anchor. "H/B" represents the embedment ratio of the anchor. As the embedment ratio increases, the ultimate tensile resistance increases in capacity. In addition to these studies, Merifield and Sloan (2006) observed the behavior of plate anchors in the sand in more detail. The research added important information to the literature on how these anchors perform in sandy environments. Similarly, Kumar and Kouzer (2008b) reported horizontal plate anchors. Also, White et al. (2008) observed the subject by investigating the tensile load capacities. Their study on the ultimate tensile load of horizontal plate anchors have further advanced the development of the field by increasing our understanding of this complex issue.

Circular anchors buried in saturated clay were the subject of several laboratory model test results compiled by Das (1980), with the undrained cohesion cu varied from 5.18 kN/m$^2$ to roughly 172.5 kN/m$^2$. The crucial embedment ratios and average plots of Fc (breakout factor) versus H/h (embedment ratio) from these experiments are displayed in Figure 2.15. information about curves a, b, c, d, and e in Figure 2.15.

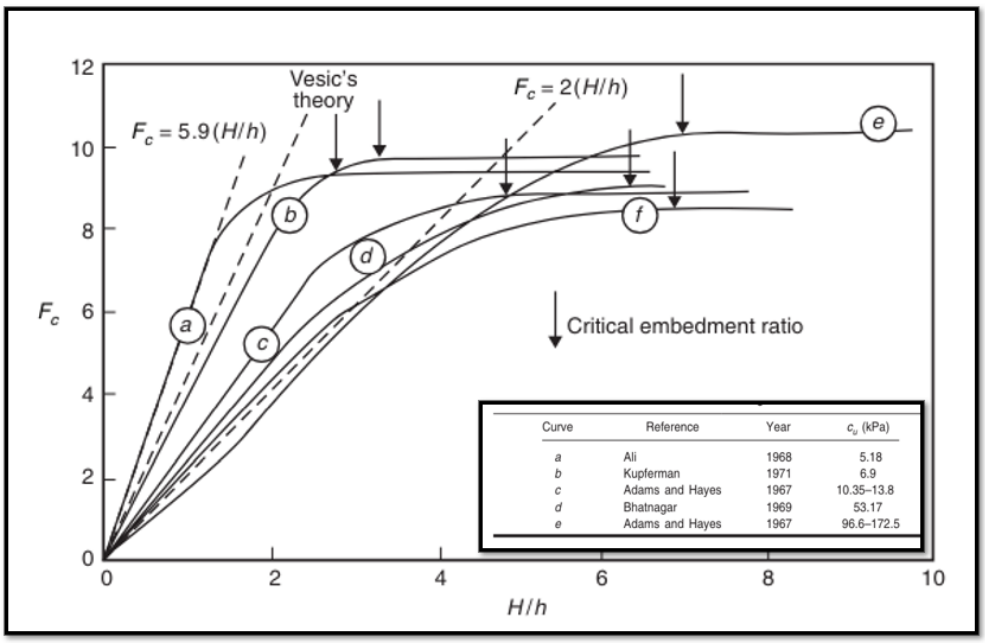


Figure 2.15 Breakout factor variation with H/h for different experimental findings (Source: Das,1980)

Figure 2.15 is valid for shallow anchors and the pull-out capacity is like Equation 2.8 for soft soils (Das, 1980).

$$P_u = BL\left[7.56 + 1.44\left(\frac{H}{h}\right)\right]C_u + \gamma\,\mathrm{H} \tag{2.8}$$

Where

B= width of the anchor

L = length of the anchor

H/h = embedment ratio of the anchor

$C_u$ = undrained shear strength parameters of the soil

Saeedy (1987) proposed an ultimate holding capacity hypothesis for circular plate anchors implanted in sand, wherein the failure surface trace was considered an arc of a logarithmic spiral, as illustrated in Figure 2.16. This situation states that the failure surface of shallow anchors reaches the earth. On the other hand, the failure surface reaches Hcr above the anchor plate for deep anchors ($H > H_{cr}$). Saeedy (1987) postulated the net ultimate uplift capacity for different values of φ and the embedment (H/h) ratio in a non-dimensional form ($Q_u = \gamma H h^2$).

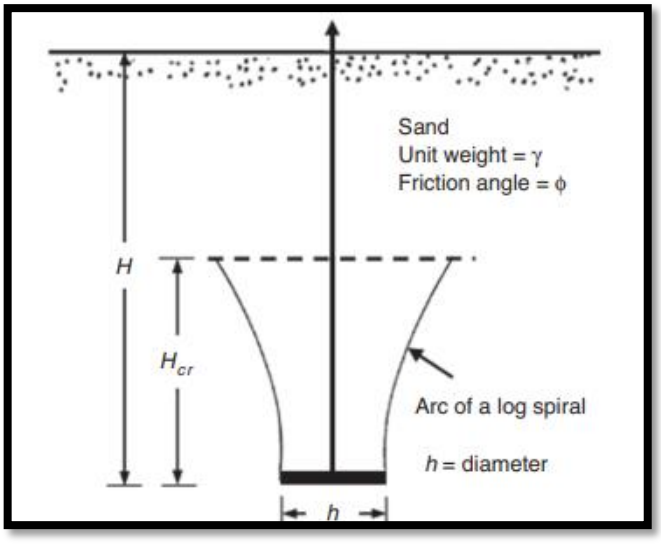


Figure 2.16 Saeedy's (1987) circular plate anchor theory(Source: Saeedy,1987)

They plot the fracture factor Fq = Qu /γAH (where A is the area of the anchor plate) against the soil friction angle ϕ, as shown in Figure 2.17. Saeedy (1987) states that the soil above the anchor gradually compresses during the pulling of the anchor, increasing the shear strength of the soil and therefore the net ultimate uplift capacity.

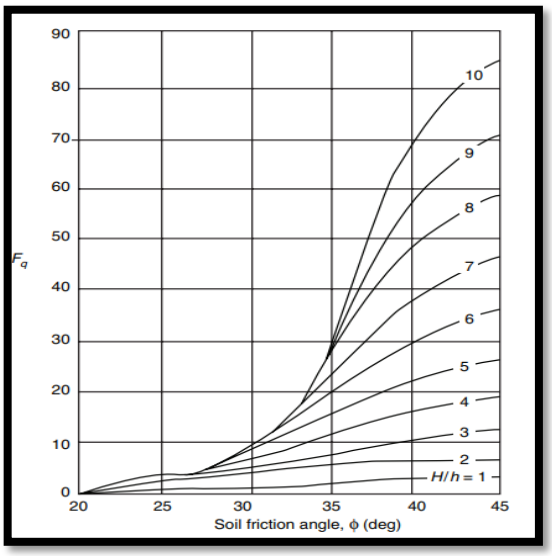


Figure 2.17 Plot Fq and soil friction angle based on Saeedy Theory (Source: Saeedy,1987)

Therefore, an empirical compression factor in the form as in Equation 2.9 was proposed.

$$\mu = 1.044D_r + 0.44 \quad (2.9)$$

Where

μ= compaction factor

$D_r$ = relative density of compaction

Equation 2.10 can be used to express the actual net ultimate capacity as a result.

$$Q_{u(actual)} = \mu\, F_q\, \gamma\, A\, H \quad (2.10)$$

Deshmukh et al. (2011) conducted a comprehensive theoretical examination of the net uplift capability of horizontal strip anchors in soils with no cohesive properties. At the limit equilibrium, the failure surface starting from the anchor edge forms an angle with the horizontal ranging from (90 - ϕ/3) to (90 - 2ϕ/3) and its average value is (90-ϕ/2) taken. The vertical soil reaction at the failure surface was applied by using the Kotter equation.Their analysis showcased a successful substitution of the Kotter equation and was verified for embedment ratios (H/h) below eight.

In a study by Liu et al. (2012), Digital Image Correlation (DIC) was employed to examine the deformation of the soil surrounding circular plate anchors utilized in dry sand uplift. The laboratory employs the experimental arrangement shown in Figure 2.18.

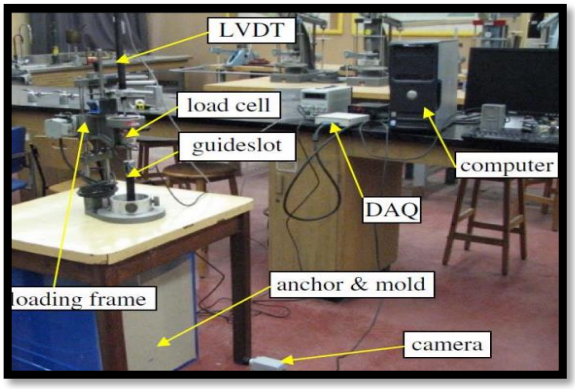


Figure 2.18 Experimental setup (Source: Liu et al.,2012)

The study found that soil compressibility in loose sand was the primary factor affecting anchor behavior for deeper buried anchors, resulting in the absence of a

significant failure surface. However, in the case of dense sand, the failure surface turned into a hybrid shape consisting of a curved cone and a truncated cone. The curved cone originates from the edges of the anchor, so it extends above the anchor plate in loose sand and tight sand to a depth of approximately three times the diameter of the anchor, as shown in Figure 2.19. In both soil density conditions, it has been observed that the width of the fracture surfaces increases in parallel with the depth of the anchor.

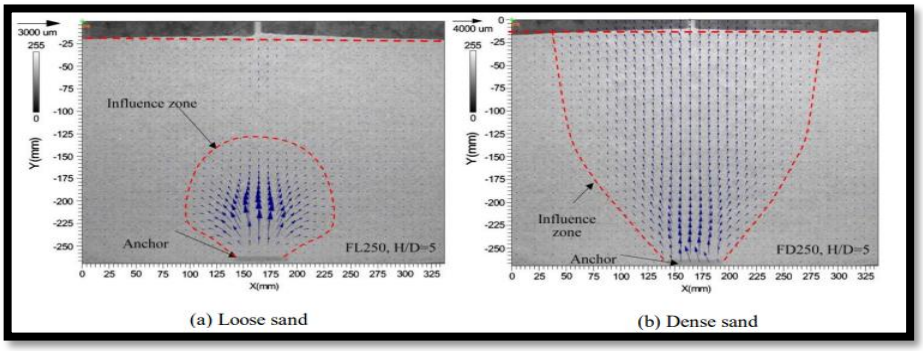


Figure 2.19 According to Liu et al. (2012), the failure surface form for H/B = 5 for (a)loose sand and (b) dense sand (Source: Al Hakeem, 2019)

More exacting numerical and analytical investigations have been done recently to estimate the maximum tensile load of horizontal plate anchors buried in clay. Rowe and Davis (1982) found that, in many cases, substantial displacement of the anchor occurs before ultimate collapse based on finite element simulations of the undrained behavior of horizontal anchor plates in water-saturated, homogeneous, isotropic clay. Their work was done on weightless soil using an elastoplastic finite-element analysis to find out the anchor's tensile capacity factor.

Several studies by researchers have delved into horizontal plate anchors in clay soil. The research by Merifield et al. (2001) undertook an analysis of plate anchor stability in undrained clay using numerical upper and lower bound methods. The study examined the impact of factors such as embedment depth, roughness coefficient, overburden pressure, and plate anchor material qualities on the pullout bearing capacity of the anchors. Tagaya and Smith (1988) conducted numerical analyses to investigate the stability of plate anchors in clay. Smith (2012) researched the stability of plate anchors in clay and made substantial contributions to the knowledge of the maximum tensile load of horizontal plate anchors embedded in clay. Smith (2012) conducted numerical research to analyze the stability of plate anchors in clay, which advanced the understanding of the

behavior of plate anchors in clay soil. The study revealed the key elements influencing the stability and maximum load capacity of horizontal plate anchors in clay. They also examined the design and performance of these anchors in geotechnical applications.

### 2.2.3.3. Vertical Plate Anchor

Vertical anchor plates are essential elements in geotechnical constructions. They offer resistance against horizontal forces in buildings like retaining walls, sea barriers, and sheet pile walls. Accurately predicting these anchor plates' maximum capacities and displacement behavior is crucial for guaranteeing these structures' structural integrity and stability (Niroumand & Kassim, 2016). Structural components known as vertical anchor plates are frequently utilized to resist tensile pressures applied to structures like sheet pile retaining walls. These structures can be either concrete anchor walls or vertical sheet piles, and their capacity to support weight is due to the passive resistance of the soil. Anchor refers to several methods of securing anything to a wall, such as slabs, a series of separate anchor plates, or a continuous system. Several factors, such as soil type, density, depth of insertion, anchor shape, and vertical surcharge pressure, influence the extraction of anchor plates. Many researchers have studied the behavior of anchors with different diameters that are anchors' behavior with different diameters embedded in different soils at various depths (El Sawwaf & Nazir, 2006).

The performance of vertical anchor plates, which are constructed using tie rods and plates, is affected by the dynamics of lateral earth pressure. This phenomenon has been explained by Rankine and Coulomb's theories (Rowe, 1952). In practical application, a vertical anchor plate comprises key geometric parameters, including height (h), width (D), and embedment depth (H), as illustrated in Figure 2.20. These dimensions are critical in determining the anchor plate's load-bearing capacity and response to lateral earth pressures. Understanding the relationship between these geometric attributes and the mechanical behavior of the anchor plate is essential for effective design and performance evaluation in geotechnical projects.

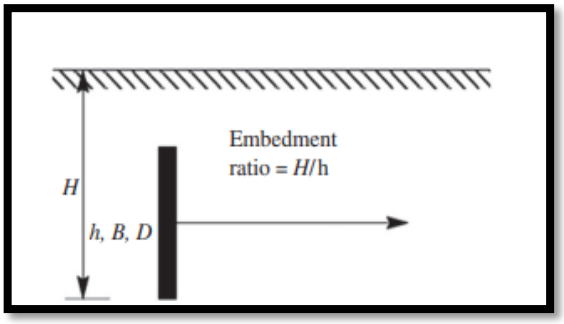


Figure 2.20 Vertical anchor and geometric parameters (Source: Niroumand & Kassim, 2016)

The literature emphasizes the importance of accurately predicting vertical anchor plates' ultimate capacities and displacement characteristics under lateral loading conditions. This necessitates a comprehensive analysis incorporating soil properties, anchor plate geometry, and loading conditions. Geotechnical engineers can optimize the design and installation of vertical anchor plates to meet the needs of each project and keep the structure stable over time by combining the theories of Rankine and Coulomb with real-world data and advanced numerical modelling methods.

Vertical anchor plates are classified based on their depth in the soil profile, distinguishing between shallow and deep anchor plates. Shallow anchor plates distribute their failure surface to the ground surface, while deep anchor plates primarily apply shear force within and around the vertical anchor plate. The distinction depends on the embedment ratio (H/h), where a low ratio suggests a shallow anchor plate with its failure surface reaching the ground surface. In contrast, a high embedment ratio signifies a deep anchor plate. The key factor in designing vertical anchor plates is ensuring that the passive force is exerted in front of the plate.

The precise placement of the vertical plate anchor is essential for efficiently stabilizing it against lateral loads. Regardless of differences in embedment ratio or depth classification, both shallow and deep anchor plates have the same property so the ultimate force capacity ($Q_u$) is equal to the net ultimate force capacity ($Qn_u$). The categorization of vertical anchor plates into shallow and deep groups enables the customized design and use of anchor systems to meet individual project needs and soil conditions.

In summary, the performance of vertical plate anchors depends on variables such as embedment depth and the properties of the soil. When analyzing the insertion of vertical anchor plates, it has been noted that the maximum tensile load can significantly impact the failure mechanism displayed by the soil (Murray & Geddes, 1987). When the

embedment ratio is relatively low, a passive failure surface develops in the soil that intersects the soil surface when the ultimate tensile load is reached. Conversely, at a higher embedment ratio, local shear failure within the soil becomes dominant at the ultimate load.

### 2.2.4. Flip Anchors (Type of Driven Earth Anchor)

In geotechnical engineering, ensuring slope stability is of paramount importance for the longevity and safety of infrastructure projects, particularly in the transport sector. Plate anchors are a common method for stabilizing slopes. Although they are effective in terms of the bearing capacity of the soil to ensure stability, plate anchors cannot be used to reinforce existing slopes due to the pre-installation requirements. However, they remain viable in scenarios where advanced installation is possible and the ground can withstand applied loads.

Flip-type anchors are specifically intended for applications with moderate loads in different soil conditions. These anchors employ a toppling plate mechanism that depends on the inherent strength of the earth to withstand tensile loads adequately. They possess versatility and can be utilized in a diverse array of applications. These anchors are used in various structures, including retaining walls, slope stabilization, pier foundations, gabion support, temporary applications, underwater applications, and erosion control.

Flip anchors predominantly employ premium materials, such as galvanized steel casting or aluminium alloys, for their construction. These materials possess outstanding strength-to-weight ratios and corrosion resistance, rendering them highly suitable for enduring outdoor applications. The high strength-to-weight ratio in flip anchors provides efficient load transfer to the surrounding soil or rock, which is essential for maintaining structural stability under various loading conditions. Minimising soil disturbance during installation is another critical advantage, as excessive disturbance can compromise soil integrity and reduce bearing capacity. Anchors with a high strength-to-weight ratio can provide significant resistance with minimal material volume, which is particularly advantageous in difficult ground conditions where larger anchors may not be practical. Precision casting or machining ensures dimensional accuracy and structural integrity, ensuring reliable performance in demanding conditions. Additionally, flip anchors are

compatible with steel rods or wire ropes of various diameters, typically ranging from 10 to 50 mm, providing flexibility in design and installation.

### 2.2.4.1. Installation of Flip Anchor

The installation process of this type of anchor consists of three stages. Installing flip anchors involves a systematic sequence of operations aimed at driving the flip anchor head to the designed depth, connecting a drive steel rod, and subsequently load locking to achieve the desired tensile strength. Initially, the flip anchor head is driven into the soil using a jackhammer or excavator, penetrating to the predetermined depth dictated by engineering specifications. This initial stage of installation is critical, as it establishes the foundation for subsequent load-bearing capacity and stability. Upon reaching the designed depth, the installation process progresses to the second stage, wherein a connected drive steel rod is utilized. This drive steel rod is pivotal in the load-locking mechanism, facilitating the anchor's securement at the desired depth. The drive steel rod is meticulously inserted into the anchor head assembly, ensuring a robust connection capable of withstanding applied loads and environmental stresses.

During the last stage of installation, load-locked occurs. This is a crucial procedure where the anchor head rotates and opens when a tensile force is applied. The application of a tensile load to the anchor induces rotation in the anchor head, thereby initiating the opening of the load-locked mechanism. This action flip anchor is firmly fixed to the adjacent soil, thereby establishing a stable hold. This action helps to provide tensile strength to the anchor. Figure 2.21 illustrates the installation procedure for this particular type of anchor.

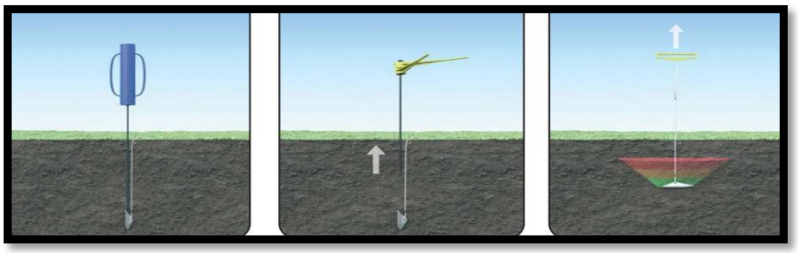

Figure 2.21 Installation of flip anchor system (Source: Platipus Civil Engineering &Construction Brochure, 2022)

The installation of a flip anchor begins by applying a load to induce rotation, allowing the anchor to transition into its load-locked position. This phase is critical as it involves both load application and extension. At the same time, the anchor advances further into the subsurface strata. This stage highlights the significance of achieving sufficient rotational movement to ensure the anchor properly engages with the surrounding soil mass, establishing the foundation for subsequent load-bearing capacity. During the anchor installation process, a frustum of soil is generated directly in front of the anchor, which creates a zone of soil disturbance. This signifies the initiation of soil displacement and mobilization, reflecting the anchor's interaction with the subsurface strata. The load transition observed during this phase reflects the evolving dynamics of soil-structure interaction, with the anchor system gradually assuming a more stable configuration.

The installation of the flip anchor is completed when it has reached its ultimate load capacity. At this point, as shown in Figure 2.22, in the initial phase (load-lock), the anchor is rotated into its load-locked position by applying a load. During the working load phase, the anchor system produces a frustum of soil close to the anchor. Typically, at this point load normally increases with minimum extension. The final stage is where the anchor reaches its ultimate load. As the bearing capacity of the soil is reached, the rate of load increase starts to slow down. This indicates that the soil has reached its bearing capacity limit, which is the equilibrium between the applied loads and the soil resistance. However, exceeding the mechanical shear strength of the soil may result in a reduction in the residual load due to the anchor shearing of the soil. An extensive evaluation of soil properties and shear strength parameters is required to ensure the integrity and performance of the anchor system.

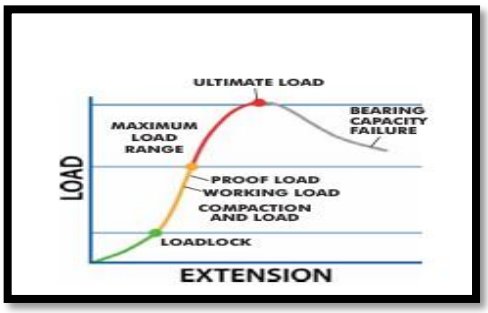


Figure 2.22 Bearing capacity of flip anchor system (Source: Platipus Civil Engineering &Construction Brochure, 2022)

In summary, the placement of anchors is complex and multi-stage and is governed by the soil-structure interaction. Each stage of this process is crucial in the performance and efficacy of the flip anchor system. A comprehensive understanding of these stages is imperative to optimize anchor performance, ensure structural stability, and mitigate geotechnical risks in engineering applications. Through careful analysis of the behavior of the soil and the anchor system at each stage of installation, engineers can refine design parameters, improve operational efficiency, and reduce potential hazards associated with soil-structure interaction. Furthermore, a comprehensive understanding of anchor installation procedures enables engineers to make informed decisions about anchor selection, placement, and performance evaluation, thereby promoting sustainable and resilient infrastructure development.

### 2.2.4.2. Models Similar to Flip Anchors and Related Studies

Flip-type anchors are available in a variety of models and sizes, including the duckbill anchors shown in Figure 2.23. Other flip-type anchor models generally resemble the "Manta Ray" shape as shown in Figure 2.24.


Figure 2.23 Example of Duckbill Flip Anchor (Source: MacLean Civil, 2022)

Flip-type anchors are driven into the ground, eliminating the necessity for pre-drilled openings and minimizing soil disturbance, in contrast to conventional methods that necessitate auguring or torquing. This system is powered by the same hydraulic source as the jackhammer and comprises a base plate, hydraulic ram, jaws, and an adapter setting bar. These anchor system's lightweight, portable design enables secure operation from ground level and effortless transportation. The driving operation is executed

efficiently by coupling sections of drive steel as required. This method is excellent for supporting poles, towers, and antennas in utility and telecom projects, as it offers a robust and environmentally friendly anchoring solution.

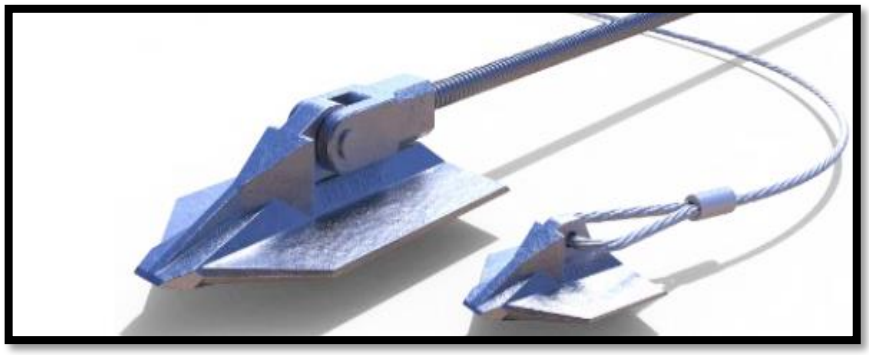

Figure 2.24 Example of flip-type anchor (Source: Anchor Rope and Rigging Pty Ltd., 2019)

A duckbill anchor typically comprises a driving steel rod or shaft with a helical or screw-like blade at one end and a flared anchor, known as a "duckbill," at the other. The helical blade enables the anchor to revolve into the earth, ensuring a tight grip, while the duckbill anchor expands during installation to resist upward or lateral stresses. These anchors are frequently employed when conventional anchor techniques are feasible or expensive, such as in concrete foundations or driven piles. The advantages of these systems are their easy installation, minimum impact on the environment, and ability to adapt to different soil conditions.

The efficiency of these anchors is contingent upon the soil's specific attributes. Clay and silt, which are cohesive soils, generally have greater shear strength and cohesion, making them more movement-resistant. Moreover, these anchors can efficiently sustain cohesive soils by offering lateral reinforcement and countering uplift forces. The effectiveness of duckbill anchors in granular soils, such as sand and gravel, can be affected by factors, including the distribution of grain sizes and the soil density. An accurate evaluation of soil parameters is essential for establishing the appropriateness of duckbill anchors in particular soil types.

The installation depth significantly influences the performance of duckbill anchors. Inadequate anchor depth in shallow installations might decrease pullout resistance and stability. Conversely, excessively deep installations may encounter challenges related to installation equipment and costs. Optimal anchor depth should be

determined based on site-specific conditions, including soil properties, anticipated loads, and desired performance criteria. Geotechnical analysis and field testing are essential for determining the appropriate installation depth for duckbill anchors. A few case studies showcase the effectiveness of duckbill flip anchor in different types and depths of soil. One such study was conducted by Asfaw et al. (2023), as shown in Figure 2.25.

Figure 2.25 Example of Duckbill flip Anchor (Source: Asfaw et al., 2023)

Their study was conducted on the field installation and performance evaluation of Percussion Driven Earth Anchors (PDEA) for slope stabilization in difficult soil conditions. Aswaf et al. (2023) investigated the methodology for driving PDEA anchors into the slope using a mini excavator with a drive rod and hammer attachment. Their study evaluates the maximum tensile strength of anchors when installed in soil predominantly sandy lean clay. The research employs a combination of field testing and empirical estimation methods to enhance our understanding of anchor behavior in real-world conditions.

The findings of their study informed optimized slope stabilization strategies and helped to support structural resilience. The methodology is a comprehensive approach to field testing and empirical estimation of anchor performance. Three anchors were strategically installed into the proposed bank slope, penetrating an average depth of 3 m. The slope layout, with an average gradient ranging from 2:1 to 2,5:1, offered a suitable surface for anchoring. The field testing began by applying an upward tensile load to the placed anchors using a hydraulic jack. Simultaneously, the load cell, linear variable

differential transformer (LVDT), and strain gauge equipment enabled the measurement of tensile load, displacement, and stresses, respectively.

Analyzing the relationship between applied loads and displacement, they methodically constructed and examined curves to understand the behavior of anchors under tension. Afterward, a practical estimating technique was used to forecast the tensile capability of the anchors, utilizing undrained shear strengths acquired from laboratory experiments or in situ Texas cone penetration (TCP) data. During the field-testing phase, insights were gained into the behavior of duckbill anchors in sandy, poorly clay soil. Data collection and analysis have comprehensively described anchor performance under different load conditions. Critical parameters for evaluating anchor response to applied loads were obtained through tensile load, displacement, and strain measurements. Investigated were basic anchor properties, including tensile load versus displacement curves, yield strength, and ultimate tensile capacity. The field-testing phase established the foundation for comprehending anchor-soil interaction dynamics and informing subsequent empirical prediction studies through observation and analysis. The ultimate tensile capacity of duckbill anchors was estimated using an empirical method based on undrained shear strengths obtained from laboratory testing or in situ TCP data. The research on field tests and empirical prediction of the ultimate tensile capacity of duckbill anchors in sandy weak clay soil has observed slope stabilization applications. The empirical estimation method, which has been validated by comparison with field-derived capacities, is a reliable approach for predicting anchor performance and guiding engineering decisions in slope stabilization projects.

Yoshida et al. (2021) meticulously investigated the dynamics of flip-type ground anchors through field pull-out tests in different substrates, especially clay and sand layers. This scientific study aimed to elucidate the operational properties of these anchors under varying land conditions, thus assessing their effectiveness in ground stabilization and pullout resistance capabilities. The centerpiece of this research was the strategic placement of 26 flip-type anchors into the terrestrial matrix at predetermined positions, as in Figure 2.26, using an impact drive apparatus, followed by their use of a hydraulic jack mechanism.

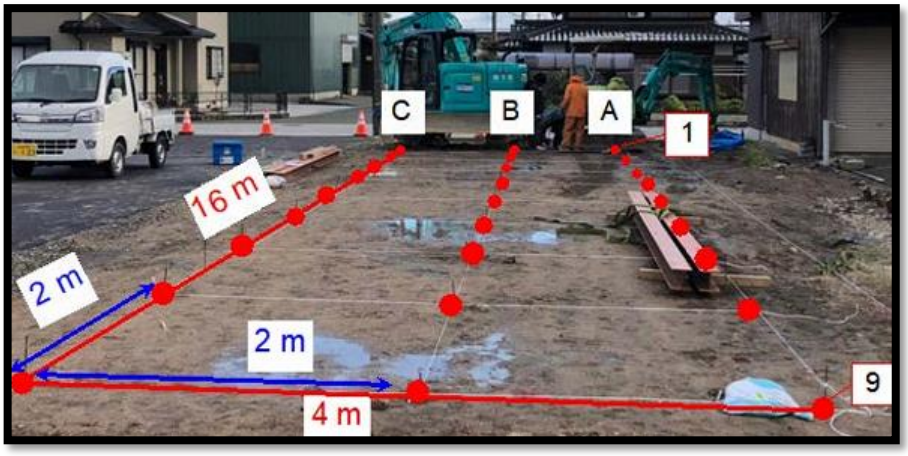


Figure 2.26 Location where the flip anchors are pull-out test (Source: Yoshida et al., 2023)

The analytical results of these experiments showed significant differences in the tensile forces exerted by anchors depending on whether they were placed in sand or clay soil (Yoshida et al.,2023). The anchors presented more tensile forces in sandy soil profiles than in clay soil profiles. This phenomenon was interconnected with the increased pressure exerted on the anchor as the effective projected area decreased, as observed only in the sand soil profile. Contrary to this, the clay soil profile consistently exerted a compressive effect on the anchor, regardless of its dimensional characteristics. Their study underlined the importance of soil composition when positioning flip-type anchors due to the considerable differences in performance and resistance between sand and clay soils (Yoshida et al.,2023).

Their study performed empirical field experiments and comparative analysis of anchor behavior with different soil types. The activity of flip-type anchors in improving soil stabilization and reducing erosion under various soil conditions was examined (Yoshida et al.,2023). As a result, flip-type anchors exhibit an interesting behavior in clay, where the area of the anchor mainly determines the tensile forces and remains relatively constant. The integration of innovative forecasting methodologies and empirical evidence provides a more comprehensive understanding of these important geotechnical developments.

Yoshida & Xiong (2023) conducted a field test for flip anchor specimens in a specific area. The specific area had dimensions of 4 m in length, 4 meters in breadth, and 2.5 m in height, as shown in Figure 2.27. 5 flip-type anchors were strategically positioned within the excavation area at a predetermined burial depth (H). These anchors

were positioned with open or closed flip anchor heads during the soil preparation phase. This setup enabled the evaluation of the accurate measurements and effectiveness of the flip anchors when they were buried at various depths.

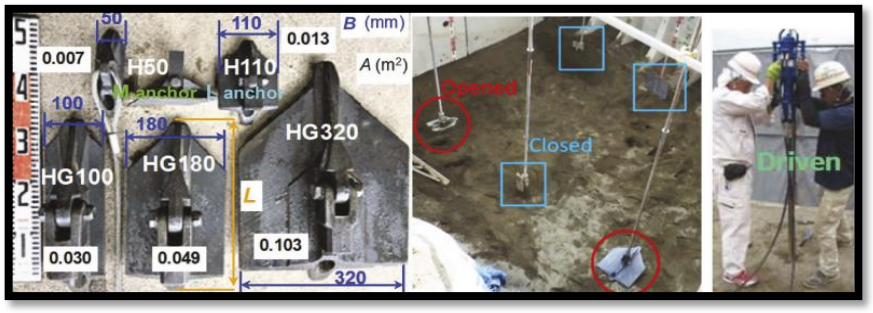


Figure 2.27 Field pull-out test conditions and flip-type anchors (Source: Yoshida &Xiong,2023)

Their study, installation of flip anchors vertically from the surface into the soil strata. Following installation, pull-out test was performed on each flip anchor using a hydraulic jack. A data acquisition system was used to record the tensile force (F) and tensile-induced displacement (w). Field experiments have shown that flip anchors must be derived by the length of the flip anchor (L) or up to 1.5 times L in order to be adequately placed in the dense sand soil profile (Yoshida and Xiong,2023). These empirical findings have led to the presentation of a new methodological approach for the calculation of the tensile strength of flip anchors in sandy soil profiles. As a result of the studies, it is proposed to calculate the maximum tensile force value for flip anchors by considering the depth until the anchor head is sufficiently seated (L or close to 1.5 times L), similar to the methodologies applied to conventional plate anchors (Yoshida & Xiong,2023). Their analysis improves the understanding of flip anchor behaviour in sandy soils and contributes to the development of design and application strategies for flip-type anchor system.

Hu et al. (2022) conducted a centrifugal model experiment to examine the tensile properties of plate anchors typically embedded in solidified clay, a substrate frequently encountered in offshore seabed conditions. This study represents a remarkable advance in the field of geotechnical engineering. This study aims to evaluate the performance of horizontal and inclined anchors by examining embedment depths and aspect ratios at different levels. The experimental setup shown in Figure 2.28 used a designed half-anchor

model (representing half the anchor length, L/2), a loading apparatus, hydraulic control mechanisms, and an array of sensors capable of precise measurements.

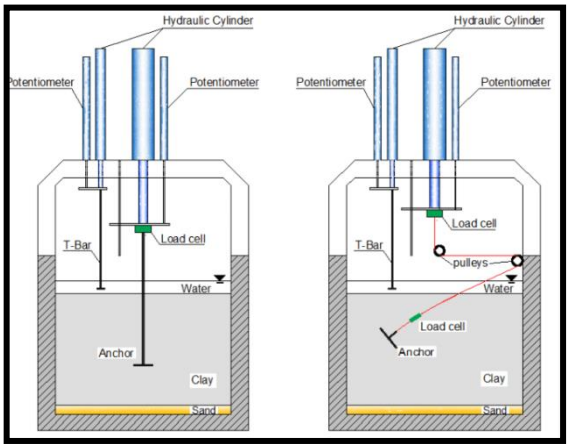


Figure 2.28 Set-up of the model (Source: Hu et al., 2022)

The experimental apparatus was equipped with a loading frame above the test container. Especially, a load cell integral to the setup provided accurate evaluations of the pull-out resistance encountered by the anchors. It was observed that, upon reaching the ultimate anchor resistance, there was no noticeable separation at the anchor-soil interface for either anchor orientation or embedment depth (Hu et al.,2022). Also, in their study, the soil displacement increased as the anchor slope increased in the soil where the inclined anchor was located. The difference in soil displacement can be attributed to the undrained shear strength of the soil adjacent to the top and bottom of the inclined anchor and so the anchor's resistance is reduced. These findings improve understanding of the interactions between plate anchors and the marine clay soil profile.

The Flying Wing Anchor® is a new anchor concept that stabilizes offshore foundations for renewable energy. The anchor, with a wing-like shape, uses its weight to penetrate the seabed by free-fall and mobilizes its full capacity by using the in-service load, so it is a new concept to optimize the sustainability of offshore foundations for renewable energy. A major challenge is to understand the trajectory of the anchor during loading because the anchor capacity depends on the final embedment depth and orientation. The project was initiated at the University of Texas at Austin and represents a groundbreaking advance in this field (Lai, 2017). This design cleverly combines the structural features of torpedo piles and vertically loaded plate anchors to maximize performance and sustainability. The Flying Wing Anchor® is strategically positioned

above the center of mass, which is critical as the anchor sinks through the water column and keeps its trajectory perpendicular to the seabed. The Flying Wing Anchor® is installed in a series of coordinated steps, as shown in Figure 2.29.

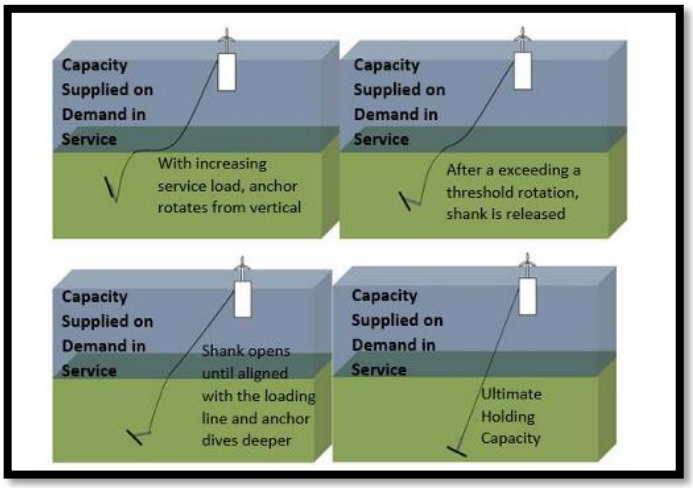


Figure 2.29 Installation process of Flying Wing Anchor (Source: Gerkus et al., 2016)

Once the installation process is complete, the anchor rod closes and locks securely if the load requirements are met automatically. If the connecting line of the anchor becomes tighter due to increased loads, the anchor is pulled upwards from its original vertical position. During the first pull-out phase, the spindle remains firmly locked. When the anchor reaches a certain angle of inclination, it returns to its original position. It is therefore very important that the anchor allows deeper penetration into the seabed under increasing tensile forces, thus increasing the anchor load-bearing capacity.

Azizian et. al, (2024) examined the performance of impact-driven earth anchors (flip anchors) under tensile loads in poorly sand properties (SP). Specifically, it was designed to investigate the extent to which the maximum tensile load is affected by changes in anchor embedment depth. The experimental design was conducted in a laboratory pull-out test using a Duckbill model 88 flip anchor with a 7.9 mm wired tendon cable embedded in an earthen box 1 meter long, 0.9 m high, and 0.3 meter wide. The laboratory experiment box is shown in Figure 2.30.

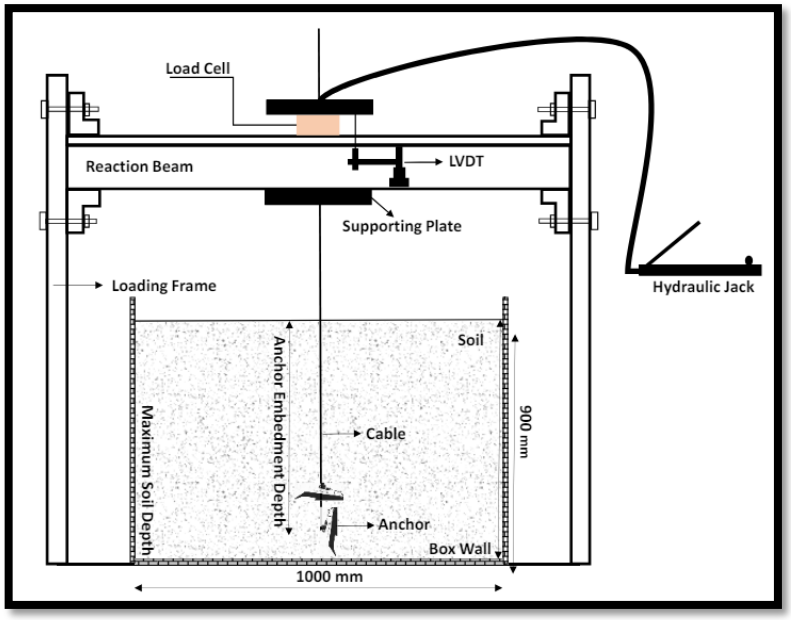


Figure 2.30 Pull-out test rig used for flip anchors in the laboratory (Source: Azizian et al., 2024)

The flip anchor was driven hydraulically to a depth of 0.75 m. Using a linear variable differential transformer (LVDT) and a load cell, the displacement of the flip anchor and the corresponding tensile force were recorded during the tensile experiments. The study also used the ABAQUS program to simulate the behavior of the anchor under retraction conditions. Numerical analysis revealed an important finding. This finding is with a 13% increase in the embedment depth of the anchor (from 0.75 m to 0.85 m), the ultimate tensile resistance ($P_{ult}$) increased from 1.8 kN to 3.9 kN (Azizian et al., 2024). At an embedding depth of approximately 1 cm increase, it now affected the final tensile strength by 78%. The reason for this is that due to the deeper embedment depth, a larger volume of soil needs to be displaced by the anchor, which corresponds to the increase in the overburden pressure acting on the anchor, thus increasing the durability of the anchor. Another reason is that the withdrawal capacity of the anchor increases with deeper embedment. It is further increased by lengthening the cutting surfaces in front of the anchor, which is facilitated. The results determined that the embedment depth directly effects of the flip anchor performance.

### 2.2.4.3. Advantages and Disadvantages of Flip Anchor

Flip anchors significantly advance slope stabilization technology, offering a versatile and efficient solution for reinforcing slopes and embankments (Aswaf et al., 2023). This method eliminates the need for advanced embedding, making it particularly suitable for improving existing slopes and fixing emergent stability concerns. Its ability to quickly adapt to different soil conditions makes it a valuable anchor a geotechnical engineering projects.

The flip anchors are resistant to corrosion. Galvanized steel flip anchors are constructed by applying a zinc layer to the steel, which prevents it from oxidizing. Zinc functions as an anode, offering protection against corrosion before steel and even in the event of a damaged coating. Additionally, these anchors are constructed with a lightweight design. In contrast to conventional anchors, they are manufactured through the use of precision casting, 3D printing, and machining. Flip anchors can be installed using portable equipment due to their lightweight design. They are capable of being directly propelled to the designated depth by the project without the need for excavation.

The flip anchors are drawn and secured in the site after being driven to the predetermined depth. The geometry of the flip anchor structure, which grasps and retains the soil while pulling it upwards or laterally, is the source of this mechanical advantage. Since flip anchors instantly provide full holding capacity to the site area, they are energy efficient, time-saving, and more cost-effective in terms of installation and labor compared to other conventional anchors.

Despite the benefits of flip anchors, they also have some disadvantages. The following are the disadvantages:

- Limited Bearing Capacity: Compared to other grouted anchor systems, flip anchors have a comparatively low bearing capacity, which is a disadvantage (Moghadam et.al, 2021). It is necessary to conduct a thorough assessment of the soil conditions and load requirements to ensure that the flip anchor can support the intended loads without experiencing excessive failure.

- Immediate Need for Pull-out Test: Pull-out tests must be conducted immediately following the installation of flip anchors, as the anchor plate rotates 90 degrees within the soil. For the flip anchor to transition from the

drive position to the load-bearing position, rotation is crucial. Nevertheless, this procedure generates uncertainty regarding the anchor's capacity to effectively support loads and its connection to the soil.

- Lack of Scientific Reports on Environmental Effects: A significant lack of scientific reports examining the effect of environmental conditions such as soil compaction on the rotation of flip anchors and the resulting load-bearing capacity has been observed (Moghadam et al. (2021).

Flip anchors provide innovative solutions for anchoring in a variety of soil conditions; however, they also have disadvantages, including the necessity of immediate pull-out tests, a limited bearing capacity, and a lack of scientific research on their environmental conditions. To optimize the performance and reliability of flip anchors in geotechnical applications, it is necessary to comprehend and mitigate these drawbacks through inclusive testing and research.

### 2.2.4.4. Relevant Case Studies of Flip Anchors

The flip anchor's system configuration has it has a minimal environmental impact, aligning with sustainability principles in engineering practices. Flip anchors have begun to take their place in infrastructure development, construction, and civil engineering projects due to their time-saving and sustainability. The durable load-locking mechanism ensures performance even in difficult soil and seismic environments, making flip anchors used tools in modern engineering applications. Some of the application areas of flip anchors are shown in the diagram in Figure 2.31.

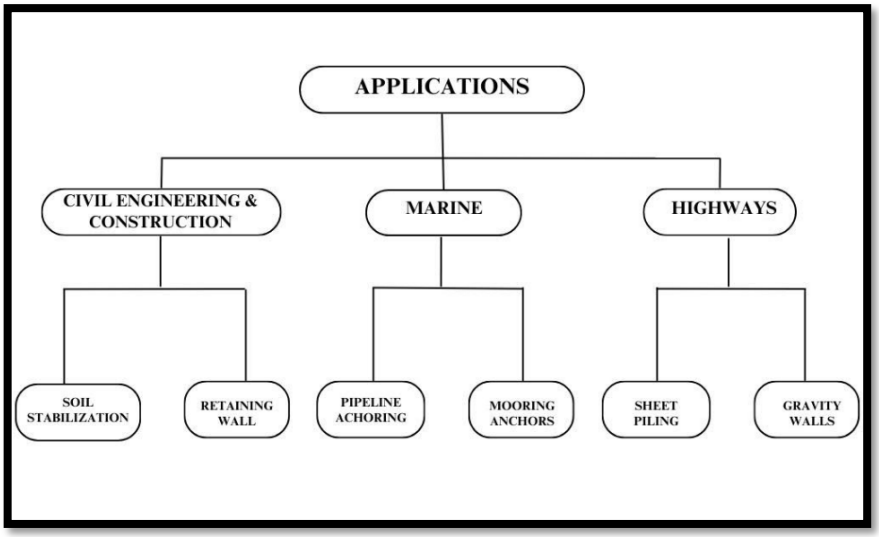


Figure 2.31 Usage areas of flip anchors

As seen in Figure 2.31, flip anchors are used as supporting elements of retaining walls and as auxiliary elements to ensure slippage or drainage in slope stability problems. Additionally, in marine projects, flip anchors are generally used as a temporary solution to attach the ship to a fixed or floating element and to keep the ship anchored during loading or unloading operations. In highway projects, where sheet piling is used, it is generally used as a support element by using flip anchors in case of tipping or slipping risks.

There are several practical examples on-site due to the benefits that flip anchors offer. The initial of these is the utilization of flip anchors in slope stability issues. A high pore water pressure was detected on an earth-covered hillside in Stubbington, Hampshire, on the south coast of England. Therefore, a drain was required to be constructed 10 m from the gravel layer into the clay. It has been determined that driven belt drains that are frequently available are not appropriate for road terrain due to the challenges associated with operating in corrosive soils. For this reason, a series of field tests were conducted to evaluate the design of flip anchors. The addition of a steel protective cover considerably increased their durability. Instead of driven band drains, the flip anchor design was determined to be appropriate, and over 300 flip anchors were inserted into the soil to mitigate erosion and landslides induced by elevated pore water pressure (Anchor System International, 2020). The application and implementation of flip anchors for this project are illustrated in Figure 2.32.

Figure 2.32 Flip anchor applied to a soil-covered hillside in Stubbington England (Source: Anchor System International, 2020)

Another application is the stabilization of marine embankments. There were flood problems and slope slide problems on the banks of the Salmons Brook River in London. The profile of a section of the shoreline was reconfigured and shore levels were raised to safeguard against floods. In order to prevent both shallow and profound collapse, ground anchors were required to stabilize slopes. It was requested that the vegetation on the slope surface be protected and that the plants at the end of the slope profile not be damaged to prevent the destruction of nature. Accordingly, flip anchors that were resistant to water and corrosion were the favored option. It has been demonstrated that the system can be determined the 100-year design life in the marine environment by utilizing stainless steel (316 class) material in the flip anchor. The proof load of 21 kN and the safety load of 17 kN of each flip anchor were determined along the slope sections, as illustrated in Figure 2.33 (Anchor System International, 2020). A natural-looking river was achieved by installing a recessed pattress plate and geo-mesh sheeting, which allowed vegetation to grow over it and hide the system.

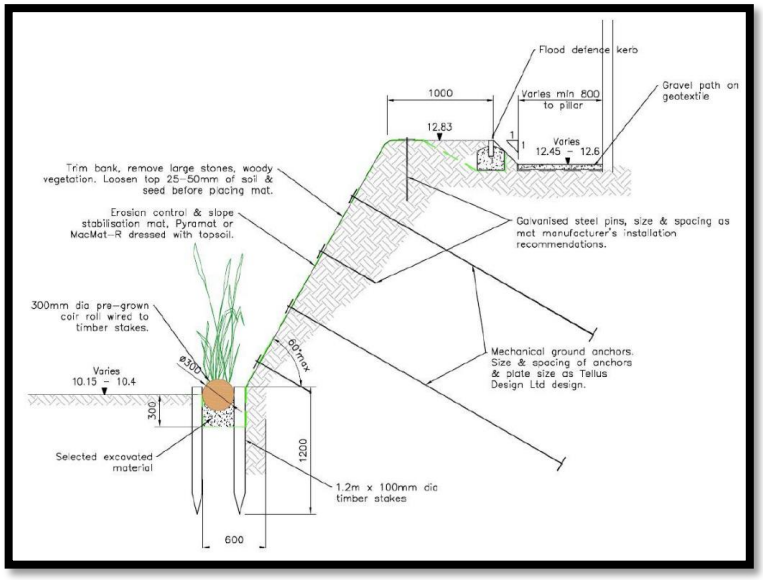


Figure 2.33 Layout of flip anchors used in Salmons Brook River (England)(Source: Anchor System International, 2020)

The installation of the flip anchors is completed in a very short time, as the flip anchor system is ready for immediate installation and use, without the need to wait for any mortar to harden before testing or applying load. During the assembly work, a 5-ton excavator, a 3-meter drive rod set, and a hand-held hydraulic jack were used. Figure 2.34 shows the completed flip anchor system in Salmons Brook River (Anchor System International, 2020).

Figure 2.34 Layout of flip anchors used in Salmons Brook River (England)(Source: Anchor System International, 2020)

In another construction project, flip anchors were used to improvement an existing old retaining wall. An urgent resolution was necessary due to the potential for the 4.5-meter-high, old retaining wall in the vicinity of the new housing project to collapse during construction. The condition of the retaining wall was also influenced by the absence of drainage behind the wall, which necessitated the implementation of a functional drainage system. Due to the high cost and environmental impact associated with completely demolishing the existing retaining wall and constructing a new reinforced concrete wall, it was determined that reinforcing the old wall using flip anchors would be a more economical and environmentally friendly solution (Source: Platipus Civil Engineering & Construction Brochure, 2022). To enhance the retaining wall and resolve drainage issues, field experiments were implemented. Initially, a diamond drilling machine was employed to drill three rows of 10 cm diameter holes in the masonry, and 60 permanent flip anchors were driven to a depth of 6.2 m, as illustrated in Figure 2.35.


Figure 2.35 Reinforcement of existing retaining wall with flip anchors England (Source: Platipus Civil Engineering & Construction Brochure, 2022)

The earth pressure acting on the wall was balanced by subjecting each anchor to durability testing, and each flip anchor was load-locked at 10kN. The drainage system and flip anchor system are combined in the lower two rows to simultaneously limit capacity and provide drainage. The carbon emissions were reduced by 96% by utilizing the flip anchor solution exclusively to enhance the wall, resulting in the emission of only 0.6 tonnes of carbon (Source: Platipus Civil Engineering & Construction Brochure, 2022).

Another area of use of flip anchors is to ensure the fixing of structures by resisting the buoyancy force. As an application of this, a new underground storage system was established in the USA without disrupting the existing infrastructure due to the inadequacy of the underground storage system in the city center. A total of 48 HDPE pipes were used in the system to be built. Field investigations concluded that the total weight of the soil and pipe was not sufficient to resist the potential vertical hydrostatic uplift of the underground storage system due to the water table and limited overburden. Flip anchors were chosen to secure this underground storage system. As seen in Figure 2.36, the flip anchors were buried directly into the ground and fixed by connecting them with a bell on top of the HDPE pipes. While the structure meets the required factor of safety (FS) 1.5, the underground system was secured with belts using flip anchors every half meter.

Figure 2.36 Flip anchor application used for hydrostatic buoyancy force (USA)
(Source:Platipus Civil Engineering & Construction Brochure, 2022)

In another application, flip anchors were used to provide additional temporary horizontal support to a 9 m high concrete adjacent pile retaining wall on the roadside in

Sydney, Australia (Source: Anchor System International, 2020). The reason for choosing flip anchors was that time is limited for the construction period and especially the construction area was saved thanks to the use of limited space. The flip anchor systems used were installed at an inclined angle as seen in Figure 2.37.

Figure 2.37 Location of flip anchors used to support pile retaining structure (Australia) (Source: Platipus Civil Engineering & Construction Brochure, 2022)

An anchor head was placed on the flip anchors placed at an angle, and the pressure applied to the anchor head increased due to the weight of the soil on it. When the flip anchors were placed and tested at a depth of 8 m in compact sandy soil, it was proven that the requirements of the predicted working loads of 50kN and 80kN were met, respectively. Figure 2.38 shows the finished installation and positioning of these flip anchors.

Figure 2.38 Flip anchor systems applied on Cranbrook Road (Australia)(Source:Platipus Civil Engineering & Construction Brochure, 2022)

As seen in Figure 2.38, installing flip anchors applied in two rows was completed within one month. Since temporary support and a quick solution were offered to the pile retaining wall structure, efficient use of the area was enabled.

## 2.3. Conclusion

In this chapter, grouted anchors, plate anchors and anchors operating on similar principles are summarised and literature studies on installation methods, advantages and holding capacities are described. Flip anchors, which are the main subject of this study, are included and similar flip anchors available in the market are explained. To enhance comprehension of vertical pull-out tests and numerical analyses of flip anchors, this study describes literature studies on flip-type anchors. Finally, to better understand the ultimate tensile resistance of flip anchors, case studies of flip anchors applied in the field are included.

# CHAPTER 3

# SITE INVESTIGATION and PULL-OUT TEST

## 3.1. Introduction

In this section, the field studies were performed in the Seferihisar district of Izmir province. First, a site investigation was performed (Figure 3.1a). At this stage, soil samples were taken from different depths by boring, and soil classification was carried out. Then, the disturbed soil samples were sieve analyzed in the laboratory, and particle size distribution and Atterberg limit tests were performed. In addition, a double-layer Multichannel Method of Analyzing Surface Waves (MASW) test was performed in the field to determine the shear wave velocity (Vs). After the site investigation was completed, vertical pull-out tests were performed on 3 different soil profiles using FPA-I anchor and 2 different soil layers using FPA-II anchor. The reason for performing pull-out tests on two different soil profiles in FPA-II anchor was that the last soil layer, 3.25 m, could not be pull-out tested because the drive steel rod was buckled in the site and became unusable. The ultimate tensile resistance of the anchors ($P_{ult}$) was manually recorded for each pull-out test using a hydraulic jack. Finally, the $P_{ult}$ recorded at the site for the FPA-I and FPA-II anchors was compared with the tensile resistance of similar types of flip anchors available in practice.


Figure 3.1 Location of the project site in Seferihisar (a) soil boring location (b) pull-out tests location

## 3.2. Site Investigation Tests

### 3.2.1. Field Tests

Soil boring was conducted on February 17, 2024, at a depth of 15 m. The boring operations employed the GEOROB-PS35, a hydraulic, automated soil drilling rig. This rig operates using a hydraulic system that provides power to the boring rig and is typically controlled by a computer system that adjusts its operation based on feedback from boring conditions. The advanced control system can precisely manage the drilling process's speed, pressure and depth.

The Standard Penetration Test (SPT) was performed for soil classification and to find the number of blow count (N) value in the soil profile. During the field application of SPT, a standard tube sampler with an outer diameter of 50 mm and an inner diameter of 34.9 mm was utilized. The sampler was driven into the soil with a 63.5 kg hammer dropped freely from a height of 76.2 cm. The procedure involved measuring the hammer blows required to penetrate the sampler to three successive depths of 15 cm each, thus reaching a total depth of 45 cm into the soil sublayer. The SPT blow count (N) was calculated by summing the number of pulses required for the second and third 15 cm penetrations. Measured SPT values were corrected to a standard energy level, $(N_{60})_1$. This correction adjusts SPT results to account for varying energy efficiencies in different test equipment and conditions, thus providing a more uniform basis for interpreting soil conditions. Equation 3.1 was used to find $(N_{60})_1$ value.

$$(N60)_1 = NC_N\, C_R C_S C_B C_E \tag{3.1}$$

$C_N$ shown in Equation 3.1 represents the depth correction coefficient. The effective vertical stress $\sigma_{vo}'$ (kN /m$^2$) at the depth where the SPT is performed is calculated. The depth correction factor is calculated by the formula (Liao and Whitman, 1986), as Equation 3.2.

$$C_N = 9.81 * \left(\frac{1}{\sigma'_{Vo}}\right) \leq 1.70 \tag{3.2}$$

The rod length correction factor ($C_R$), the sample receiver type correction coefficient ($C_S$), the drill hole diameter correction coefficient ($C_B$) and the energy

correction factor ($C_E$) values shown in Equation 3.1 are shown in Table 3.1 (TDBY, 2018).

Table 3.1 Correction factors of Standard Penetration Test (Source:TDBY, 2018)

| Correction Coefficient | Variation | Values |
|---|---|---|
| $C_R$ | Between 3m and 4m | 0.75 |
| | Between 4m and 4m | 0.85 |
| | Between 6m and 10m | 0.95 |
| | Deeper than 10m | 1.00 |
| Cs | Standard Sample Receiver | 1.00 |
| | Sample receiver without an inner tube | 1.10-1.30 |
| $C_B$ | Diameter between 65mm - 115mm | 1.00 |
| | Diameter 150 mm | 1.05 |
| | Diameter 200 mm | 1.15 |
| $C_E$ | Safety Hammer | 0.6 - 1.17 |
| | Ringed Hammer | 0.45 - 1.00 |
| | Automatic pulsed Hammer | 0.90 - 1.60 |

The SPT-N corrected and uncorrected correlations and the effective vertical stress at three different depth ranges are shown in Table 3.2. The SPT test was conducted up to 4.95 m, as illustrated in the table. The SPT test was unable to be conducted due to the sandstone turning grey and the alternation that was observed at a depth of 5 m in the site investigation area. The soil at a depth of 1.5 m was classified as idealized clayey sand soil as a consequence of the SPT test. This classification denotes a soil composition that is characterized by a narrow range of particulate sizes, which typically leads to diminished porosity and compaction properties. At a depth of 2.5 m, a silty granular soil profile was identified. This stratum is distinguished by a higher concentration of silt particles intermixed with sand, which can impact the soil's mechanical properties and drainage. At a depth of 3.25 m, the classification of low-plastic clay was identified. This variety of sand is distinguished by its low plasticity and minimal clay content. The stratification of these soil types suggests a multifaceted depositional history that poses a variety of challenges and considerations for engineering applications, particularly in the design of foundations and the implementation of soil stabilization strategies.

Table 3.2 SPT Test Results

| Depth(m) | SPT-N | $\sigma'_{vo}$ (kN/m²) | $N_{60}$ | $(N_{60})_1$ |
|---|---|---|---|---|
| 1.50-1.95 | 2 | 27 | 2 | 3 |
| 3.00-3.45 | 24 | 51.8 | 20 | 28 |
| 4.50 4.95 | 15 | 78.8 | 13 | 14 |

Additionally, Multi-Channel Analysis of Surface Wave (MASW) test was performed to identify the sub-surface's dynamic parameters and map the sub-surface's continuity and specific locations. In the seismic studies, the GEODE model, an American-made 12-channel seismic signal processor, was used (Figure 3.2a). Figure 3.2(b) shows geophysical survey directions. The configuration of the geophone arrays was determined according to various factors, their specific characteristics, and the optimum spacing required by the structural characteristics of the terrain. The layout of the seismic emanations was strategically designed, ensuring offset spacings were aligned in proportion to the geophone placements.

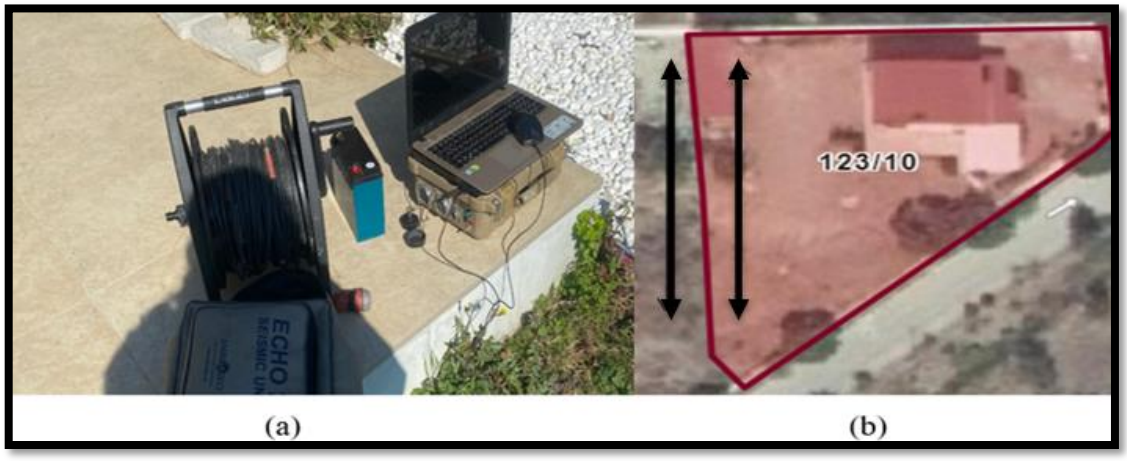


Figure 3.2 MASW Test (a) 12 Channel GEODE seismograph used in the geophysica survey (b) Geopyhsical survey directions

A 10 kg sledgehammer was used to strike a steel plate precisely and vertically to create P waves for seismic energy generation. These waves were then detected using 14 Hz vertical geophones specifically selected for their sensitivity to the vertical propagation of P waves. Seismic measurements focused on recording types of longitudinally propagating seismic waves in the subsurface ($V_p$ waves). These longitudinal seismic waves were measured from both directions to increase the accuracy of the velocity data.

The speed of $V_p$ seismic waves was specifically targeted to detect deeper underground structural formations. Data was collected by recording, analyzing, and modelling reciprocal P wave captures across all profiles. Since the study area was relatively unaffected by traffic and anthropogenic noise, seismic measurements were carried out under controlled conditions during daylight hours to minimize possible disturbances and ensure data integrity.

In the application of the MASW methodology, enhancing the bandwidth, depth, and resolution of the investigation substantially improves the signal-to-noise ratio, thereby yielding high precision in the resultant frequency-dependent phase velocity curves. Data derived from higher modes enable deeper exploration than is possible with fundamental mode data. Moreover, the utilization of higher mode data enables a significant enhancement in the resolution of the inferred S-wave velocity profiles. This is influenced not only by frequency but also by the source-to-receiver distance. Several multichannel recordings were initially captured in the conventional Common Depth Point (CDP) format to facilitate comprehensive surface wave analysis. For the effective acquisition of surface wave data, receivers were typically chosen with low response frequencies, usually below 4 to 5 Hz, to accommodate the characteristics of pulse-type sources interacting with the surface. After data collection, the seismic records were digitized and transferred to computational platforms for processing.

Utilizing the Seisimager SW software suite, necessary signal filtering and corrections were applied to ensure data integrity. Following this preprocessing step, the distribution curve was generated through ten iterations using WaveEq Software. The analytical phase resulted in the inversion of the distribution curve, where shear wave ($V_s$) velocities and corresponding depths were quantified at successive stratigraphic levels. This detailed inversion analysis facilitated the layered interpretation of subsurface velocities and provided important geophysical information regarding stratigraphic configuration. As a result of the seismic test, at each level $V_s$ velocities and measured $V_p$ were found level by level as a result of the inversion evaluation of the obtained curve. The $V_p$ and $V_s$ values are given in Table 3.3.

Table 3.3 MASW Test Results

| Depth (m) | $V_p$ (m/s) | $V_s$ (m/s) |
|---|---|---|
| 1.5 | 379 | 200 |
| 2.5 | 465 | 264 |
| 3.25 | 331 | 343 |

## 3.3. Laboratory Tests

The disturbed soil samples were collected from the field. The particle size distribution of these samples was determined through sieve analysis testing, which is a critical factor in the comprehension of soil characteristics. The sieve analysis was conducted according to the TS-EN ISO 17892-4 standard. This standard establishes a comprehensive methodology for the mechanical analysis of soils, ensuring the accuracy and reproducibility of the results. The process entailed the passing of the soil samples through a sequence of standardized sieves with progressively smaller apertures to separate the soil particles by size. The grain size distribution curve was constructed by measuring the bulk of soil retained on each sieve. The gradation curve that results, as shown in Figure 3.3, demonstrates the particle size distribution of the soil.

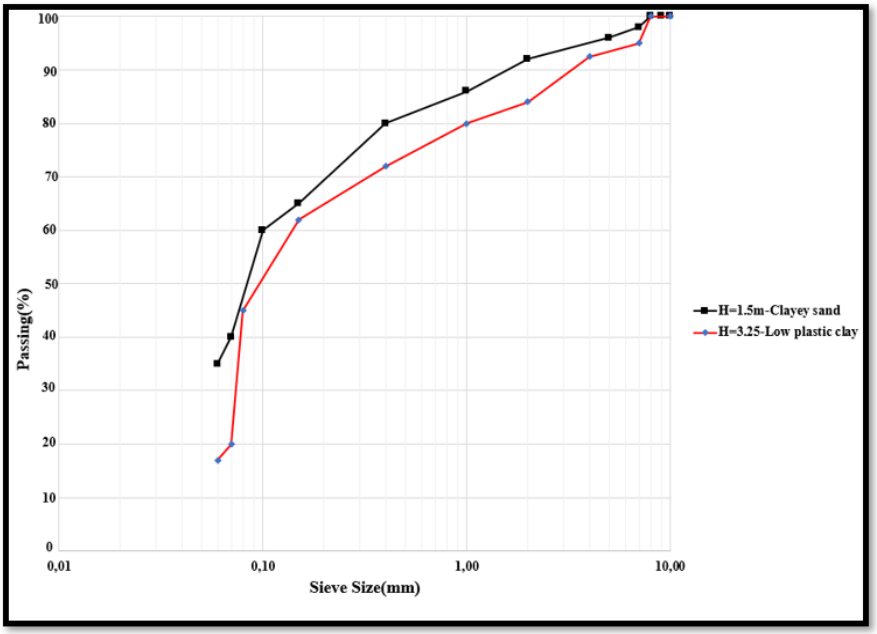


Figure 3.3 Gradation of curves of soils

The Atterberg Limits test was conducted according to the TS-17892-12 standard for determining the plasticity characteristics of fine-grained soils. The Atterberg Limits include the Liquid Limit (LL), Plastic Limit (PL), and Plasticity Index (PI). The Atterberg limit test results and the TS standard classification are listed in Table 3.4.

Table 3.4 Atterberg Limit Test Results

| Sample | | Atterberg Limit Test | | | Soil Classification (TS) | Soil Classification (TS) |
|---|---|---|---|---|---|---|
| No | Depth(m) | LL (%) | PL (%) | PI (%) | | |
| 1 | 1.5-1.95 | 34 | 20 | 14 | ciSa | Clayey sand |
| 2 | 2-2.95 | -- | NP | -- | siSa | Silty sand |
| 3 | 3-3.5 | 33 | 17 | 16 | CIL | Low-plastic clay |

## 3.4. Flip Anchor Pull-Out Tests

The site investigation and laboratory tests were completed, and the site shown in Figure 3.1(b) was prepared for the pull-out experiments for flip anchors. Figure 3.4 shows the predefined 6 points labelled A, B, C, A', B', and C'. For FPA-I anchor, point A represents the points driven into the soil at a depth of 1.5 m, point B at 2.5 m, and point C at 3.25 m. The FPA-II anchor was driven into the soil at points A' (at a depth of 1.5 m), B' (at a depth of 2.5 m), and C' (at a depth of 3.25 m). The distance of 1.5 m horizontally and 1 m vertically was determined according to the length of the flip anchors (approximately 2-3 times the length of the flip anchors). An attempt was made to avoid interaction between the flip anchors, which could affect the stress distribution and distort the test results. In order to maintain the integrity of the pull-out test, an effort was made to provide a more accurate representation of the capacity of each flip anchor.

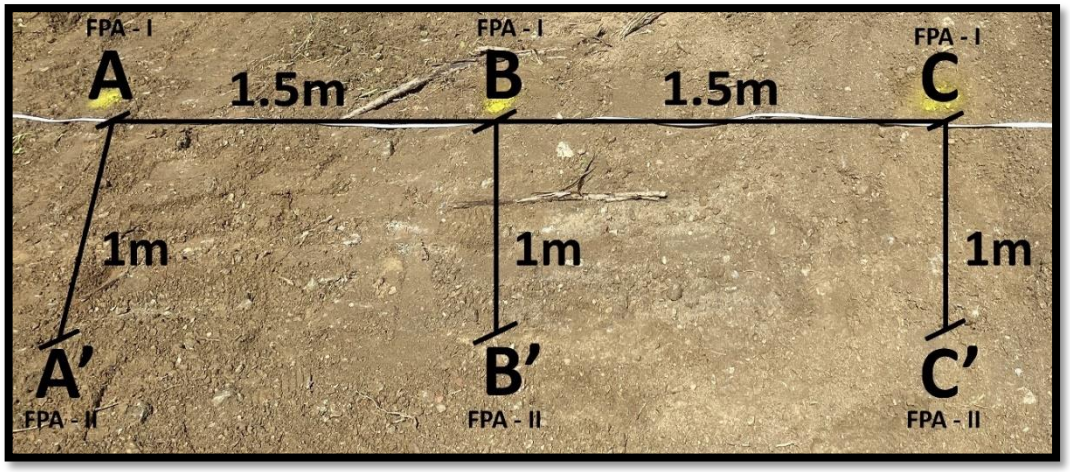


Figure 3.4 Location of the points to be pull-out test for flip anchors

The reason for choosing three different depths for the experiment is to investigate the $P_{ult}$ of the flip anchor specimen in various soil profiles. The FPA-I anchor was driven into three different soil types and pulled out with a hydraulic jack, and the maximum tensile force at each depth was manually recorded from the pressure gauge. The FPA-II anchor was tested in two different soil types (two different depths) because the drive steel rod was bent and could not be driven into the soil at 3.25 m. The reason for this is that the person using the excavator cannot adjust the excavator's head while driving the drive steel rod and suddenly applied force. In all other pull-out tests, the drive steel rod was driven into the soil in a gradual and controlled manner. The $P_{ult}$ of the FPA-II anchor was determined using the same procedures as the FPA-I anchor.

### 3.4.1. Materials, devices and flip anchor samples used during the Pull-out Tests

Pull-out tests were performed in the field for 2 different flip anchors with different geometries. Figure 3.5 (a) shows the schematic dimensions and Figure 3.5 (b) illustrates the photo of the FPA-I flip anchor.

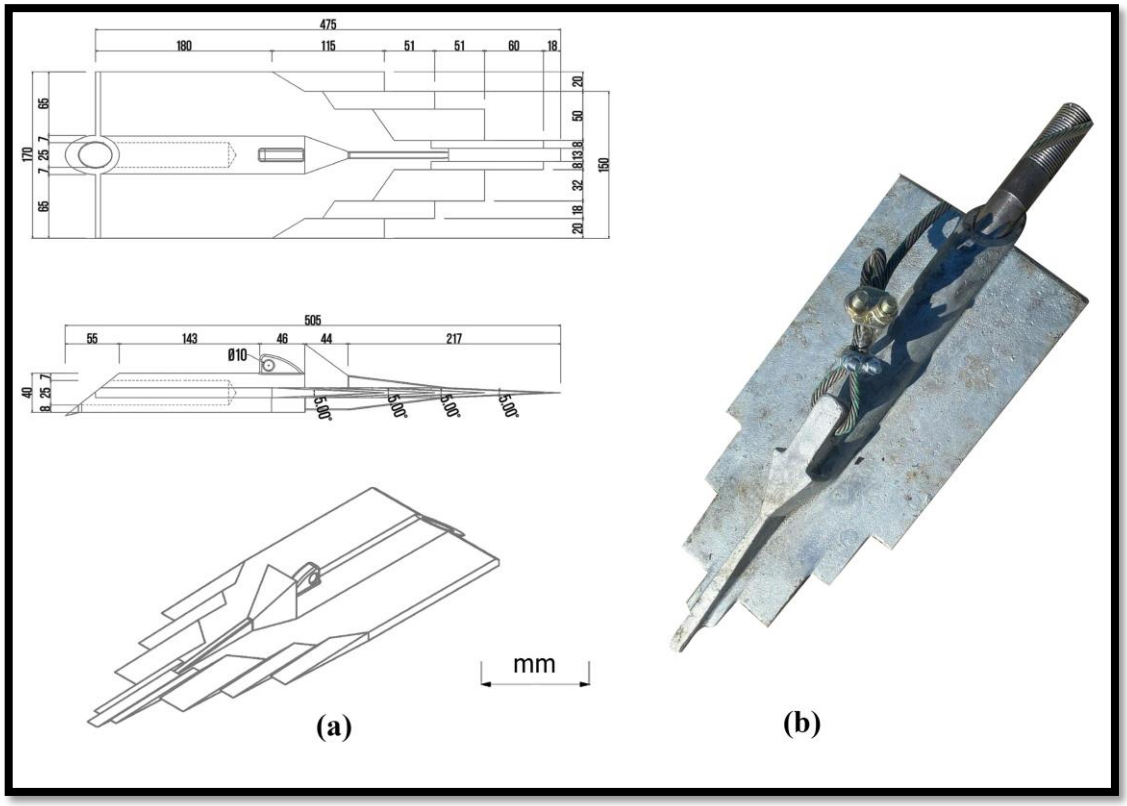


Figure 3.5(a) Schematic drawing and dimensions of the FPA-I anchor (b) illustrates the photo of the FPA-I flip anchor

As shown in the Figure 3.5(a), the FPA-I anchor had a width of 17 cm and a length of 47.5 cm. The mass of this anchor was measured with a weighing scale and recorded as approximately 10 kg. These characteristics are important in assessing the suitability and performance of the FPA-I anchor. Figure 3.6 (a) shows the schematic dimensions and Figure 3.6 (b) illustrates the photo of the FPA-II flip anchor. As shown in the figure the FPA-II anchor was 4 cm wide and about 16.28 cm long. The mass of this anchor was measured with a weighing scale and recorded as approximately 5 kg.

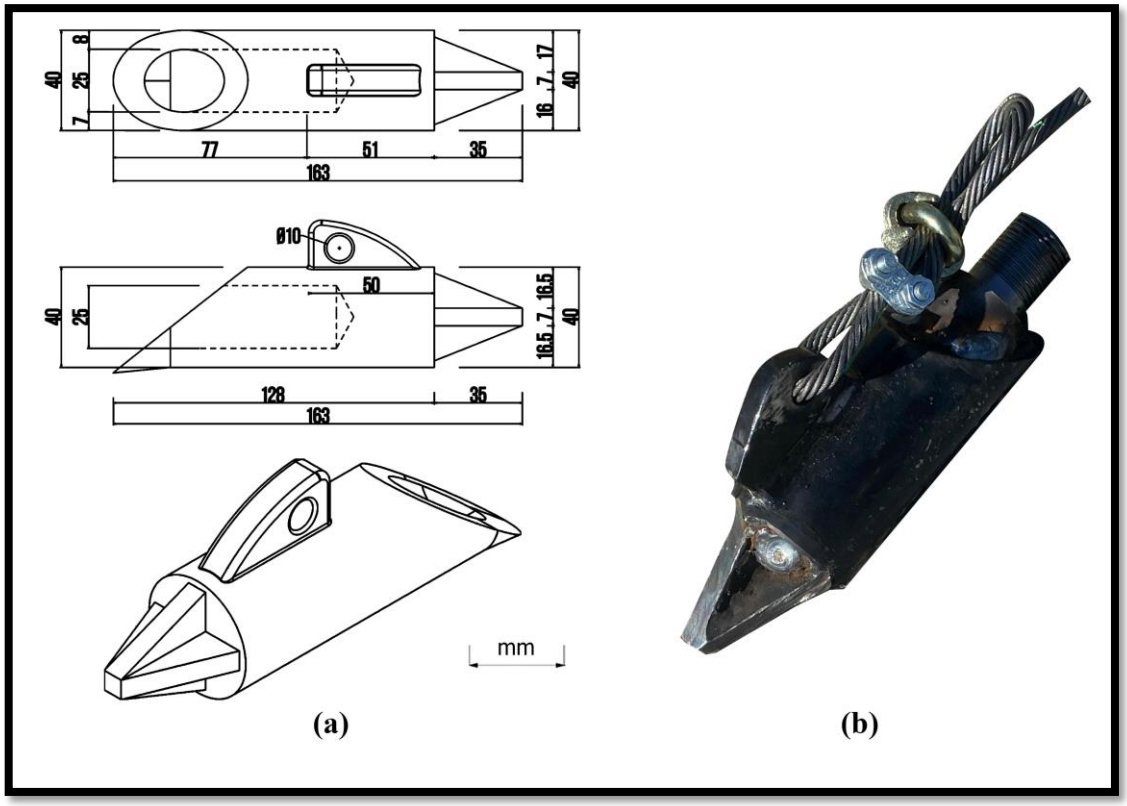


Figure 3.6 (a) Schematic drawing and dimensions of the FPA-II anchor (b) illustrates the photo of the FPA-II flip anchor

During the installation of the flip anchors to the soil. The following steps were performed:

1. Drive steel rod suitable for the flip anchor shown in Figure 3.7(a) was placed to a depth where tests would conduct.
2. The anchor rope was locked as appropriate clamp shown in Figure 3.7(b). The anchor rope is made of high-carbon steel material. Although the tensile capacity of these ropes varies according to the number of wires, the average tensile capacity is 300 kPa.
3. Flip anchors were placed vertically at the predetermined points in Figure 3.4. They were pushed into the ground with the help of an excavator. The flip anchors were pushed into the soil with the anchor rope and the drive steel rod.
4. After the flip anchors were pushed to the predetermined installation depth, the drive steel rod was carefully removed.
5. A bearing plate was placed where the anchor rope was located as shown in Figure 3.9. This plate was distributed load and provided a stable

response point for the hydraulic jack. Additionally, Mechanical connectors (tapered jaws) were placed around the anchor rope. It was securely tightened by the tapered jaws and the anchor rope was fixed on top of the hydraulic cylinder.

6. Then, the hydraulic jack was placed aligning it with the anchor rope. Finally, the pull-out test was performed by hydraulic jack. The $P_{ult}$ of the flip anchors were manually observed and recorded.


Figure 3.7 (a) Drive steel rods used in the pull-out tests, and (b) the anchor rope and locking process used in the withdrawal of FPA-I and FPA-II anchors in the pull-out test

### 3.4.2. Pull-out Test for FPA-I and FPA-II Anchor

In the field pull-out test, the FPA-I anchor was first pushed 1.5 m into clayey sand (point A shown in Figure 3.4), then 2.5 m into silty sand (point B shown in Figure 3.4), and finally 3.25 m into low plastic clay (point C shown in Figure 3.4). An 18-ton excavator was used to push the flip anchor into the soil. Various soil profiles and depths (1.5 m, 2.5 m, and 3.25 m) were used to evaluate the $P_{ult}$ performance of the FPA-I anchor. Figure 3.8 shows the FPA-I anchor pushing into the soil.

Figure 3.8 The installation of the FPA-I anchor vertically to the soil

During the process of driving the FPA-I anchor into the soil, it was driven with the anchor rope and driven steel rod. Following the removal of the steel rod, a bearing plate was strategically placed where the anchor rope was located. This bearing plate distributed the applied load evenly and provided a stable point of response for the subsequent application of the hydraulic jack. To facilitate the pull-out test, mechanical connectors, specifically tapered jaws, were positioned around the anchor rope. These connectors ensured a firm grip on the rope, enabling an accurate transfer of force during the test. Then, the hydraulic jack was aligned with the anchor rope, ensuring that the direction of the applied force would be directly along the axis of the anchor ropeAfter that, pull-out test was performed with the help of a hydraulic jack with a capacity of 700 bar. The hydraulic jack is equipped with a pressure gauge that allows manual observation of the applied force. The hydraulic jack was used because it effectively applies a measurable and controlled tensile force, which is a critical feature in determining the ultimate tensile resistance of flip anchors. The test setup shown in Figure 3.9 shows the pull-out test performed with a hydraulic jack.

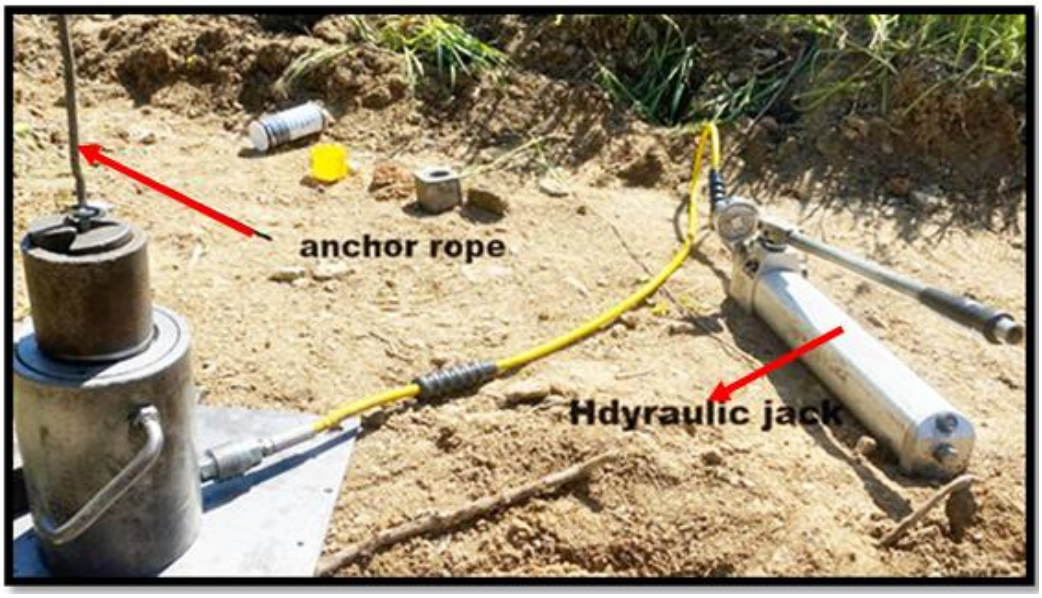


Figure 3.9 The pull-out test performed to FPA-I anchor by a hydraulic jack

The maximum tensile force of the flip anchor in the load-locking position was recorded manually by observing the pressure gauge. These findings provided information about the behavior of the FPA-I anchor under load and thus provided preliminary information on the design and installation techniques of the flip anchor system. The results of these tests provided preliminary information for the optimization of flip anchor design and installation techniques for geotechnical engineering applications, especially in environments with heterogeneous soil layers. Investigating the response of flip anchors versus the ultimate tensile resistance of flip anchors in various soil types contributed to the empirical component of the thesis, providing a simple basis for analysis in real-world scenarios. Also, numerical analysis was performed using data obtained from the field.

In the second stage, the FPA-II anchor was driven into the soil from points A' (at a depth of 1.5 m) and B' (at a depth of 2.5 m) as shown in Figure 3.4. FPA-II anchors C' (at a depth of 3.25 m) could not be pushed. This was because the drive steel rod buckled and became unusable. Figure 3.10 shows driving this anchor to the soil by an excavator. The pull-out tests were performed at predetermined locations (A’, B’ and C’), following the same testing steps as for the FPA-I anchor sample. The methodology used for these tests was established in a controlled experimental setup to ensure consistency in test conditions and facilitate direct comparison of results under the same test conditions.

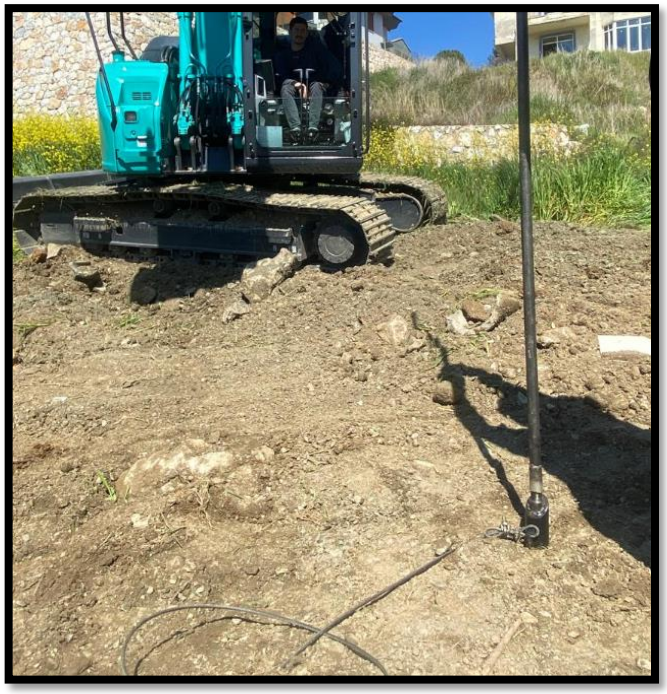

Figure 3.10 The installation of the FPA-II anchor to the soil

The use of the same test apparatus for FPA-I and FPA-II anchors was critical to validating the experimental model and ensuring that the data collected in the field were directly comparable to those obtained under controlled conditions. Table 3.5 shows the ultimate tensile resistances of the FPA-I and FPA-II anchors pull-out test results at each depth.

Table 3.5 Ultimate tensile resistance at each depth for FPA-I and FPA-II anchors

| Anchor type | Depth (m) | Pult (kN) |
|---|---|---|
| FPA-I | 1.5 | 61.6 |
| | 2.5 | 86.2 |
| | 3.25 | 154 |
| FPA-II | 1.5 | 37 |
| | 2.5 | 52.4 |

By analyzing the pull-out tests, the $P_{ult}$ values and performance characteristics of FPA-I and FPA-II anchors under different depths and soil conditions were evaluated. Moreover, the preliminary information was obtained on how soil composition and density affect the flip anchor systems.

### 3.4.3. The Pull-Out Test Result of FPA-I Anchor and Comparison with Similar Flip-Type Anchors

As explained in Section 3.3.2 of the thesis, pull-out tests of the FPA-I anchor were carried out in the field at 1.5, 2.5, and 3.25 m. These investigations were performed to measure the ultimate tensile resistance of flip anchors under different subsurface soil conditions. The results of these tests were expressed to correspond to the maximum tensile load that the flip anchor could withstand at each specified depth. In order to conduct an additional investigation, the $(N_{60})_1$ for the applicable soil strata was incorporated into the study based on the results of the SPT tests. An $P_{ult}$ of 61.6 kN was determined in the clayey sand layer at a depth of 1.5 m. Clayey sand layers are soil types containing both sand and clay particles. The ratio of these components can significantly affect the behavior and properties of the soil. These soils often have unequal particle sizes, resulting in less efficient force transfer. In silty sand layers (at a depth of 2.5m), it was found to be 86.2 kN. The reason for obtaining a higher ultimate tensile resistance is generally because this type of soil provides more resistance to tensile forces due to better interlocking of the particles.

In the low plastic clay layer at 3.25 m, the $P_{ult}$ value of the FPA-I anchor was 154 kN. Low plastic clays may have higher tensile resistance than other soil layers due to better particle arrangement and less shrink-swell behavior. As the depth increases, the overburden pressure increases due to the weight of the soil above. Due to the increase in overburden pressure, the density of this low-plastic clay soil may increase as the air voids due to compression in the low-plastic clay soil decrease. It was observed that the tensile resistance increased as the density increased, providing better interlocking between particles and greater resistance to movement. Another factor is the cohesion (c) and internal friction ($\phi$) parameters of the soil.

The relationship between the $P_{ult}$ of the FPA-I anchor and the $(N_{60})_1$ is illustrated in Figure 3.11(a). The graphical representation provided a view of how the $P_{ult}$ of FPA-I anchor varies in response to changes in soil conditions. The relationship between the $P_{ult}$ of FPA-I anchor and the characteristics of the soil has been examined. There are also various types of flip anchors available in practice. Several studies of these similar flip anchors are described in the literature survey (Chapter 2). Based on the available technical data sheets, a comparative analysis was made of the $P_{ult}$ resulting from the same $(N_{60})_1$ on

different but similar soil properties. Pull-out tests were carried out on three different soil types; clayey sand, silty sand and low plasticit clay. Although the soils corresponding to the ultimate tensile resistances of the similar flip anchors shown in Table 3.6 are not exactly the same soil properties, an estimated comparison was made with different proportions of medium sandy and similar soils. Table 3.6 shows the geometry properties of similar flip anchors (SMA-1, SMA-2, SMA-3 and SMA-4) and the $P_{ult}$ values in the similar soil profiles. In the technical data sheets of the flip anchors with similar geometry, the $P_{ult}$ values are given as a range according to $(N_{60})_1$. $P_{ult}$ values were found by ratio-proportion within the given range according to $(N_{60})_1$.

Table 3.6 Dimension (L=length, W=witdh, H=Height) and $P_{ult}$ values of flip anchors similar to FPA-I anchor

| **Flip Anchor** | **$(N_{60})_1$** | **L x H x W (cm)** | **$P_{ult}$ (kN)** |
|---|---|---|---|
| **SMA-1** | 3-5 | 40x20x11 | 53 |
| | 5-20 | | 89 |
| | 20-30 | | 160 |
| **SMA-2** | 3-5 | 34x18x10 | 56 |
| | 5-20 | | 95 |
| | 20-30 | | 170 |
| **SMA-3** | 3-5 | 34x21x9 | 60 |
| | 5-20 | | 100 |
| | 20-30 | | 130 |
| **SMA-4** | 3-5 | 37x18x19 | 65 |
| | 5-20 | | 90 |
| | 20-30 | | 125 |
| **FPA-I** | 3-5 | 47.5x17x5 | 61.6 |
| | 5-20 | | 86.2 |
| | 20-30 | | 154 |

In Figure 3.11(b), the $P_{ult}$ of flip anchors with similar dimensional features is compared with the ultimate tensile resistance ($P_{ult}$) of FPA-I anchor tested in this study.

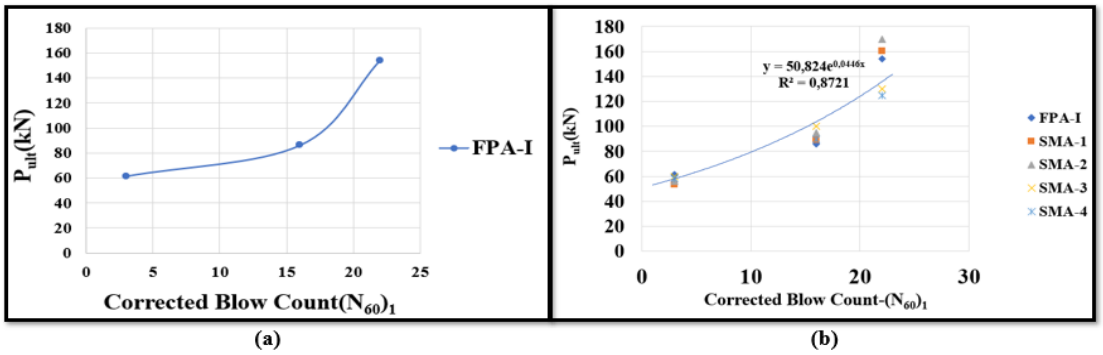


Figure 3.11 (a) $P_{ult}$ obtained from pull-out tests at different depths for FPA-I anchor (b) comparison of the Pult of the FPA-I anchor with other similar flip anchors

The graph shown in Figure 3.11(b) reveals that at similar $(N_{60})_1$ value, the ultimate tensile resistances ($P_{ult}$) are close to each other, so the results from field tests are consistent. An exponential function was developed between the $(N_{60})_1$ and the $P_{ult}$ (Equation 3.3).

$$P_{ult} = 50.824\, e^{0.0446(N_{60})_1} \tag{3.3}$$

Comparison of tensile resistance between similar flip anchors is of great importance, especially in evaluating and improving the structural integrity and operational feasibility of these types of anchors. By analyzing these forces under $(N_{60})_1$, researchers can evaluate the mechanical strength and load-carrying capacity of different flip anchor designs in similar soil conditions. This increases the accuracy of predictions regarding the behavior of flip anchors under different loading conditions, thus facilitating the verification of theoretical models.

### 3.4.4. The Pull-Out Test Result of FPA-II Anchor and Comparison with Similar Flip-Type Anchors

The field pull-out test of the FPA-II flip anchor consisted of experiments conducted at depths of 1.5 and 2.5 m, as detailed in Section 3.3.2. The correlation between SPT results and the tensile performance of the FPA-II anchor revealed details about the relationship between the $P_{ult}$ of the FPA-II anchor and the quality of the soil. The $P_{ult}$ relationship for FPA-II anchor by applying pull-out tests at two different depths with $(N_{60})_1$ is given in Figure 3.12(a). The $P_{ult}$ of the FPA-II anchor was measured as 37 kN at

a depth of 1.5 m in clayey sand layer. The $P_{ult}$ of 52.4 kN was measured in the silty sand layer at a depth of 2.5 m. The results show that, as the depth increased the ultimate tensile resistance of the flip anchor increased. Then, the ultimate tensile resistance of FPA-II anchors and similar flip anchors (SMA-I, SMA-2, and SMA-3) with similar dimensional characteristics as FPA-II were taken from technical data sheets. Table 3.7 shows the dimensions and $P_{ult}$ values of flip anchors similar to FPA-II. Figure 3.12(b) compares the $P_{ult}$ values of FPA-II and similar types of flip anchors. In the technical data sheets of the flip anchors with similar geometry, the $P_{ult}$ values are given as a range according to $(N_{60})_1$. $P_{ult}$ values were found by ratio-proportion within the given range according to $(N_{60})_1$.

Table 3.7 Dimension (L=length, W=witdh, H=Height) and $P_{ult}$ values of flip anchors similar to FPA-I anchor

| Flip Anchor | $(N_{60})_1$ | Lx Wx H (cm) | $P_{ult}$(kN) |
|---|---|---|---|
| **SMA-1** | 3-5 | 16x4.5x6 | 31 |
| | 5-20 | | 52 |
| **SMA-2** | 3-5 | 16.3x4.8x6 | 30 |
| | 5-20 | | 50 |
| **SMA-3** | 3-5 | 15x4x5 | 20 |
| | 5-20 | | 46 |
| **FPA-II** | 3-5 | 16.3x4x4 | 37 |
| | 5-20 | | 52.4 |

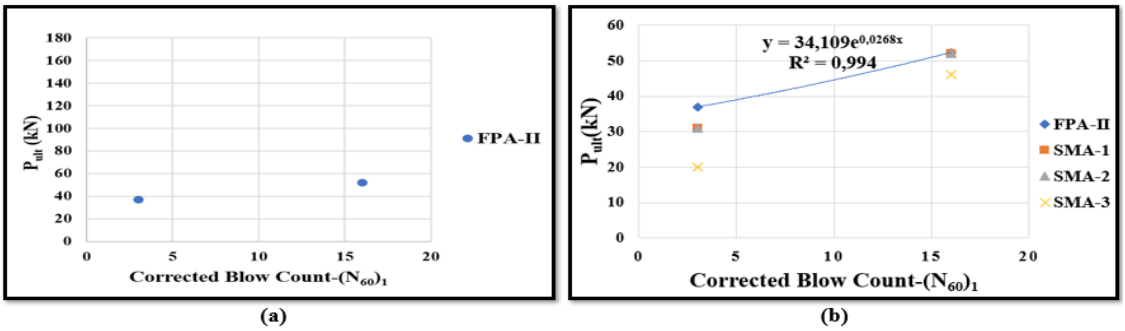


Figure 3.12 (a) Pult obtained from pull-out tests at different depths for FPA-II anchor (b) comparison of the Pult of the FPA-II with other similar flip anchor

An exponential function was developed between the $(N_{60})_1$ and the $P_{ult}$ for FPA-II anchor (Equation 3.4).

$$P_{ult} = 34.109\, e^{0.0268(N_{60})_1} \tag{3.4}$$

Similar $P_{ult}$ values were observed at corresponding $(N_{60})_1$ value, as depicted in Figure 3.12(b). Nevertheless, the maximum tensile resistance of SMA-3 was lower than that of the FPA-II anchor. This could be related to the somewhat smaller surface area of SMA-3 (60 $cm^2$) in comparison to other SMA's and FPA-II anchor.

### 3.4.5. The Comparison of FPA-I and FPA-II Anchors, and Similar Flip-Type Anchors

Combining Figures 3.11(b) and 3.12(b) Figure 3.13 plotted to compare the two flip anchors (FPA-I and FPA-II anchors) and other flip-type anchors available in practice.

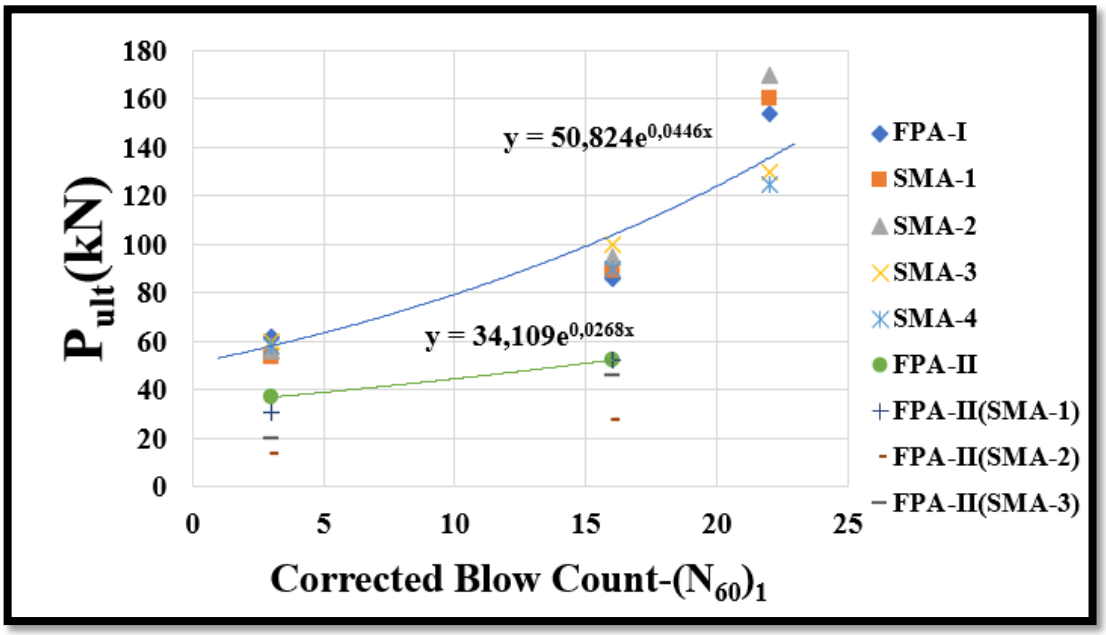


Figure 3.13 Comparison of the $P_{ult}$ of the FPA-I, FPA-II anchors and similar flip anchors

Figure 3.13 shows that FPA-I anchor and similar flip anchors have a higher ultimate tensile resistance than FPA-II anchor and similar flip anchors. This is because FPA-I and similar flip anchors have a larger area of anchors than FPA-II anchor and

similar flip anchors. Additionally, the FPA-I anchor exhibits a more recessed and protruding shape when viewed from the perspective of its geometry, whereas the FPA-II's geometry is flatter than FPA-I anchor. The FPA-I's geometry has demonstrated a higher tensile resistance by optimizing the load-lock mechanism in the soil by adjusting the angle of the indentation and edges.

It is important to note that this comparison was based on estimates due to the lack of detailed technical specifications for flip anchors from alternative sources. Data on ultimate tensile resistance was approximately obtained from available source information. Although comprehensive technical sheets were not available, the exponential equation obtained using the approximation method of FPA-I and FPA-II anchors has been determined by making predictions to facilitate a comparative understanding of the performance characteristics of similar-sized flip anchors under equivalent impact conditions. This approach provides a preliminary and informative analysis of the performance of these flip anchors, laying the foundation for empirical research in this field of study.

In the study of Emirler et al., (2016), laboratory model tests were carried out on single and group anchor plates to investigate the effect of anchor plates on pull-out capacity. They used the breakout factor (Fq) from dimensionless parameters to compare the test results. They compared this to the breakout factor as in Equation 3.5.

$$F_q = \frac{Q_u}{\gamma_d \, \mathrm{H} \, \mathrm{A}} \tag{3.5}$$

"Fq" in Equation 3.5 represents the breakout factor, "A" is the area of the anchor plate, "γd" is the dry unit weight of the soil, and "H" is the embedment depth. Based on Equation 3.5, a relationship as in Equation 3.6 was developed for flip anchors. This comparison is between the ultimate pull-out factor ($P_{ult(fac)}$) and $(N_{60})_1$. The ultimate pull-out factor is defined in Equation 3.6:

$$P_{ult(fac)} = \frac{P_{ult}}{\gamma \, \mathrm{H} \, \mathrm{A}} \tag{3.6}$$

For the dimensionless parameters comparison (ultimate pull-out factor) of FPA-I and other similar flip anchors used in practice (SMA-1, SMA-2, SMA-4 and SMA-4), the Pult values in Table 3.6 were used and the γ values were compared according to the soil

unit weight values at the field where the tests were performed. The pull-out factor – $(N_{60})_1$ comparison of FPA-I and other similar anchors is as shown in Figure 3.14.

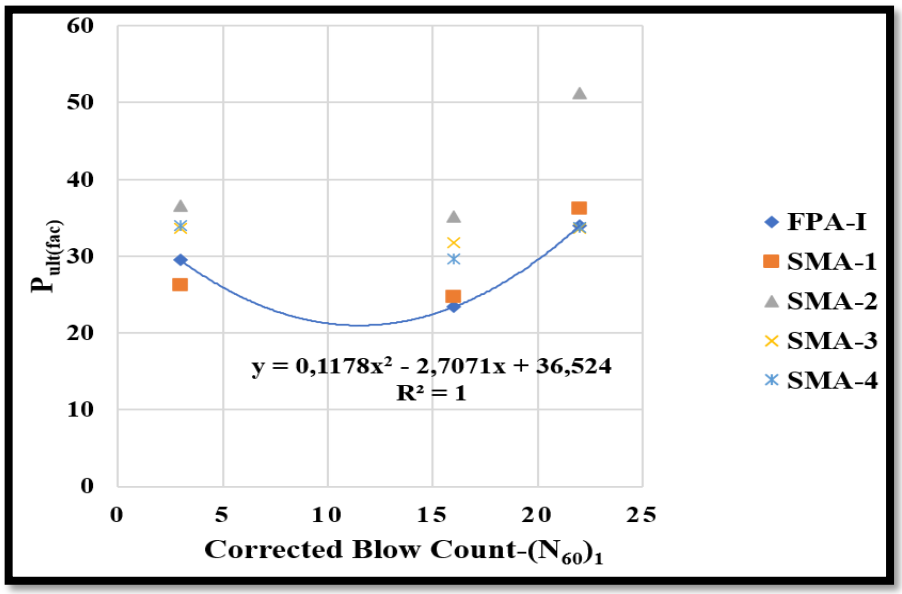


Figure 3.14 Comparison of the $P_{ult(fac)}$ of the FPA-I anchor with other similar flip anchors

In the graph shown in Figure 3.14, a polynomial function was developed between (N60)1 and the pull-out factor Pult(fac) using dimensionless parameters (Equation 3.7).

$$Pult_{(fac)} = 0.12(N_{60})_1{}^2 - 2.71(N_{60})_1 + 36.52 \quad (3.7)$$

The equation in Figure 3.14 shows that the pull-out factor initially decreases, reaches a minimum, and then increases with increasing blow count. This suggests an optimal range of corrected blow counts where the pull-out resistance is minimized before growing again. This behavior results from complex interactions between soil density, compaction, and tensile resistance mechanisms.

Using the same procedure for FPA-II and similar flip anchors used in practice, the ultimate pullout values ($P_{ult}$) in Table 3.7 were used. Applying Equation 3.6, the relationship between the $P_{ult(fac)}$ and $(N_{60})_1$ is shown in Figure 3.15.

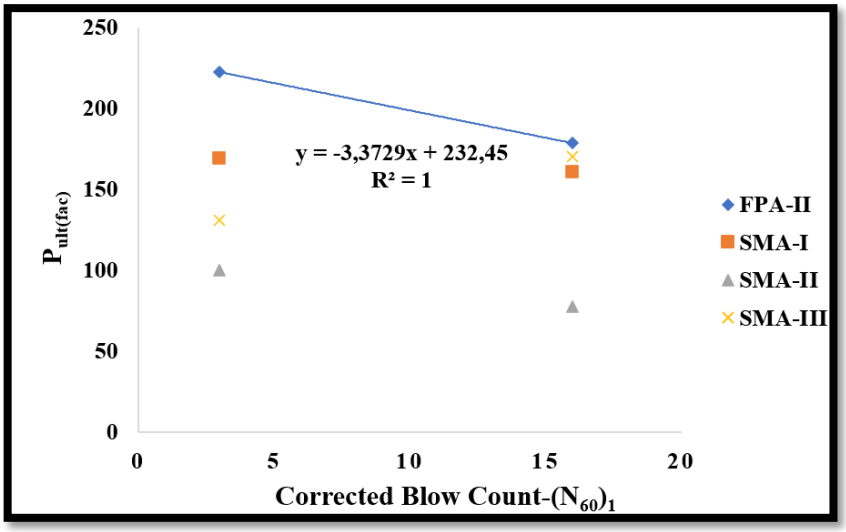


Figure 3.15 Comparison of the $P_{ult(fac)}$ of the FPA-II anchor with other similar flip anchors

In the graph shown in Figure 3.16, a polynomial function was developed between $(N_{60})_1$ and the pull-out factor $P_{ult(fac)}$ using dimensionless parameters (Equation 3.8).

$$Pult_{(fac)} = -3.37(N_{60})_1 + 232.45 \quad (3.8)$$

Higher corrected blow counts$(N_{60})_1$ typically indicates denser or more compact soils, as shown in Figure 3.15. The decrease in ultimate tensile resistance with the increasing $(N_{60})_1$ demonstrates that flip anchors may perform differently in dense soils than loose ones. In dense soils, mechanical interlocking and friction between soil particles can be reduced by flip anchor, which can lead to lower tensile resistance. In soils with a high corrected impact number, alternative fixing methods or assembly methods can be developed to achieve the desired tensile resistance. Accurate predictions of tensile resistance ensure that the anchor system performs as expected under various loading conditions, improving the overall safety and reliability of the structure.

The combination of Figures 3.14 and 3.15 Figure 3.16 plotted to compare the two flip anchors (FPA-I and FPA-II anchors) and other flip-type anchors available in practice.

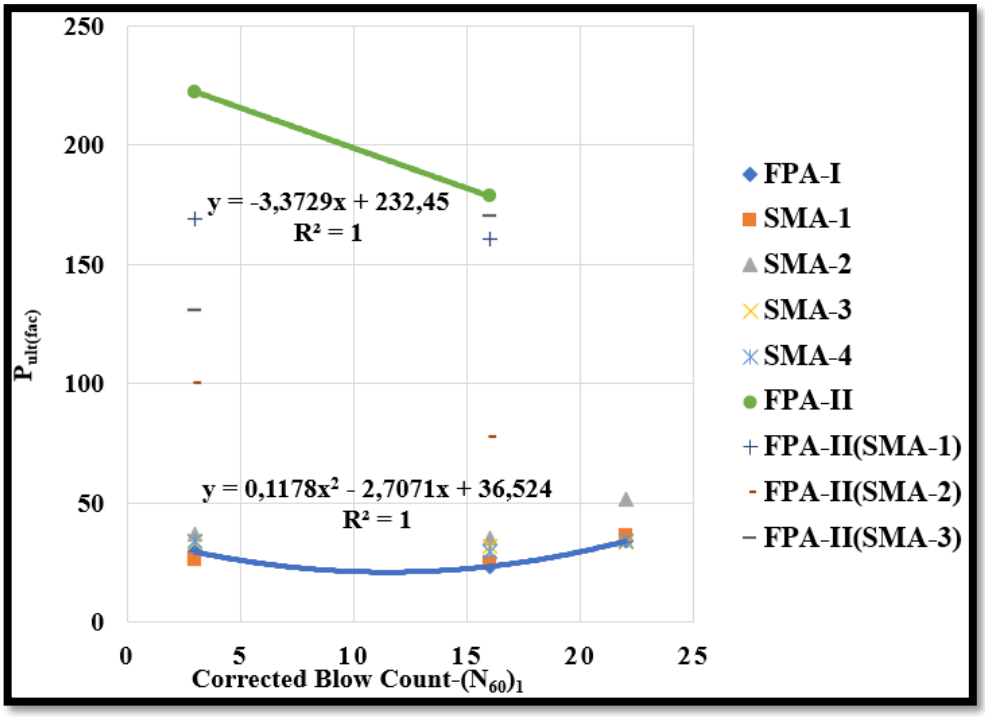


Figure 3.16 Comparison of the $P_{ult(fac)}$ of the FPA-I, FPA-II and similar flip anchors

As shown in Figure 3.16, the FPA-II anchor appears to experience a steady decrease in resistance as the soil becomes more compact (higher number of corrected blow counts). This may be due to the loss of interlock between soil particles and the flip anchor surface as compaction increases, or it may be due to a temporary condition such as soil expansion, where the initial resistance decreases with the increasing $(N_{60})_1$. The FPA-I anchor may be more efficient in certain soil conditions because it can take advantage of increased compression to regain or even improve tensile resistance after the initial decline.

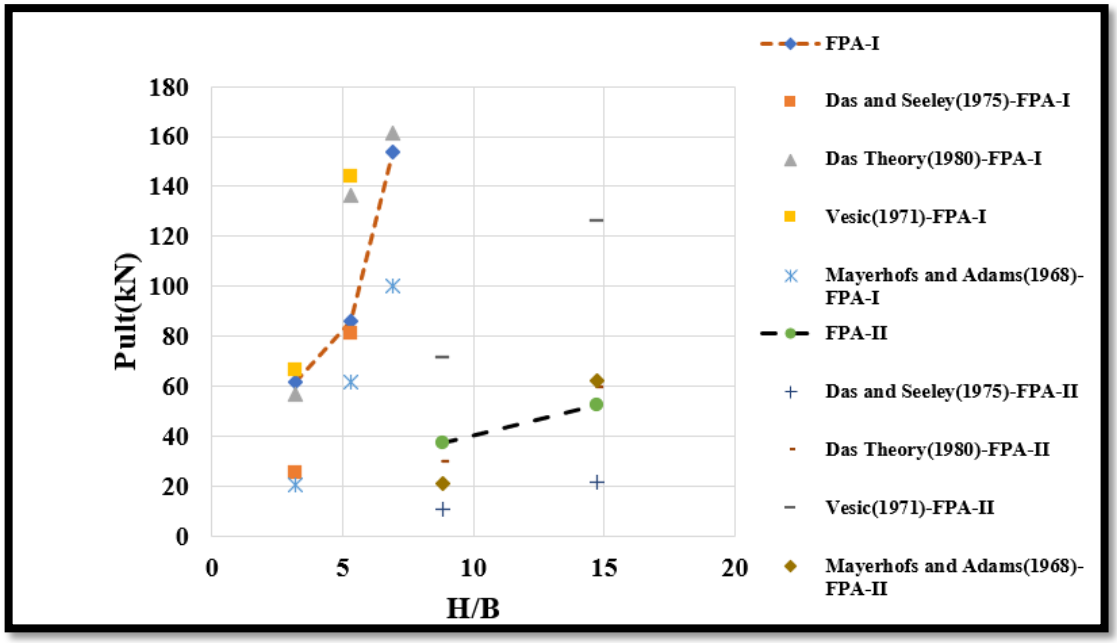


Figure 3.17 The comparison of FPA-I and FPA-II anchors with $P_{ult}$ formulas in the literature

In general, examination of formulas in other literature and FPA-I anchoring demonstrated satisfactory concordance at lower H/B ratios (H/B ≈ 5), yet field results diverged significantly at higher H/B ratios. In FPA-II, the trend was comparable to the field results at lower H/B ratios, yet a discrepancy emerged as H/B increased. Discrepancies between field results and theoretical models underscore the intricacy of soil-flip anchor interactions. While models offer valuable insights, it is essential to exercise caution when interpreting their results, given the variability in soil properties and behaviour observed in the field.

## 3.5. Conclusion

Total of 5 pull-out tests were performed by a hydraulic jack for FPA-I and FPA-II anchors, at designated points in the field. The ultimate tensile capacities of FPA-I anchor were found in 3 different soil profiles and it was seen that the highest tensile resistance was 3.25 m in low plastic clay soil. Then, the ultimate tensile capacities of FPA-I anchor and similar flip anchors on the practice were compared in similar soil properties. As a result of the comparison, it was seen that FPA-I anchor and similar flip anchors had similar ultimate tensile resistances. The same analyses were carried out on 2

different soil profiles in FPA-II anchor, providing preliminary information about the ultimate tensile resistance.

In general, it was observed that the ultimate tensile resistance increases as the depth increases in both flip anchors. In the same soil profiles, the ultimate tensile resistance of FPA-I anchor was approximately 50% higher than the ultimate tensile resistance of FPA-II anchors. This is because the dimensions and geometric design of FPA-I anchor are different from FPA-II anchor and it is better with the soil interaction. In the numerical studies, the $P_{ult}$ that was obtained from the field were used as input values in the numerical model that will be explain in Chapter 4. The displacement of the soil during the pull of the flip anchors and the total principal stress changes in the soil were analysed.

# CHAPTER 4

# NUMERICAL MODELING OF FLIP ANCHORS

## 4.1. Introduction

In the numerical modeling, the 2D finite element method (FEM) was used to analyze FPA-I and FPA-II anchors. They were evaluated under ultimate tensile forces obtained from the field tests Chapter 3. The load phase input values for the program were $P_{ult}$ values obtained from the pull-out test at the site. The research was performed at different placement depths using the commercially available finite element program, PLAXIS-2D. The results provided an accurate representation of the operating environment of the flip anchors. An investigation into the total principal stress response and displacement of the soil strata surrounding the flip anchors was the principal aim of the numeric modeling.

## 4.2. Geometry of the Model

The numerical model generated to reflect distinct soil profiles identified during field experiments must accurately represent the physical characteristics of the field conditions. This is one of the most critical aspects of numerical analysis. Figure 4.1 shows the 2D finite element models of soil, FPAI, and FPA-II anchors. The flip anchors were placed at the desired depths of soil within the model to simulate their effective interaction with the soil. In order to effectively investigate the displacement of the soil pattern and the total principal stress distribution due to the applied tensile force, it is crucial to position the flip anchors and ensure adequate soil coverage.

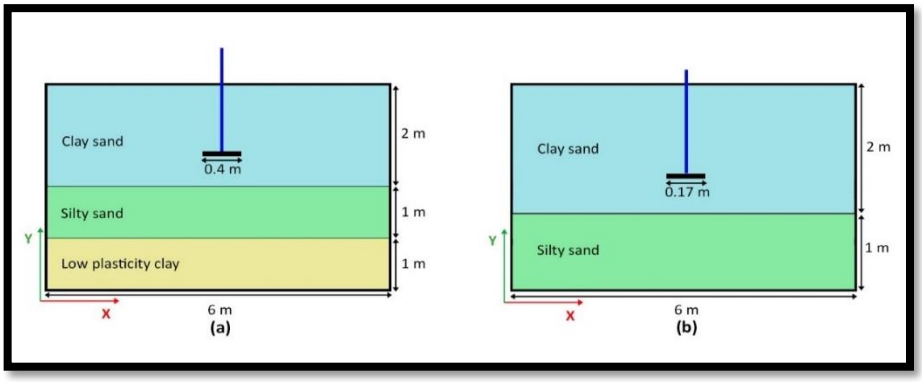


Figure 4.1 2D model geometry a)FPA-I, and b)FPA-II anchors

## 4.3. Boundary Conditions and Mesh in Numerical Model

The model focused on the vertical orientation of the primary stress and displacement responses, which are crucial for the performance of the flip anchor under tensile applied load. Figure 4.2 shows the side and bottom boundary conditions of the model. This was achieved by restricting horizontal and vertical movement. The free upper bound enabled the surface to respond naturally to applied tensile loads, allowing surface deformations and displacements to be captured realistically.

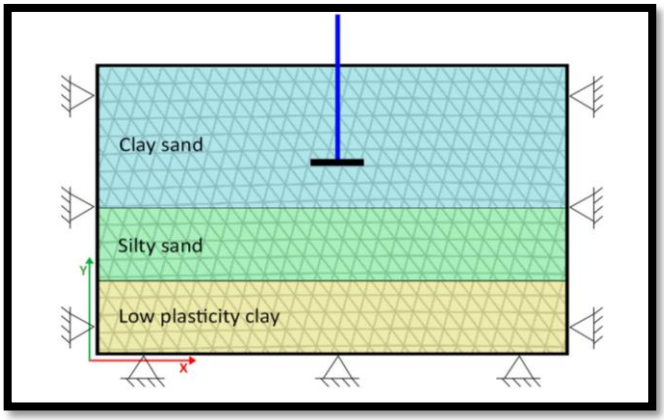


Figure 4.2 Boundary conditions of the model

It was also examined at 8 m and 10 m, as well as at 6 m, to observe the lateral effect. In the examination, by applying a load of 124 kN, which is the ultimate tensile force, at the shallowest depth (1.5m), the principal stress change at 8 m is shown in Figure 4.3(a) and the principal stress change at 10m is shown in Figure 4.3(b).

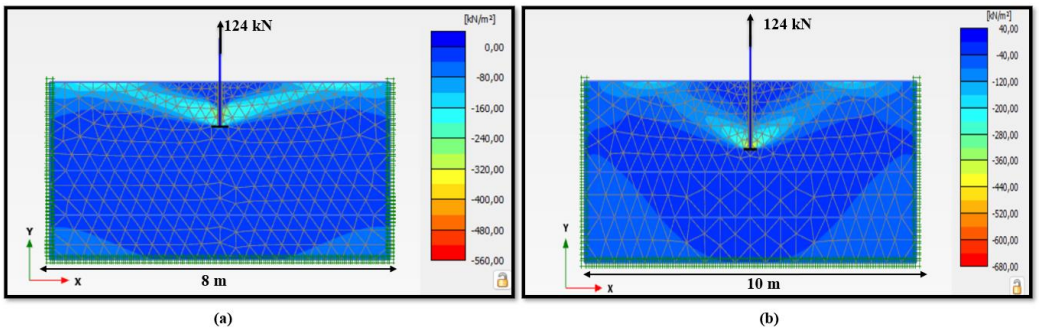


Figure 4.3 (a) x = 8 m principal stress change in the soil (b) x = 10 m principal stress change in the soil

In examining the lateral effect of 6 m, 8 m, and 10 m, it was observed that while the principal stress remained consistent in both 6 m and 8 m, the principal stress change rate in 10 m exhibited an approximate 20% increase in comparison to both 6 m and 8 m. Furthermore, the displacement changes in the soil at x = 8 m are illustrated in Figure 4.4(a), while displacement changes in the soil at x = 10 m are presented in Figure 4.4(b).

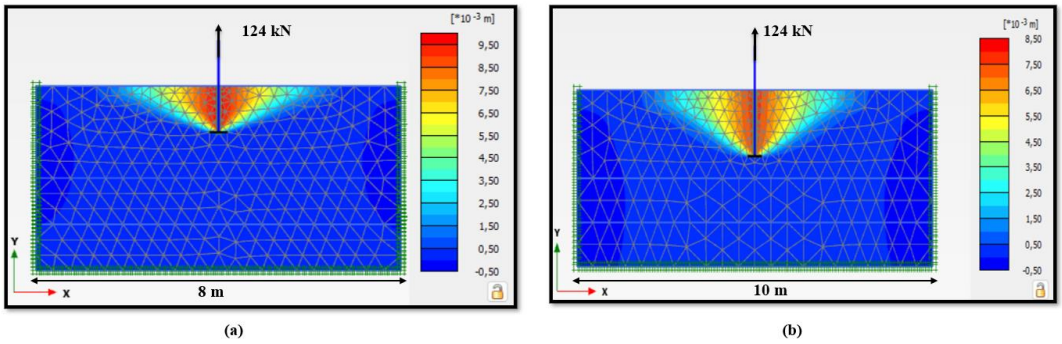


Figure 4.4 (a) x = 8 m displacement changes in the soil (b) x = 10 m displacement changes in the soil

In an examination of Figure 4.4(a) and (b), the displacement appears to decrease as the lateral distance increases. In the model's geometry, when x (lateral distance) was increased from 6 m to 8 m, the displacement changes on the ground decreased by approximately 15%, while when it was increased from 8 to 10 m, it decreased by approximately 10%. Considering the displacement and principal stresses in the soil, numerical analyze was made as x = 6 m, since x = 6 m (lateral distance) gives more realistic results for the field.

In numerical analysis, especially in the context of FEM, the selection of mesh spacings plays a critical role in defining the level of detail and accuracy of simulation results. The choice of mesh spacings is crucial for the analysis of numerical model results and the determination of soil properties, as it directly influences the solution with which the model can represent physical phenomena. The frequency of network intervals is very important in increasing the precision of analysis results (Wu et al., 2020). A finer mesh typically allows for a more detailed representation of soil properties and interactions between different model elements, such as interfaces between soil layers or soil-flip anchor interactions. In order to obtain detailed information about the soil behavior around a flip anchor, this study has constructed a finite element model with a particularly fine mesh. When the analyses were performed on the medium mesh and coarse mesh, close soil displacements and stress variations were observed between all meshes. In the numerical analysis section, a comparison of the mesh change when the largest tensile force is applied for the larger anchor FPA-I is performed. However, by setting $R_{inter}$ to 0.8 for soil-flip anchor interaction, the interaction between the anchor surface and the soil was modeled weaker than the surrounding soil. Considering the results, the Rinter was chosen as rigid ($R_{inter}$ =1) since similar results were obtained in displacement and stress changes between 1 and 0.8.

## 4.4. Soil Parameters and Materials Used

The Mohr-Coulomb model was selected for soil modeling to facilitate a fundamental investigation of soil behavior under varying load conditions. The selection of this model is driven by its relative simplicity and the basic nature of its parameters, which are readily available from standard geotechnical testing procedures. Other more advanced constitutive models, such as the Hardening Soil Model, were not utilized due to the unavailability of specific parameters required for their accurate application. These parameters include but are not limited to, the secant stiffness in drained triaxial tests and the tangent stiffness for oedometer loading. Acquiring and accurately determining these parameters would necessitate extensive and sophisticated testing, which was beyond the scope of this study. Additionally, purely elastic models were deemed inappropriate for this analysis, as they failed to capture the inherent plasticity and non-linear behavior of soil during the pullout of anchors. The soil's response to loading and unloading involves

irreversible deformations and non-linear stress-strain relationships, which an elastic model cannot accurately represent. This decision was supported by the fact that the model is based on fundamental but critical soil parameters, such as cohesion (c) and angle of internal friction (ϕ), which are important in determining the shear strength of the soil. Since the unit weight of soil could not be determined exactly in laboratory tests and the direct shear test was not performed, the weight of the soil and elasticity modulus of the soil at the desired depth were determined using the formulas suggested by Tezcan et al. (2009):

$$\gamma = \gamma 0 + 0.002 Vp \quad (4.1)$$

In the equation $V_p$ is P-wave velocity in m/s, $\gamma_0$ reference unit weight values in kN/m$^3$. As a result of the MASW test, which is the seismic method performed in the field, the $V_p$ values measured at the specified depth in Table 3.2 were used in the equation to find the unit weight of each soil profile at each depth. Unit soil weights were calculated by taking $\gamma_0$ = 16 kN/m$^3$ for, silty sand, poorly sand and clayey soils and $\gamma_0$ = 17 kN/m$^3$ for sand. The shear modulus (G) of the soils was calculated using Equation 4.2:

$$G = \gamma Vs\ 2/g \quad (4.2)$$

G is the shear modulus of the soil and $V_s$ is the shear wave velocity (m/s). These values were obtained from the seismic tests performed in the site investigations. After finding the G of each soil, the elastic modulus (E) of each soil was calculated using Equation 4.3. The E is derived from the fundamental linear relationship observed between strain during elastic deformation and the corresponding normal stress, which is both tensile and compressive forces.

$$E = 2G\ (1+v) \quad (4.3)$$

In Equation 4.3, E is the modulus of elasticity in the soil (kPa), and v represents the Poisson's ratio. The friction angle (ϕ) value for clayey sand layer was calculated using Equation 4.4 (Bashar, 2000).

$$\phi = 7.1 \log_{10} N + 29.8 \quad (4.4)$$

The value of N shown in the equation represents the number of blow counts obtained at 1.5 m in the SPT. The friction angle for silty sand and low plastic clay layer was obtained using Equation 4.5 proposed by Hatinaka and Uchida (1996).

$$\phi = \left(\sqrt{20(N_1)_{60}}\right) + 20 \quad (4.5)$$

Sivrikaya (2009) used an artificial neural network model to determine the cohesion relationship between SPT, water content (w), LL (liquid limit), and PI (plasticity index) using data obtained from Turkish construction companies and laboratories and developed an equation as in Equation 4.6.

$$c = 2.41N - 0.82w + 0.14LL + 1.44\text{PI} \quad (4.6)$$

Cohesion values for clayey sand and low plasticity clay was found using Equation 4.6 and for silty sand using Equation 4.7 (Sivrikaya & Toğrol, 2006).

$$c = 4.68N_{field} \quad (4.7)$$

In Equation 4.7, the cohesion value for silty sand was calculated according to the SPT-N at the depth of 2.5m. The soil parameters used in the numerical model related to the equations given above are shown in Table 4.1.

Table 4.1 Soil parameters used in the model

| Soil Parameters | Clayey Sand(ciSa) | Silty Sand(siSa) | Low Plastic Clay (CIL) |
|---|---|---|---|
| $V_p$ (m/sn) | 379 | 465 | 331 |
| $\gamma$ (kN/m$^3$) | 17 | 18 | 17 |
| $V_s$(m/sn) | 200 | 264 | 343 |
| G(kPa) | 72408 | 120281 | 203806 |
| E (kPa) | 188260 | 300702 | 529540 |
| $\phi$($^o$) | 33 | 38 | 41 |
| c(kN/m$^2$) | 32 | 75 | 76 |

The anchor rope that was used in the field was defined as the plate in the set type of the Plaxis 2D program. A flip anchor is defined as the anchor. Since the flip anchor is made of galvanized cast steel, the elasticity modulus taken from the manufactured factory was used. The anchor rope was made of high carbon steel. Table 4.2 shows the parameters entered for the flip anchor and anchor rope in the numerical model.

Table 4.2 The properties of the anchor rope and flip anchor used in the FEM model

| Material | Anchor Rope | Flip Anchor |
|---|---|---|
| Elastic Modulus (kPa) | $1.98x10^8$ | $9.8x10^5$ |
| Moment Of Inertia (I) | 0.052 | 0.002 |
| EI | $1.041x10^7$ | N/A |
| EA | N/A | $6.7x10^4$ |

## 4.5. Pull-out Force in Numerical Model

Field pull-out tests were performed on FPA-I and FPA-II anchors, as described in Chapter 3. For this numerical study, the ultimate tensile resistances shown in Figure 3.13 (a) and Figure 3.14 (a) were used. Thereby, the ultimate tensile resistance of the FPA-I anchor found at the site at 1.5 m was taken as the input value of the load phase in the numerical model. Additionally, an interface was created to facilitate the interaction (positive (+) and negative interface (-) between the flip anchor and the surrounding soil during the load phase. This interface is crucial in determining potential relative displacements and principal stress changes between the flip anchor and the soil.

A numerical analyze was performed to evaluate the behavior of FPA-I anchor by modeling different $P_{ult}$ at 3 different depths (1.5 m, 2.5 m, and 3.25 m). Similarly, numerical analyses were carried out at depths of 1.5 m and 2.5 m for the FPA-II anchor. Analyses were conducted with a focus on evaluating the principal stresses and displacements of the surrounding soils around the flip anchor. The results of these analyses were carried out to obtain information about the performance of FPA-I and FPA-II anchors and their behavior in different soil profiles.

### 4.5.1. Numerical Analysis Results

The numerical analysis consisted of two phases, as explained below:

1. In the first part, numerical analyze was performed by applying a load obtained from the field pull out test results given in Figure 3.11(b) and Figure 3.12(b) in Chapter 3 for FPA-I and FPA-II anchors, respectively. The tensile forces obtained from the equations were used as load phase input values in the numerical program. As a result, the maximum

displacement and maximum principal stress changes in the soil were observed under different tensile load conditions at different depths.

2. In the second part, as a result of the first part for FPA-I and FPA-II anchors, certain stress points and node points were determined in the soil. The selected poits were at the upper side and lower side of the soil surrounding the flip anchors. As a result, the displacement and soil principal stress changes in the soil surrounding the flip anchor at different depths were closely examined.

#### 4.5.1.1. Numerical Analysis with Empirical Equations

For FPA-I anchor, Equation 3.3 obtained from Figure 3.11(b) was used. Equation 3.3 shows a relationship between $(N_{60})_1$ and $P_{ult}$. Firstly, for FPA-I at 1.5 m, $(N_{60})_1$ was gradually increased until the soil body collapsed. The $P_{ult}$ values corresponding to each $(N_{60})_1$ obtained from Equation 3.3 were entered into the numerical model as tensile load input values, respectively, and numerical analysis was carried out. Table 4.3 shows the $P_{ult}$ values corresponding to $(N_{60})_1$ for each depth.

Table 4.3 Tensile applied load ($P_{ult}$) for FPA-I anchor in numerical analysis

| Anchor name | Depth(m) | $(N_{60})_1$ | $P_{ult}$(kN) (From eq 3.3) |
|---|---|---|---|
| FPA-I | 1.5 | 3 | 61.6 |
| | | 10 | 79.4 |
| | | 15 | 99.2 |
| | | 20 | 124 |
| FPA-I | 2.5 | 3 | 61.6 |
| | | 10 | 79.4 |
| | | 15 | 99.2 |
| | | 20 | 124 |
| FPA-I | 3.25 | 3 | 61.6 |
| | | 10 | 79.4 |
| | | 15 | 99.2 |
| | | 20 | 124 |

The maximum displacements and maximum total principal stresses corresponding to each applied tensile force were recorded from the numerical output results. The maximum displacements corresponding to each applied tensile load ($P_{ult}$) of FPA-I anchor at 1.5 m are shown in Figure 4.5.

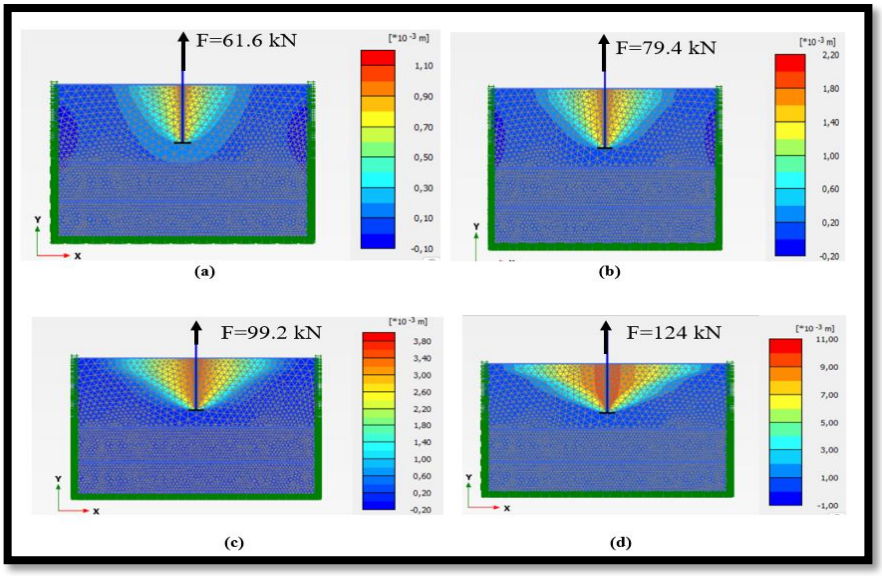


Figure 4.5 For the FPA-I anchor, the maximum displacement versus applied tensile loads obtained from Eq. 3.3 at a depth of 1.5 m a) F= 61.6 kN b) F=79.4 kN c) F=99.2 kN, and d)F=124 kN

The $P_{ult}$ derived from Equation 3.3 at 2.5 and 3.25 m for FPA-I anchor were utilized as input values in the numerical study. The maximum displacements on the soil that corresponded to these $P_{ult}$ were observed using the same methodology. Figure 4.6 shows the maximum displacement of FPA-I anchor in the soil at 2.5 m, while Figure 4.7 shows the maximum displacement of this anchor in the soil at 3.25 m.

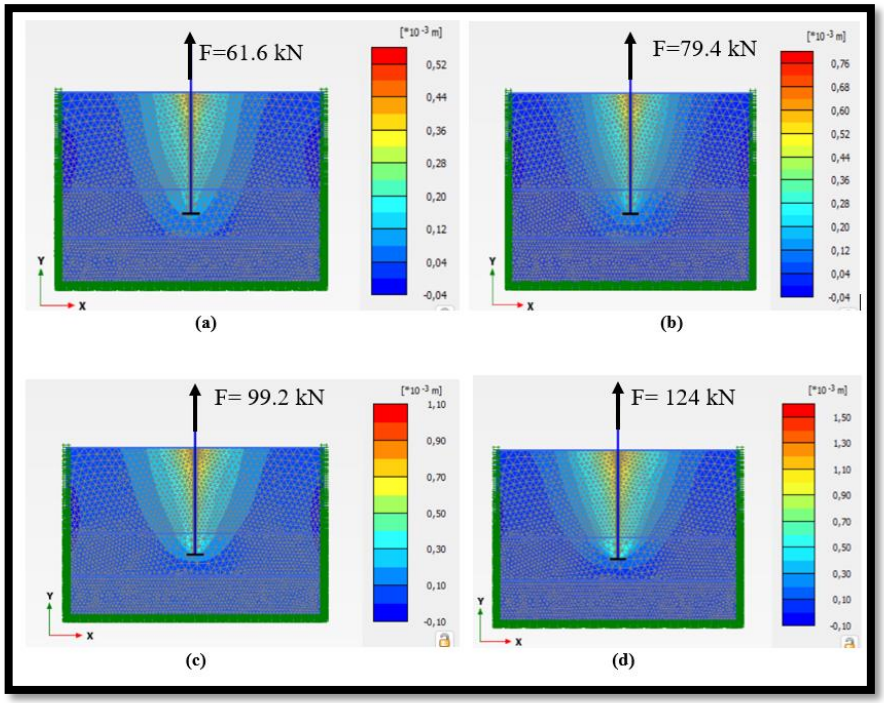


Figure 4.6 For the FPA-I anchor, the maximum displacement versus applied tensile loads obtained from Eq. 3.3 at a depth of 2.5 m. a) F= 61.6 kN b) F=79.4 kN c) F=99.2 kN, and d) F=124 kN

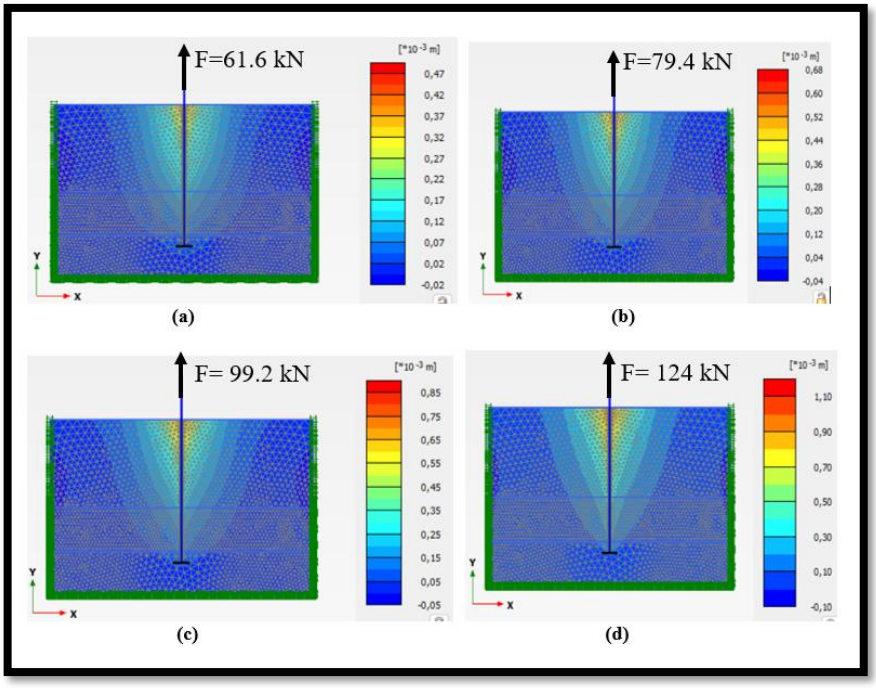


Figure 4.7 For the FPA-I anchor, the maximum displacement versus applied tensile loads obtained from Eq. 3.3 at a depth of 3.25 m a) F=61.6 kN b) F= 79.4 kN c)F=99.2kN, and d)F =124 kN

When Figures 4.5, 4.6 and 4.7 were examined, the displacement of the soil around the anchor rope found higher in 1.5 m of clayey sand, which is the soil layer closest to where the tensile force is applied. The soil layer closest to where the tensile force is applied experiences the greatest displacement concentration. When clayey sand is at a depth of 1.5 m, it is directly subjected to tensile force, resulting in increased displacement. As the depth increases, the total principal stress the tensile force creates spreads over a larger soil volume, and the displacement noticed in the deeper layers' decreases.

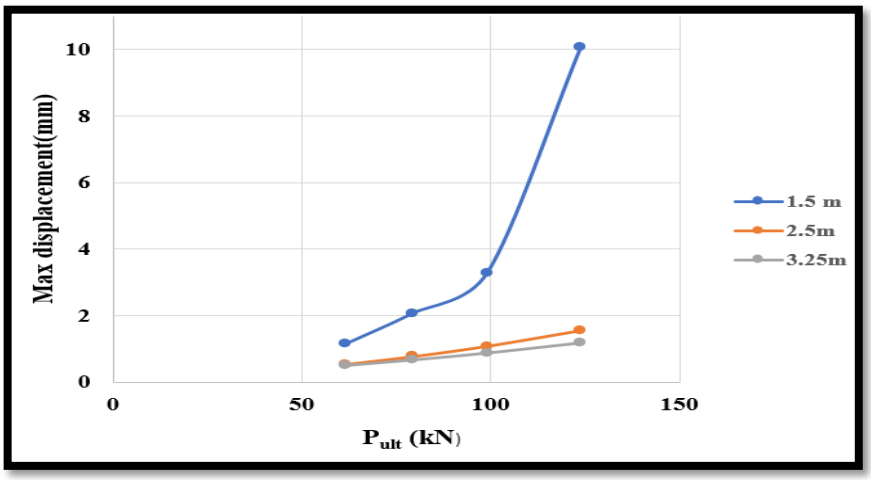


Figure 4.8 Maximum displacement -tensile applied load ($P_{ult}$) correlation for FPA-I anchor obtained from Eq. 3.3

Figure 4.8 shows the maximum displacements resulting from applying tensile loads at different depths. The figure shows that for the same applied $P_{ult}$, the maximum displacement decreases approximately 65% between 1.5 m and 2.5 m and 20% between 2.5 m and 3.25 m as the depth increases. Since the depths of 2.5 m and 3.25 m are close to each other, less displacement was observed compared to the other layer. Furthermore, the clayey sandy soil profile at a depth of 1.5 m generally exhibits a reduced shear strength in comparison to low-plasticity clay soil. When the flip anchor was pulled, the layer of clayey sand soil experienced greater displacements as a result of reduced shear strength and frictional resistance. Low plastic clay soil generally exhibits greater shear strength and frictional resistance compared to sandy soils. Moreover, the reduced particle size of clay enhances the interlocking mechanism between particles, hence augmenting the frictional resistance. Additionally, the maximum soil displacement comparison in Figure 4.8 was made using a fine mesh. For FPA-I, the coarse and medium mesh was used to observe the displacement changes between the shallow depth (1.5 m) and maximum

tensile force (124 kN) between comparisons, as shown in Figure 4.7. Figure 4.9(a) represents the displacement contour resulting from the coarse mesh and Figure 4.9(b) represents the displacement contour resulting from the medium mesh. When fine, coarse, and medium meshes are applied, the same displacement changes are observed at 61.6 kN, 79.4 kN, and 99.2 kN, while a difference of 20% is observed when 124 kN tensile load is applied. Since the difference was negligible, numerical analysis was continued with the fine mesh.

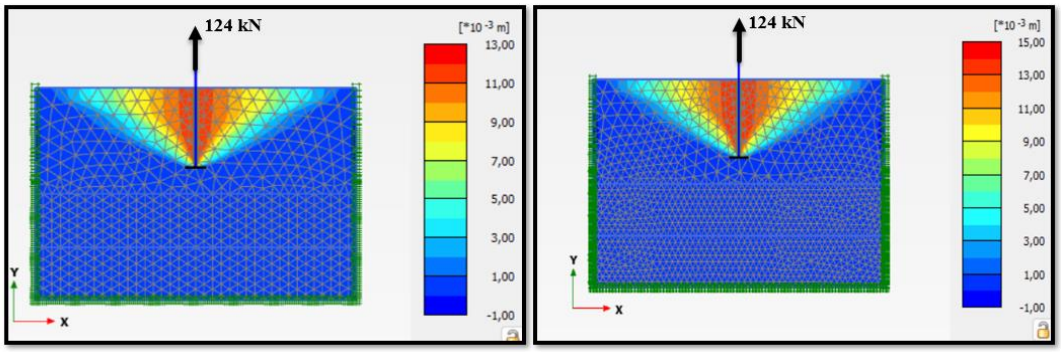


Figure 4.9 (a) Soil displacement change resulting from using coarse mesh (b) Soil displacement change resulting from using medium mesh

Applying the same procedures (using Equation 3.3), maximum total principal stresses were observed in the response of the soil to tensile load at each depth. Figure 4.10 shows the maximum total principal stress versus applied tensile loads obtained from Eq. 3.3 at a depth of 1.5 m.

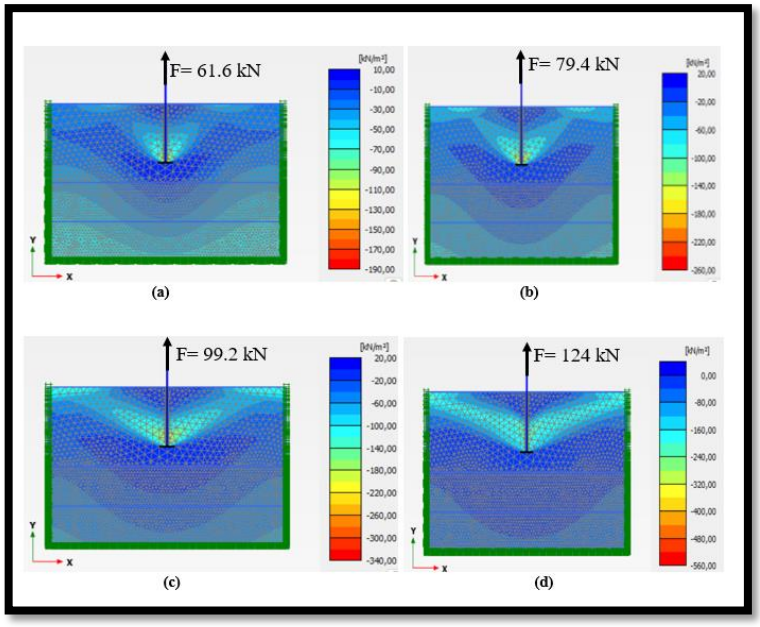


Figure 4.10 For the FPA-I anchor the maximum total principal stress versus applied from Eq. 3.3 at a depth of 1.5 m a) F=61.6 kN b) F=79.4kN c) F=99.2 kN and d)F=124 kN

Figure 4.11 shows the maximum total principal stress versus applied tensile loads obtained from Eq. 3.3 at a depth of 2.5 m and Figure 4.12 shows the maximum total principal stress changes in the soil at 3.25 m.

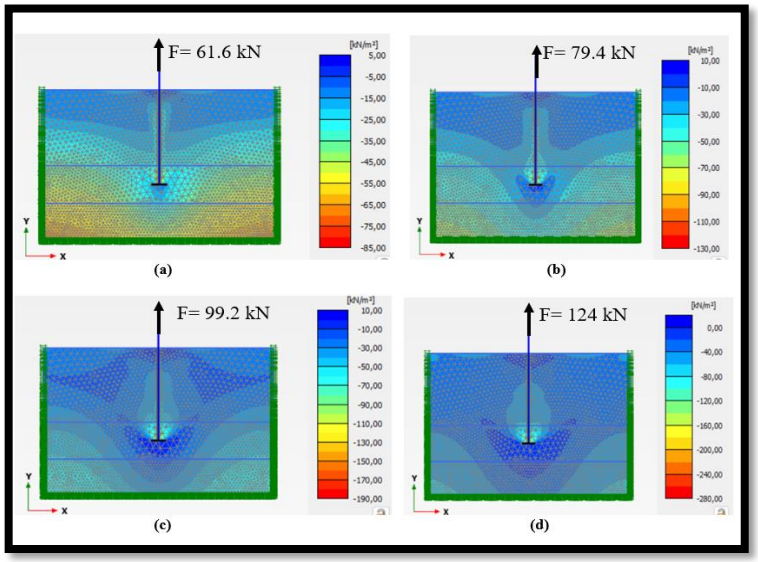


Figure 4.11 For the FPA-I anchor, the maximum total principal stress versus applied tensile loads obtained from Eq. 3.3 at a depth of 2.5 m a) F=61.6 kN b) F= 79.4 kN c) F =99.2 kN, and d) F=124 kN

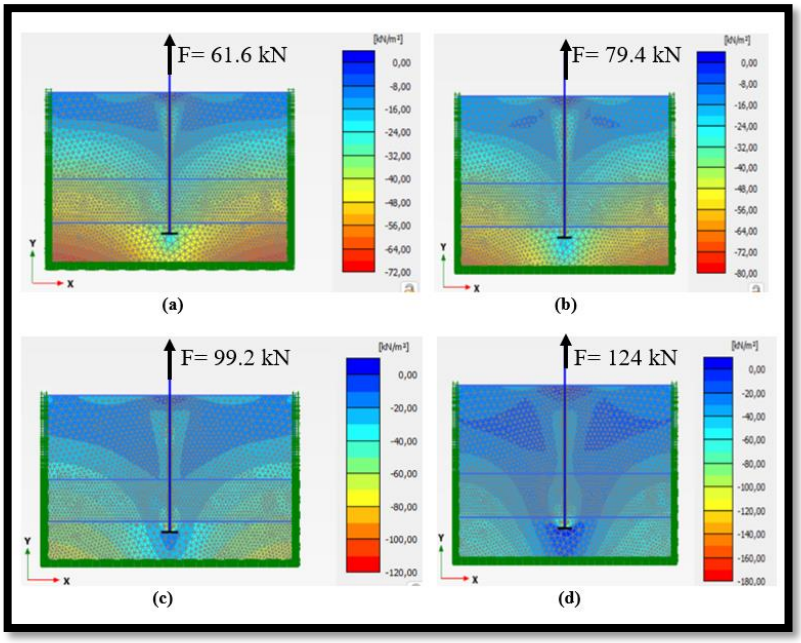


Figure 4.12 For the FPA-I anchor, the maximum total principal stress versus applied tensile loads obtained from Eq. 3.3 at a depth of 3.25 a) 61.6 kN b)79.4 kN c)99.2kN,and d)124 kN

Figures 4.10, 4.11, and 4.12 show that there was significant maximum total principal stress in the soil at a depth of 1.5 m near the surface. When $P_{ult}$ was applied from a distance of 1.5 m, the soil layer at the bottom of the anchor showed more negative swelling than the soil layers at different depths, causing the soil to rise in the opposite direction of the applied stress. Silty sand soils result in a more uniform weight distribution because they consist of fine particles with moderate cohesion and shear strength. Low plasticity clay, due to its cohesive nature and plasticity, can provide a relatively stable and uniform stress distribution under loads compared to more compressible and heterogeneous soils.

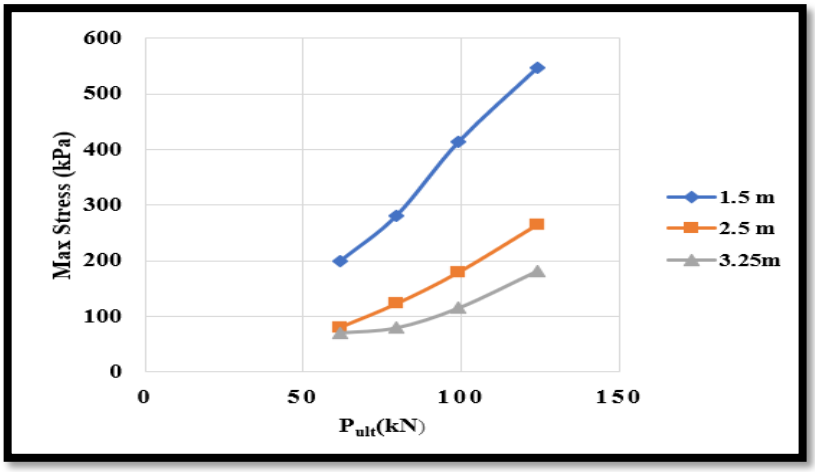


Figure 4.13 Maximum total principal stress at a depth - tensile applied load correlation($P_{ult}$) for FPA-I anchor obtained from Eq. 3.3

Figure 4.13 shows the maximum total principal stress levels experienced at 3 different depths depending on $P_{ult}$. In the context of FPA-I anchor, the maximum total principal stress of soils increased in proportion to the $P_{ult}$ applied at the same depth. The soil profile analysis indicates that the maximum total principal stress is considerably elevated in the clayey sand layer, which is the closest soil layer to the point of application of the tensile force. In contrast, the maximum total principal stress increase of the soil layer at 2.5 m silty sand soil layer and 3.25 m in the low plastic clay soil profile decreased relatively. Figure 4.10 illustrates that the maximum total principal stress decreased by approximately 55% between 1.5 m and 2.5 m and by 30% between 2.5 m and 3.25 m as the depth increased, under the same $P_{ult}$.

In addition, the maximum principal stress variations in the soil shown in the graph in Figure 4.13 was made using a fine mesh. For FPA-I, the coarse and medium mesh was used to observe the maximum principal stresses in the soil between comparisons between the shallow depth (1.5 m) and maximum tensile force (124 kN), as shown in Figure 4.14. Figure 4.14(a) represents the contour of the variation of principal stresses in the soil due to coarse mesh. Figure 4.14(b) illustrates the contour of the variation of principal stresses in the soil due to medium mesh. When fine, coarse, and medium meshes were applied, when looking at the contour lines, the mesh with the highest principal stress change in the soil was the fine mesh. Therefore, the finer mesh was selected and analyzed to give more reliable results.

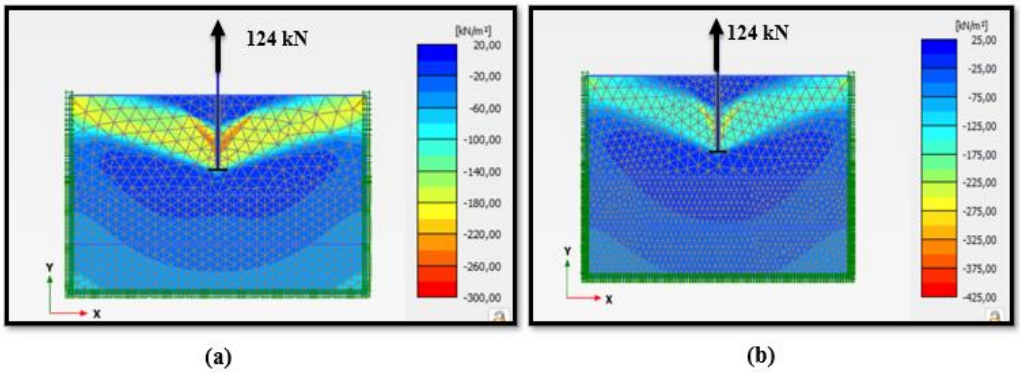


Figure 4.14 (a) Soil principal stresses change resulting from using coarse mesh (b) Soil principal stresses change resulting from using medium mesh

Similarly, Equation 3.4 obtained from Figure 3.12(b) was used for the FPA-II anchor. Equation 3.4 shows the relationship between $(N_{60})_1$ and $P_{ult}$. Firstly, for FPA-II at 1.5 m, $(N_{60})_1$ was gradually increased until the soil body collapsed. The $P_{ult}$ values corresponding to each $(N_{60})_1$ obtained from Equation 3.4 were entered into the numerical model as tensile load input values respectively and the numerical analysis was performed. Table 4.4 shows the $P_{ult}$ values corresponding to $(N_{60})_1$ for each depth.

Table 4.4 Tensile applied load ($P_{ult}$) for FPA-II anchor in numerical analysis

| Anchor name | Depth (m) | $(N_{60})_1$ | $P_{ult}$ (kN) (From eq 3.4.) |
|---|---|---|---|
| FPA-II | 1.5 | 3 | 37 |
| | | 10 | 44.6 |
| | | 20 | 58.3 |
| | | 30 | 76.2 |
| | | 40 | 99.6 |
| FPA-II | 2.5 | 3 | 37 |
| | | 10 | 44.6 |
| | | 20 | 58.3 |
| | | 30 | 76.2 |
| | | 40 | 99.6 |

The maximum displacements and maximum principal stresses corresponding to each applied tensile force were recorded from the numerical output results. The maximum displacements corresponding to each applied tensile load of FPA-II anchor at 1.5 m are

shown in Figure 4.15 and Figure 4.16 shows the maximum displacement of this anchor in the soil in response to increasing applied tensile load at 2.5 m.

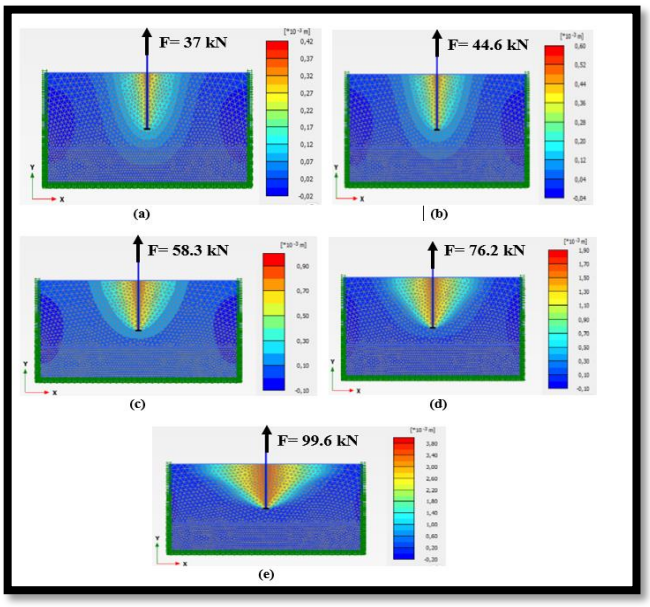


Figure 4.15 For the FPA-II anchor, the maximum displacement versus applied tensile loads obtained from Eq. 3.4 at a depth of 1.5 m a) F=37 kN b) F=44.6 kN c) F=58.3 kN d) F=76.2 kN, and e)F= 99.6 kN

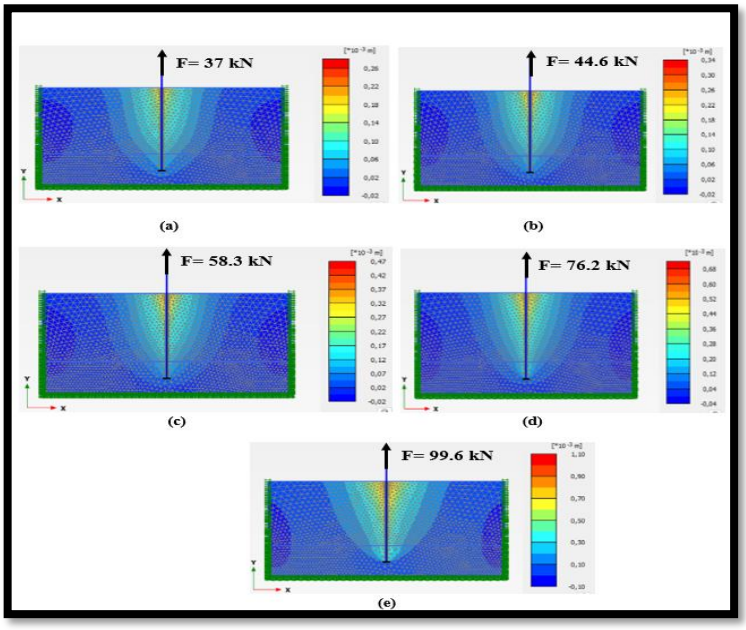


Figure 4.16 For the FPA-II anchor, the maximum displacement versus applied tensile loads obtained from Eq. 3.4 at a depth of 2.5 m a)F= 37 kN b) F=44.6 kN c) F=58.3 kN d)F=76.2 kN, and e)F= 99.6 kN

When Figure 4.15 and Figure 4.16 are analyzed, it was observed that the displacements are generally higher in the soil layer close to the anchor rope than in the soil layer lower side. In particular, in Figure 4.15, at $P_{ult}$ values of 76.2 kN and 99.6 kN applied at 1.5 m, more soil displacement was observed in and around the soil layer close to the anchor rope compared to other applied tensile load value. The corresponding maximum displacements and $P_{ult}$ at each depth in Figure 4.15 and Figure 4.16 above are shown graphically in Figure 4.17.

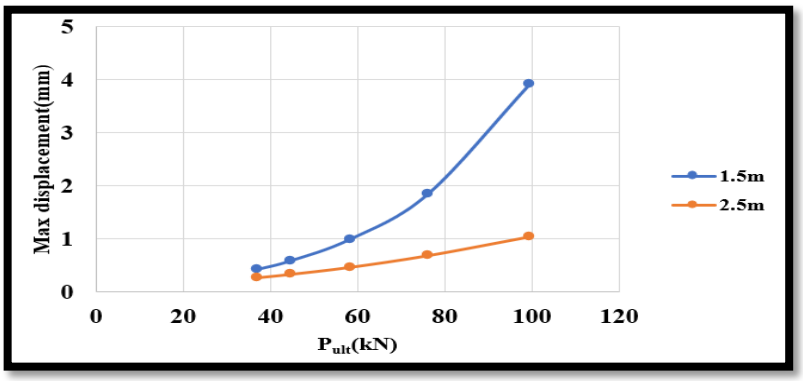


Figure 4.17 Maximum displacement - tensile applied load ($P_{ult}$) correlation for FPA-II anchor obtained from Eq. 3.4

A comparison of the results presented in Figures 4.8 and 4.17 reveals a similarity. In a similar situation, as in FPA-I anchor, it was determined that the displacement of the soil profile in clayey sand, which is the soil layer closest to the point where the $P_{ult}$ is applied, was higher than the other soil profile. However, when FPA-I and FPA-II anchors were compared at the same depth and with a similar $P_{ult}$, it was found that the maximum displacement of FPA-I anchor was larger than that of FPA-II anchor. This difference may be due to the larger surface area of FPA-I anchor than FPA-II anchors. In addition to surface area difference, the flip anchor shape (geometry) and design of FPA-I and FPA-II anchors differ. Considering the design and geometry, FPA-I anchor has an angled shape, which affects the more tensile resistance between the flip anchor and the soil. This has been observed to lead to more displacement due to the soil's response to increased surface contact. However, the larger size of the FPA-I anchor may cause greater soil disruption during installation, potentially leading to different compaction levels around the anchor. This affects the behavior of the soil under tensile load.

Similarly, maximum total principal stresses in the soil were observed using Equation 3.4 for each installation depth. Figure 4.18 and Figure 4.19 show the maximum

total principal stress of the soils in response to different applied tensile load values for FPA-II anchor at 1.5 m and 2.5 m.

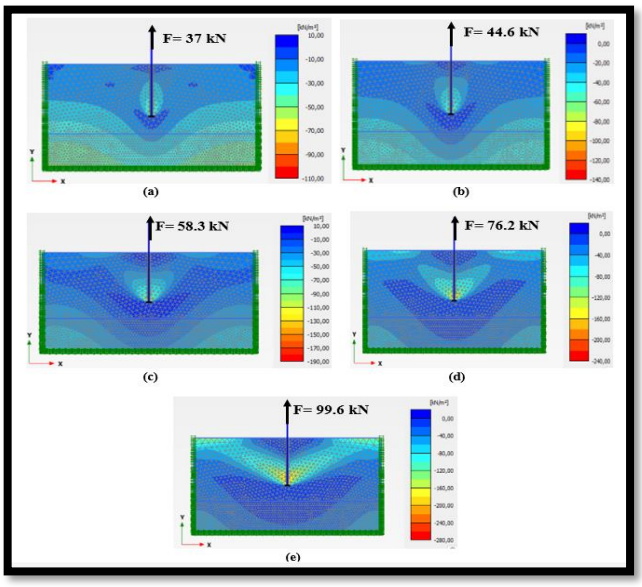


Figure 4.18 For the FPA-II anchor, the maximum total principal stress versus applied tensile loads obtained from Eq. 3.4 at a depth of 1.5 a) F=37 kN b) F=44.6 kN c) F=58.3 kN d) F=76.2 kN, and e) F=99.6 kN

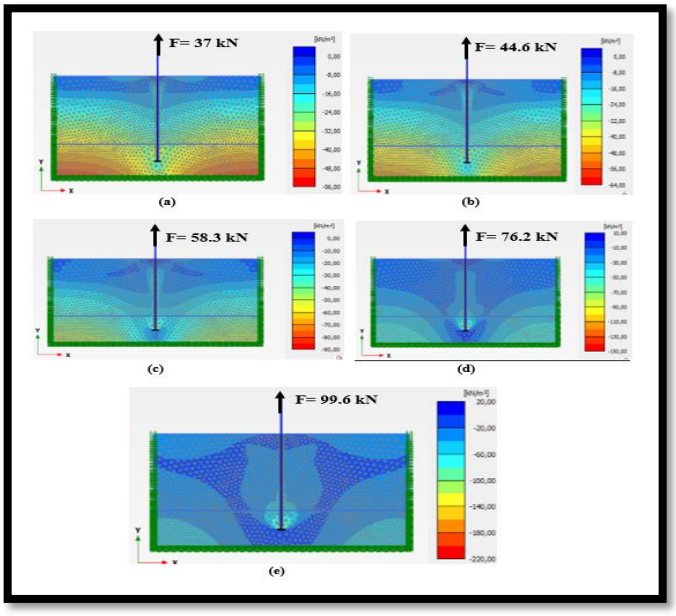


Figure 4.19 For the FPA-II anchor, the maximum total principal stress versus applied tensile loads obtained from Eq. 3.4 at a depth of 2.5 a)F=37 kN b)F=44.6 c)F= 58.3 kN d)F=76.2 kN, and e)F= 99.6 kN

When Figures 4.18 and 4.19 were examined, maximum total principal stress changes similar to those in FPA-I anchor were seen. When the applied tensile load ($P_{ult}$) at the same depth was increased, the maximum total principal stress of the soil increased. More principal stress change was observed in the soil layer located in the direction of the applied tensile load, than in the soil layer in the opposite direction of the tensile resistance. Using the same procedure, Figure 4.20 shows graphically the maximum total principal stress at depths of 1.5 m and 2.5 m and under different tensile load.

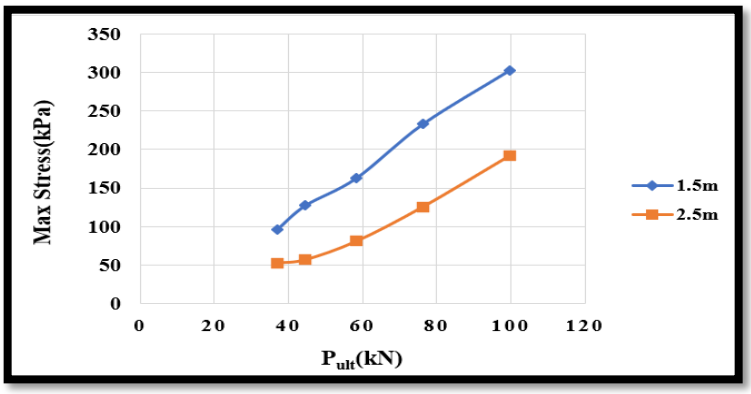


Figure 4.20 Maximum total principal stress at a depth - tensile applied load ($P_{ult}$)- $P_{ult}$ correlation for FPA-II anchor obtained from Eq. 3.4

As shown in Figure 4.20, when the same $P_{ult}$ was applied, the maximum total principal stress change in the soil decreases by approximately 45% on average as the depth increased. Figures 4.13 and 4.20 show that when two flip anchors (FPA-I and FPA-II anchors) were compared at the same depth (1.5 m) and closely applied tensile resistance (99.2 kN and 99.6kN), the maximum total principal stress of FPA-I anchor was approximately that of FPA-II anchor has greater by 35%. Since FPA-I anchor has a larger surface area than FPA-II anchor, more principal stress changes were observed in the soil at the same depth.

### 4.5.1.2. Displacement and Stress Analysis in the Soil Surrounding the Flip Anchor

This section focused on the changes in total principal stresses and displacements in the soil surrounding the flip anchors. Therefore, to closely examined the soil displacement and principal total stress changes at 1.5 m, 2.5 m, and 3.25 m of the FPA-I

anchor at the upper and lower sides of this anchor, the $P_{ult}$(kN) values applied in Table 4.3 were used to observe the total principal stress change and displacement change in the soil at the determined stress and node points, respectively. For FPA-II anchor, the ultimate resistance forces ($P_{ult}$) values specified in Table 4.4 were applied. The soil profile surrounding the upper and lower sides of the surrounding soil FPA-II anchor was closely analyzed by the same method. Figure 4.21 shows a visualization of how the stress and node point selection process is performed from the soil surrounding the flip anchors.

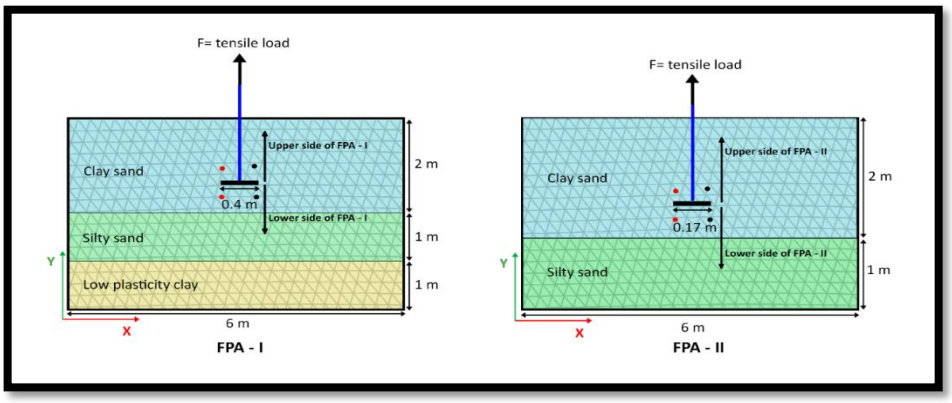


Figure 4.21 Determined points from the upper side and lower side of the soil surrounding the flip anchors

After selecting the stresses and node points at each depth for FPA-I anchor, Table 4.5 clearly shows the total principal stresses and displacements at the selected points on the upper and lower sides of the soil surrounding the FPA-I anchor.

Table 4.5 Soil displacement and total principal stress change at the lower and upper side of the FPA-I anchor

| Depth(m) | $P_{ult}$ (kN) | upper side of stress point | upper side of anchor stress(kPa) | upper side of node point | upper side of disp.(mm) | lower side of stress point | lower side of anchor stress(kPa) | Lower side of node point | lower side of disp.(mm) |
|---|---|---|---|---|---|---|---|---|---|
| 1.5 | 62 | 16968 | 23 | 24669 | 0.507 | 16975 | -49 | 24676 | -0.386 |
| | 79 | 16968 | 45 | 24669 | 0.989 | 16975 | -71 | 24676 | -0.666 |
| | 99 | 16968 | 79 | 24669 | 1.825 | 16975 | -90 | 24676 | -0.938 |
| | 124 | 16968 | 144 | 24669 | 3.532 | 16975 | -116 | 24676 | -1.120 |
| 2.5 | 62 | 23419 | 43 | 27042 | 0.141 | 23426 | -24 | 27580 | -0.130 |
| | 79 | 23419 | 72 | 27042 | 0.239 | 23426 | -42 | 27580 | -0.216 |
| | 99 | 23419 | 107 | 27042 | 0.392 | 23426 | -48 | 27580 | -0.344 |
| | 124 | 23419 | 159 | 27042 | 0.656 | 23426 | -82 | 27580 | -0.555 |
| 3.25 | 62 | 64953 | 59 | 33428 | 0.039 | 47941 | -25 | 33443 | -0.035 |
| | 79 | 64953 | 80 | 33428 | 0.052 | 47941 | -25 | 33443 | -0.046 |
| | 99 | 64953 | 115 | 33428 | 0.069 | 47941 | 26 | 33443 | -0.056 |
| | 124 | 64953 | 181 | 33428 | 0.114 | 47941 | 26.5 | 33443 | -0.069 |

From the data given in Table 4.5, the total principal stress variations of the soil surrounding the upper and lower sides of the selected stress points for FPA-I anchor at each depth (1.5 m, 2.5 m, and 3.5 m), corresponding to the applied $P_{ult}$ are shown in Figure 4.22(a).

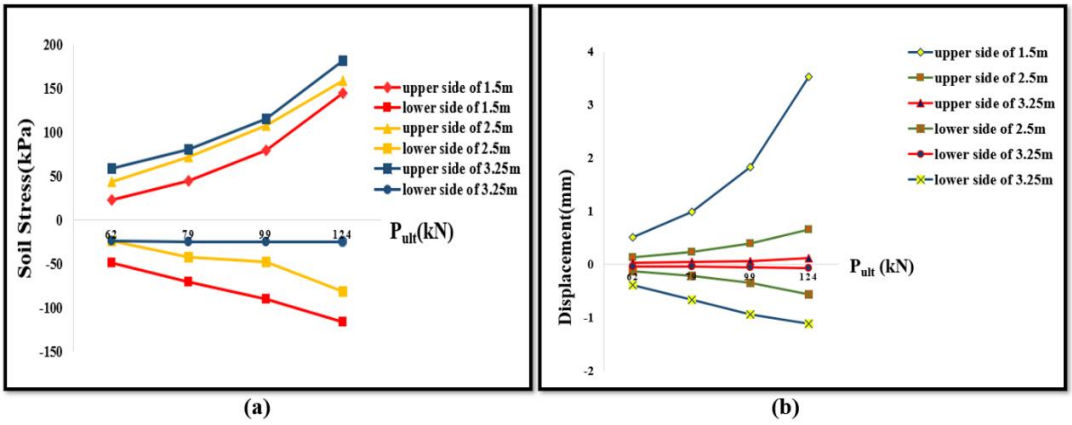


Figure 4.22 (a) Total principal stress distribution for FPA-I anchor b) Displacement of soil distribution for FPA-I anchor

When Figure 4.22(a) was examined, it was seen that as the depth increases in the direction of the $P_{ult}$ (surrounding soil of the upper part of the anchor) the total principal stress in the soil increases proportionally. Conversely, as the depth increases, the total principal stress of the soil decreases in the (-) opposite direction of the applied force on the soil lower side the anchor. The adjacent soil mass confines the soil as it approaches the applied force. This compaction limits the soil's capacity to move laterally and causes increased total principal stress. The surrounding soil of the upper part of the flip anchor instantly transfers the applied force to the ground at that depth. This direct force transfer can increase the total principal stress within soil particles. Contrary to the direction of the applied force, the pressure applied to the soil decreased as the depth increased. The force transmitted at the lower side of the flip anchor is distributed over a larger surface area, resulting in lower stress levels compared to the surrounding soil at the upper part of the flip anchor. The variation of total principal stress with depth, as seen at selected stress points along the flip anchor, is a result of the complex interplay of confining effects, direct load transfer, and force distribution within the soil mass.

The displacement at each node was recorded with the determined node points in Table 4.5. Figure 4.22(b) shows the displacement of soil (mm) at that depth about the $P_{ult}$(kN). The soil displacement increased as $P_{ult}$ applied at the same depth

increased. Conversely, as depth increased, displacement decreased proportionately because as depth increased, the soil became denser and more compact, limiting its ability to displace. However, some types of soil are more prone to deformation under load, resulting in more soil displacement. Upon analyzing the soil profiles, it is apparent that the clayey sand soil exhibits the lowest cohesiveness value. Therefore, there is a higher level of displacement compared to the other layers of soil. In other words, the resistance to movement in the same direction as the applied force can easily be overcome at the upper side of the flip anchor, resulting in further displacement. In general, the complex relationship between soil quality, compaction, load transfer mechanisms, and frictional resistance results in a situation where soil principal stress and displacement are opposite and directly related in various aspects related to the applied force.

Pull-out tests were performed at FPA-II anchor at two specific depths of 1.5 m and 2.5 m. By applying, Equation 3.4, the $P_{ult}$ applied for both depths was found. Table 4.6 shows, for each depth, the total principal stress values corresponding to the stress points at the upper and lower sides of the soil surrounding the FPA-II anchor and the displacement values corresponding to the node points in the FPA-II anchor.

Table 4.6 Soil displacement and principal total stress change at the lower and upper side of the FPA-II anchor

| Depth | $P_{ult}$(kN) | upper side of stress point | upper side of stress(kPa) | lower side of stress point | lower side of stress(kPa) | upper side of node point | upper side of disp.(mm) | lower side of point | lowe side of disp.(mm) |
|---|---|---|---|---|---|---|---|---|---|
| 1.5 | 37 | 23863 | 7 | 23856 | -10 | 19210 | 0.202 | 19737 | -0.126 |
| | 45 | 23863 | 9 | 23856 | -12 | 19210 | 0.301 | 19737 | -0.156 |
| | 58 | 23863 | 24 | 23856 | -20 | 19210 | 0.578 | 19737 | -0.219 |
| | 76 | 23863 | 63 | 23856 | -30 | 19210 | 1.196 | 19737 | -0.333 |
| | 100 | 23863 | 138 | 23856 | -48 | 19210 | 2.520 | 19737 | -0.546 |
| 2.5 | 37 | 41198 | 52 | 29029 | -3 | 18555 | 0.044 | 18746 | -0.036 |
| | 45 | 41198 | 55 | 29029 | -5 | 18555 | 0.056 | 18746 | -0.042 |
| | 58 | 41198 | 56 | 29029 | -15 | 18555 | 0.084 | 18746 | -0.051 |
| | 76 | 41198 | 80 | 29029 | -22 | 18555 | 0.163 | 18746 | -0.060 |
| | 100 | 41198 | 150 | 29029 | -25 | 18555 | 0.331 | 18746 | -0.065 |

The graph in Figure 4.23(a) was generated using the changes in total principal stress points upper and lower sides of the FPA-II anchor surrounding soil seen in Table 4.6 above.

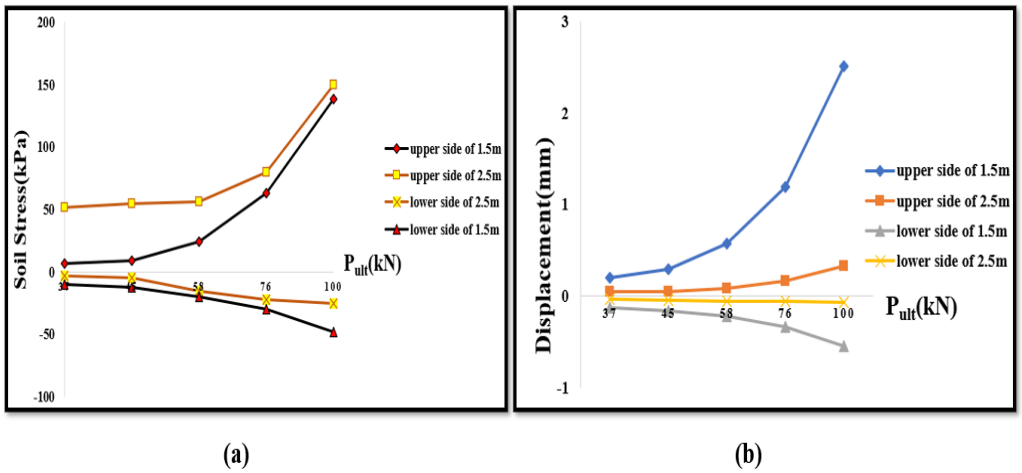


(a) (b)

Figure 4.23 (a) Principal total stress distribution for FPA-II anchor b) Displacement of soil distribution for FPA-II anchor

As seen in Figure 4.23(a), when the $P_{ult}$ increased at the same depth, the principal total stress in the soil lower and upper parts of the soil surrounding the FPA-II anchor increased proportionally. As the depth increased in the direction of the applied $P_{ult}$, the principal total stress in the soil increased, but as the depth increased in the opposite direction of the applied $P_{ult}$, the principal total stress in the lower part of the soil surrounding the FPA-II decreased. Similar results were observed in terms of FPA-I and FPA-II anchors in soil principal total stress distribution. Additionally, the soil displacement data recorded in Table 4.6 has been used to show soil displacement in response to applied tensile force for the FPA-II anchor, as shown in Figure 4.23(b). The results shown in Figure 4.22(b) are consistent with the decrease in soil displacement shown in Figure 4.23 (b) as depth increases. As the depth increases, the soil is exposed to the weight of the soil layers above it, leading to compaction and densification. This is a result of the weight of the overlying soil, which applies pressure, compressing the soil particles together, reducing pore spaces, and increasing density. Additionally, the interaction between particles in clayey sand and silty sand soils strengthens the interlocking and structural integrity of soil particles. This prevents displacement from spreading throughout the soil mass.

## 4.6. Conclusion

In this section, the $P_{ult}$ values, which were derived from field pull-out tests for FPA-I and FPA-II anchors were applied to the numerical analysis. New $P_{ult}$ values were derived from $(N_{60})_1$ using the equations given in Chapter 3, and these $P_{ult}$ values were utilized as load phase input values in the numerical analysis. Numerical analysis was conducted using PLAXIS-2D. The numerical analyze was conducted by simulating the placement of flip anchors in the soil at varying depths and in distinct soil profiles. The impact of the anchors on the adjacent soil was assessed by applying tensile forces after they were driven. The primary objective of these analyses was to investigate the principal total stresses and displacements that result in the soil. To monitor changes in principal total stress and displacement, specific stress and node points surrounding the soils of the upper and lower parts of the flip anchors were identified. Potential failure mechanisms were identified, and the efficiency of flip anchors in various soil conditions was assessed through the examination of these modifications. The integration of numerical analysis with field test data fulfils the critical objectives of this study. These analyses aimed to generate contour lines representing principal total stress distribution around flip anchors, providing a detailed understanding of how applied tensile forces are transmitted through the surrounding soil matrix. By monitoring displacement patterns around the flip anchors, preliminary insights were ensured into the deformation behavior of the soil under varying $P_{ult}$ values. This method is essential for predicting potential failure mechanisms and ensuring that flip anchors maintain their tensile resistance without causing excessive soil movement.

# CHAPTER 5

# CONCLUSION

Flip anchors have gained significant popularity in recent years due to their remarkable efficacy in using slope stabilization applications and providing dependable reinforcement in a variety of construction applications. They play a critical role in avoiding soil erosion and landslides, thereby preserving slope stability and retaining structures. Flip anchors are highly favored in the field due to their economic and practical benefits, as well as their ability to intend moderate loads. Understanding the tensile resistance and behavior of flip anchors is crucial to optimizing their use and ensuring the permanent stability of structures. This thesis presents the evaluation of the ultimate tensile resistances of 2 flip anchors (FPA-I and FPA-II anchors) through both field experiments and numerical analysis.

During the field testing, a driven steel rod was used to drive the flip anchors into the soil using an excavator until the rod reached the desired depth. Once the required depth was reached, the load-lock procedure was initiated. After removing the driven steel rod, the flip anchor was securely fixed using an anchor rope and the rope was pulled using a hydraulic jack. A pressure gauge is integrated into the hydraulic jack to enable manual monitoring of the applied force. A total of 5 pull-out tests performed with hydraulic jacks at designated locations determined the ultimate tensile resistances of FPA-I and FPA-II anchors. It has been observed that the differences in tensile resistance between two flip anchors at the same depth and in the same soil profile are due to the size and design differences of the flip anchors. Additionally, when the tensile resistances of the FPA-I anchor and other similar flip anchor types commonly used in commercial applications were compared, it was determined that their performances were similar. However, some differences were observed between the tensile capacities of the FPA-II anchor and other similar types of commercially available flip anchors. This may be because there is limited information in the technical sheets of commercially available similar flip anchors, and, more importantly, the FPA-II anchor design has a flatter surface geometry, while other similar flip anchors have a more recessed and pointed geometry. The model of the field test was simulated by finite element program Plaxis 2D and the $P_{ult}$ values obtained in the field were used as the pulling force input. Principal total stress changes and displacements

were observed especially in the upper and lower parts of the soil surrounding the flip anchors. Considering the numerical results, it was determined that FPA-I anchor, which has a larger surface area, had higher principal total stresses and displacements in the same soil profiles compared to FPA-II anchor. Additionally, not only the ultimate tensile resistances found in the field were used in the numerical analysis, but also new tensile forces were found using Equation 3.3 and Equation 3.4. obtained from the graphs in Figure 3.11(b) and Figure 3.12(b).

Many analyses were obtained by taking the new $P_{ult}$ values in the loading phase as input values. In general, in FPA-I and FPA-II anchors, it was observed that the soil displacements were higher close to the surface, and the soil displacements decreased as they were far away from the surface (as the depth increased). In both anchors (FPA-I and FPA-II anchors), as the depth increases in the direction of the tensile force (in the soil profiles at the upper part of the anchor), the principal total stresses in the soil increase, and as the depth increases in the opposite direction, the principal total stresses in the soil decrease relatively. Since the pressure in the soil decreases as the depth increases in the opposite direction of the applied load, lower principal total stress levels were obtained in the surrounding soil of lower parts of the flip anchor due to the distribution of the force transferred by the flip anchor. Integrating numerical analysis with field test data has been effective in explaining the performance of flip anchors under various soil conditions. This approach contributes to the improvement of flip anchor design and installation techniques, highlighting the importance of a study of the principal total stresses and displacements caused by flip anchors in soil. The findings of this study provide a basis for further research and development aimed at optimizing the performance and reliability of flip anchors in geotechnical applications.

## 5.1. Recommendation for Future Work

This thesis briefly overviews the preliminary field-testing procedures and results for two anchor types (FPA-I and FPA-II), highlighting the main differences in their pull-out capacities depending on the design and installation methods. The following items are proposed to better understand these principles and explore their potential applications.

- Load and displacement monitoring technologies such as strain gauges, load cells, and data acquisition systems can be applied to improve the

accuracy of field tests. The tests can be performed in the laboratory Modern sensor technologies can be used to evaluate characteristics such as load retention, corrosion rates, and material degradation to evaluate the long-term performance and durability of FPA-I and FPA-II anchors in different soil conditions. This extended field monitoring can span over multiple years.

- Other similar available flip anchors can be field tested using the same procedures in the field environment.
- Field tests can be conducted to observe the performance of FPA-I and FPA-II anchors in soil profiles comprising various soil types (e.g., clay, gravel, limestone, etc.), densities, and moisture contents.
- There is a limitation of comparative studies that evaluate the performance advantages and disadvantages of flip anchors as compared to conventional anchor methods. Hence, carrying out direct field tests and numerical analyses that compare FPA-I and FPA-II anchors to conventional anchors such as helical anchors and driven piles may accurately evaluate parameters such as load capacity, installation time, and cost-effectiveness of these various anchor types.
- The tests were applied at static loading conditions. Dynamic analysis can be performed to observe the performance of the FPA-I and FPA-II anchors.

# REFERENCES


Abdi, M. R., and M. A. Arjomand. 2011. "Pullout Tests Conducted on Clay Reinforced with Geogrid Encapsulated in Thin Layers of Sand." *Geotextiles and Geomembranes* 29, no. 6: 588–595. https://doi.org/10.1016/j.geotexmem.2011.04.004.

Al Hakeem, Nabil M. Ali Hameed. 2019. "Finite Element Investigation into The Performance of Embedded Plate Anchors in Sand." Ph.D. Dissertation, Texas A&M University. Available electronically from https://hdl.handle.net/1969.1/186938.

Ali, A. H. H. 1968. "The Resistance of Clay to Penetration by Anchor Flukes." *Proceedings of the Institution of Civil Engineers* 40, no. 2: 395–416. https://doi.org/10.1680/iicep.1968.7864.

Anchoring Rope and Rigging Pty Ltd. 2019. https://hulkearthanchors.com. Accessed June 19, 2024.

Anchor Systems International. 2020. "Projects & Case Studies from Anchor Systems International Ltd." https://www.anchorsystems.co.uk/projects/. Accessed June 15, 2024.

Asfaw, N. T., G. Lei, M. Azizian, A. Poudel, L. Hoyos, and X. Yu. 2023. "Field Pull-out Tests of Percussion-Driven Earth Anchors." *Applied Sciences* 13, no. 4: 2132. https://doi.org/10.3390/app13042132.

Aubeny, Charles P. 2017. *Geomechanics of Marine Anchors.* Boca Raton, FL: CRC Press. https://doi.org/10.4324/9781351237376.

Azizian, M., N. Kaneza, A. Poudel, N. T. Asfaw, G. Lei, and X. Yu. 2024. "Numerical and Experimental Analyses of Percussion-Driven Earth Anchors (PDEAs) under Monotonic Pullout Tests." *IFCEE 2024.* https://doi.org/10.1061/9780784485415.004.

Balla, A. 1961. "The Resistance to Breaking out of Mushroom Foundations for Pylons." *Proceedings of the 5th International Conference on Soil Mechanics and Foundation Engineering* 1: 569–576.

Barley, A. D., and D. Mothersille. 2007. *Ground Anchorages and Anchored Structures.* "https://doi.org/10.1680/gaaasis.35614.

Barron, B. B. 2014. "An Investigation into the Keying Behavior and the Capacity of Plate Anchors in Sand." Master of Engineering Thesis, Institute of Technology Sligo.

Bhatnagar, R. L. 1969. "Bearing Capacity of Strip Footings on Sand Under Eccentric and Inclined Loads." Ph.D. Dissertation, University of Roorkee.

Bildik, S., M. Laman, and M. T. Suleiman. 2013. "Uplift Behavior of Anchor Plates in Slope." *Geo-Congress 2013.* https://doi.org/10.1061/9780784412787.179.

Brown, A., and B. Green. 2022. "Load Transfer Behaviour of Instrumented Prestressed Ground Anchors in Sandy Soil." *Journal of Geotechnical Engineering* 148, no. 7: 1-15. https://doi.org/10.1590/s1983-41952021000600012.

Chan, Scott D., and E. W. M. Lam. 2002. "Framework of Success Criteria for Design/Build Projects." *Journal of Management in Engineering* 18, no. 3: 120–128. https://doi.org/10.1061/(asce)0742.

Chen, H., J. Chen, C. Leung, Y. K. Chow, and Z. Li. 2021. "Pull-out Mechanism of Horizontal and Inclined Plate Anchors in Normally Consolidated Clay." *Journal of Marine Science and Engineering* 9, no. 10: 1103. https://doi.org/10.3390/jmse9101103.

Das, B. M., and G. R. Seeley. 1975. "Breakout Resistance of Shallow Horizontal Anchors." *Journal of Geotechnical and Geoenvironmental Engineering* 101: 999-1003.

Das, B. M. 1990. *Earth Anchors.* Amsterdam, Netherlands: Elsevier Science Publishing Company Inc.

Das, B. M. 2010. *Principles of Foundation Engineering.* Cengage Learning.

Das, B. M., and S. K. Shukla. 2013. *Earth Anchors.* 2nd ed. Florida, USA: J. Ross Publishing Inc. ISBN 978-1-60427-077-8.

Davis, C. 2023. "Optimization of Screw Anchors in Tension for Renewable Energy Applications." *Renewable Energy Journal* 66, no. 1: 56-72. https://doi.org/10.1016/j.oceaneng.2020.108010.

Deshmukh, V. B., D. M. Dewaikar, and D. Choudhary. 2011. "Uplift Capacity of Horizontal Strip Anchors in Cohesionless Soil." *Geotechnical and Geological Engineering* 29, no. 6: 977–988. https://doi.org/10.1007/s10706-011-9430-0.

Elton, D. J., and L. B. Whitbeck. 1997. *Ground Anchors.* Transportation Research Record.

El Sawwaf, M., and A. Nazir. 2006. "The Effect of Soil Reinforcement on Pullout Resistance of an Existing Vertical Anchor Plate in Sand." *Computers and Geotechnics* 33, no. 3: 167–176. https://doi.org/10.1016/j.compgeo.2006.04.001.

Emirler, B., M. Tolun, and M. Laman. 2016. "Experimental Investigation of the Uplift Capacity of Group Anchor Plates Embedded in Sand." *Geomechanics and Engineering* 11, no. 5: 691–711. https://doi.org/10.12989/gae.2016.11.5.691.

Fang, H. Y. 1991. *Foundation Engineering Handbook.* Springer.

Forcelini, M., S. Maghous, and F. Schnaid. 2023. "A Limit Analysis Approach to Uplift Bearing Capacity of Shallow Plate Anchors in Marine Environments." *International Journal for Numerical and Analytical Methods in Geomechanics* 48, no. 4: 1060-1093. https://doi.org/10.1002/nag.3676.

Gerkus, H., J. R. Giampa, A. I. Senanayake, Y. Lai, Y. Huang, J. E. Iturriaga Flores, N. B. Breithaupt, S. Sivarajah, A. S. Bradshaw, and R. B. Gilbert. 2016. "Preliminary Development of a New Concept to Improve the Sustainability of Offshore Foundations." *Geo-Chicago 2016.* https://doi.org/10.1061/9780784480137.044.

Gore, M., M. Theaker, S. Howell-Smith, H. Rahnejat, and P. D. King. 2013. "Direct Measurement of Piston Friction of Internal-Combustion Engines Using the Floating-Liner Principle." *Proceedings of the Institution of Mechanical Engineers, Part D: Journal of Automobile Engineering* 228, no. 3: 344–354. https://doi.org/10.1177/0954407013511795.

Gue, S. S., and Y. C. Tan. 1998. "Design and Construction Considerations for Deep Excavation." Lecture, IEM Northern Branch, September 26, 1998, Penang.

Gui, F., J. Kong, D. Feng, X. Qu, F. Zhu, and Y. You. 2021. "Uplift Resistance Capacity of Anchor Piles Used in Marine Aquaculture." *Scientific Reports* 11, no. 1. https://doi.org/10.1038/s41598-021-99817.

Hatanaka, M., and A. Uchida. 1996. "Empirical Correlation Between Penetration Resistance and Internal Friction Angle of Sandy Soils." *Soils and Foundations* 36, no. 4: 1-9.

Hu, S., L. Zhao, Y. Tan, Y. Luo, and Z. Zeng. 2022. "Three-Dimensional Upper-Bound Limit Analysis of Ultimate Pullout Capacity of Plate Anchors in Undrained Clay Considering Embedment Depth." *Marine Georesources & Geotechnology* 41, no. 4: 400-414. https://doi.org/10.1080/1064119X.2022.2087589.

Jalali Moghadam, M., N. Dastaran, and A. Zad. 2021. "Introducing Expandable Mechanical Plate Anchors for Onshore and Offshore Anchoring." *Marine Georesources & Geotechnology* 40 (3): 329–48. https://doi.org/10.1080/1064119x.2021.1894274.

Johnson, K. 2020. "Specialized Anchor Systems for Diverse Structures." *Journal of Civil Engineering* 126 (4): 300–10.

Kalaga, S. 2018. "Uplift Capacity of Plate Anchors: Application to Transmission Poles." *Journal of Structural Engineering* 45 (3).

Kumar, J. 2001. "Seismic Vertical Uplift Capacity of Strip Anchors." *Geotechnique* 51 (3):275–79. https://doi.org/10.1680/geot.51.3.275.39368.

Kumar, J., and K. M. Kouzer. 2008. "Vertical Uplift Capacity of Horizontal Anchors Using Upper Bound Limit Analysis and Finite Elements." *Canadian Geotechnical Journal* 45: 698–704. https://doi.org/10.1139/t08-005.

Kumar, J., and O. Rahaman. 2019. "Vertical Uplift Resistance of Horizontal Plate Anchors for Eccentric and Inclined Loads." *Canadian Geotechnical Journal* 56 (2): 290-99. https://doi.org/10.1139/cgj-2017-0515.

Lai, Y. 2017. "Laboratory Model Tests on Drag and Dynamically Embedded Plate Anchors in Layered Clay Profiles." PhD diss., Texas A&M University.

Liao, S. S. C., and R. V. Whitman. 1986. "Overburden Correction Factors for SPT in Sand." *Journal of the Geotechnical Engineering Division, ASCE* 112 (GT3): 373-77.

Little, A. L. 1961. *Foundations*. London: Edward Arnold (Publishers) Ltd.

Liu, J., M. Liu, and Z. Zhu. 2012. "Sand Deformation around an Uplift Plate Anchor." *Journal of Geotechnical and Geoenvironmental Engineering* 138 (6): 728-37. https://doi.org/10.1061/(asce)gt.1943-5606.0000633.

Liu, H., Y. Yang, and J. Peng. 2021. "A Unified Model for Analyzing Comprehensive Behaviors of Deepwater Anchors." *Journal of Marine Science and Engineering* 9 (8): 913. https://doi.org/10.3390/jmse9080913.

"Manta Ray Building Anchors." Maclean Civil. Accessed June 10, 2024. https://www.macleancivilproducts.com/product/manta-ray.

Merifield, R. S., A. V. Lyamin, and S. W. Sloan. 2001. "Stability of Plate Anchors in Undrained Clay." *Geotechnique* 51 (2): 141-55. https://doi.org/10.1680/geot.2001.51.2.141.

Merifield, J., and S. Sloan. 2006. "The Ultimate Pullout Capacity of Anchors in Frictional Soils." *Canadian Geotechnical Journal* 43 (6): 624-37. https://doi.org/10.1139/t06-052.

Meyerhof, G. G., and J. I. Adams. 1968. "Uplift Resistance of Anchors." *Canadian Geotechnical Journal* 5 (4): 225-44.

Meyerhof, G. G. 1973. "Uplift Resistance of Inclined Anchors and Piles." In *Proceedings of the 8th International Conference on Soil Mechanics and Foundation Engineering*, Vol. 2, 167-72. U.S.S.R

Murray, E. J., and J. Geddes. 1987. "Uplift of Anchor Plates in Sand." *Journal of Geotechnical Engineering* 113 (3): 202-15. https://doi.org/10.1061/(asce)0733-9410(1987)113:3(202).

Niroumand, H., and K. A. Kassim. "Anchor Plates." In *Design and Construction of Soil Anchor Plates*, 17–30. https://doi.org/10.1016/b978-0-12-420115-6.00002-3.

O'Loughlin, C. D., A. P. Blake, M. D. Richardson, M. F. Randolph, and C. Gaudin. 2014. "Installation and Capacity of Dynamically Embedded Plate Anchors as Assessed through Centrifuge Tests." *Ocean Engineering* 88: 204–13. https://doi.org/10.1016/j.oceaneng.2014.06.020.

O'Neill, M. W., and L. C. Reese. 1999. "Drilled Shafts: Construction Procedures and Design Methods." Report No. FHWA-SA-99-019, Federal Highway Administration, Washington, D.C.

Osman, B. H. 2023. "Correlation of Cohesion and Friction Angle Based on SPT-N Values: A Comprehensive Review." *Civil Engineering Beyond Limits* 4 (3): 1–9. https://doi.org/10.36937/cebel.2023.1821.

"Platipus Civil Engineering & Construction Brochure." Quicksupplyco.com. Accessed June 1, 2024. https://www.quicksupplyco.com/userdocs/products/platipus-civil-engineering-construction-brochure-qsc.pdf.

Radhakrishna, H. S., and J. I. Adams. 1973. "Long-term Uplift Capacity of Augered Footings in Fissured Clay." *Canadian Geotechnical Journal* 10 (4): 647–52. https://doi.org/10.1139/t73-061.

Randolph, M., and S. Gourvenec. 2011. *Offshore Geotechnical Engineering*. Spon Press, Taylor and Francis, Abingdon, Oxon.

Richardson, M. 2008. "An Overview of Anchor Systems." *Journal of Offshore Mechanics and Arctic Engineering* 130 (3). https://doi.org/10.1093/oso/9780195134513.003.0003.

Robertson, P. K. 2009. "Interpretation of Cone Penetration Tests - A Unified Approach." *Canadian Geotechnical Journal* 46 (11): 1337-55. https://doi.org/10.1139/t09-065.

Rowe, R. K. 1952. "The Application of Rankine's Earth Pressure Theory to the Design of Retaining Structures." *Geotechnique* 2 (3): 158-70.

Rowe, R. K., and E. H. Davis. 1982. "The Behaviour of Anchor Plates in Clay." *Geotechnique* 32 (1): 9-23. https://doi.org/10.1680/geot.1982.32.1.9.

Roy, A., C. O'Loughlin, S. H. Chow, and M. Randolph. 2022. "Inclined Loading of Horizontal Plate Anchors in Sand." *Geotechnique* 72 (12): 1051-67. https://doi.org/10.1680/jgeot.20.p.119.

Saeedy, H. S. 1987. "Stability of Circular Vertical Earth Anchors." *Canadian Geotechnical Journal* 24 (3): 452–56.

Shanker, K., P. K. Basudhar, and N. R. Patra. 2006. "Uplift Capacity of Single Piles: Predictions and Performance." *Geotechnical and Geological Engineering* 25 (2): 151-61. https://doi.org/10.1007/s10706-006-9000-z.

Sharma, A., and R. K. Sharma. 2020. "Uplift Behaviour of Axial Granular Pile Anchor Encased with Geogrid in Cohesionless Soil." *Journal of Engineering, Design and Technology* 19 (2): 588-602. https://doi.org/10.1108/jedt-06-2020-0222.

Sivrikaya, O., and E. Toğrol. 2006. "Determination of Undrained Strength of Fine-Grained Soils by Means of SPT and its Application in Turkey." *Engineering Geology* 86 (1): 52-69. https://doi.org/10.101

Sivrikaya, O. 2009. "Comparison of Artificial Neural Network Models with Correlative Works on Undrained Shear Strength." *Eurasian Soil Science* 42 (13): 1487. https://doi.org/10.1134/s1064229309130092.

Smith, C. 1998. "Limit Loads for an Anchor/Trapdoor Embedded in an Associative Coulomb Soil." *International Journal for Numerical and Analytical Methods in Geomechanics* 22 (11): 855–865

Smith, C. C. 2012. "Limit Loads for a Shallow Anchor/Trapdoor Embedded in Non-associative Coulomb Soil." *Géotechnique* 62 (7): 563–571. https://doi.org/10.1177/0734242x241227378.

Smith, J. M. 2012. "Further Studies on the Stability of Plate Anchors in Clay." *Computers and Geotechnics* 44: 1-15. https://doi.org/10.1016/j.compgeo.2012.04.004.

Strom, K. B., and M. D. Ebeling. 2001. *Ground Anchors and Anchored Systems*. US Army Corps of Engineers.

Su, Q., X. Zhang, Y. Peng, and W. Zhao. 2014. "Ultimate Capacity Analysis and Determination of the Position of Failure Surface for Uplift Piles." *Mathematical Problems in Engineering* 2014: 1-6. https://doi.org/10.1155/2014/540143.

Tagaya, K., A. Tanaka, and H. Aboshi. 1983. "Application of Finite Element Method to Pullout Resistance of Buried Anchor." *Soils and Foundations* 23 (3): 91–104

Tagaya, K., R. F. Scott, and H. Aboshi. 1988. "Pullout Resistance of Buried Anchor in Sand." *Soils and Foundations* 28 (3): 114–130.

Tagaya, T., and J. M. Smith. 1988. "Numerical Studies on the Stability of Plate Anchors in Clay." *Computers and Geotechnics* 5 (4): 287-303. https://doi.org/10.1016/0266-352x(88)90002-3.

Tan, S. A., and S. G. Paikowsky. 2008. "Performance of Sheet Pile Walls in Peat." *Journal of Geotechnical and Geoenvironmental Engineering* 134 (9). https://doi.org/10.1061/(asce)1090-0241(2008)134:4(445).

Tezcan, S. S., Z. Özdemir, and A. Keceli. 2009. "Seismic Technique to Determine the Allowable Bearing Pressure for Shallow Foundations in Soils and Rocks." *Acta Geophysica* 57 (2): 400–412. https://doi.org/10.2478/s11600-008-0077-z.

Turkish Building Earthquake Code. 2018. Section 16. Ankara: Afet ve Acil Durum Yönetimi Başkanlığı.

Vesic, A. S. 1971. "Breakout Resistance of Objects Embedded in Ocean Bottom." *Journal of the Soil Mechanics and Foundations Division, ASCE* 97 (9): 1183-1205. https://doi.org/10.1061/jsfeaq.0001659.

Wang, D., R. S. Merifield, and C. Gaudin. 2013. "Uplift Behaviour of Helical Anchors in Clay." *Canadian Geotechnical Journal* 50 (6): 575-584. https://doi.org/10.1139/cgj-2012-0350.

White, D. J., C. Y. Cheuk, and M. D. Bolton. 2008. "The Uplift Resistance of Pipes and Plate Anchors Buried in Sand." *Géotechnique* 58 (10): 771–779. https://doi.org/10.1680/geot.2008.3692.

Williams, M. 2021. "Bearing Capacity of High-Strength Steel Screw Anchors in Various Soil Conditions." *Soil Mechanics Journal* 152 (8).

Wu, F., M. Q. Gong, L. Y. Yao, M. Hu, and J. Jie. 2020. "High Precision Interval Analysis of the Frequency Response of Structural-Acoustic Systems with Uncertain-but-Bounded Parameters." *Engineering Analysis with Boundary Elements* 119: 190–202. https://doi.org/10.1016/j.enganabound.2020.07.016.

Xanthakos, P. P. 1991. *Ground Anchors and Anchored Structures*. New York: John Wiley & Sons, Inc.

Yoshida, S. 2021. "Effect of Sugarcane Bagasse Ash on Alkali Silica Reaction of Concrete with Soda Lime Glass as Aggregates." *International Journal of GEOMATE* 20 (78). https://doi.org/10.21660/2021.78.gx147.

Yoshida, S., and X. Xiong. 2023. "A Limit Equilibrium Method for Estimating Pull-out Resistance of Flip-type Ground Anchors in Sand Grounds." In *Smart Geotechnics for Smart Societies*, 1076–1080. https://doi.org/10.1201/9781003299127-150.

Yu, L., J. Liu, X. Kong, and Y. Hu. 2011. "Numerical Study on Plate Anchor Stability in Clay." *Géotechnique* 61 (3): 235-246. https://doi.org/10.1680/geot.8.p.071.

Zhou, Y., Y. Chen, and R. Chen. 2016. "Correction of Earth Pressure and Deformation Analysis for Double-Row Piles in Foundation Excavation." *Journal of Geotechnical and Geoenvironmental Engineering* 142 (10). https://doi.org/10.1155/2016/9818160.